CANADIAN JOURNAL OF RESEARCH

VOLUME 27 JULY, 1949 NUMBER 4

— SECTION A —

PHYSICAL SCIENCES

Contents

Page

Contributions to the Theory of Wave Guides—*W. Z. Chien, L. Infeld, J. R. Pounder, A. F. Stevenson, and J. L. Synge* - - 69

Veiling Glare in Aerial Photography—*K. M. Baird* - - - 130

Relative Yields of the D-D Reactions at Low Energies—*T. P. Pepper* - - - - - - - - - - - - - 143

The Specific Heat of Napalm-Gasoline Gels—*G. O. Langstroth and K. H. Hart* - - - - - - - - - - - - - 151

The Nuclear Moments of P^{31}—*M. F. Crawford and J. Levinson* - 156

The Gamma Rays of Radium (B + C)—*K. C. Mann and M. J. Ozeroff* - - - - - - - - - - - - - 164

NATIONAL RESEARCH COUNCIL
OTTAWA, CANADA

CANADIAN JOURNAL OF RESEARCH

The *Canadian Journal of Research* is issued in six sections, as follows:

A. Physical Sciences	D. Zoological Sciences
B. Chemical Sciences	E. Medical Sciences
C. Botanical Sciences	F. Technology

For the present, Sections A, C, D, and E are to be issued six times annually, and Sections B and F, twelve times annually, each under separate cover. with separate pagination.

The *Canadian Journal of Research* is published by the National Research Council of Canada under authority of the Chairman of the Committee of the Privy Council on Scientific and Industrial Research. The *Canadian Journal of Research* is edited by a joint Editorial Board consisting of members of the National Research Council of Canada, the Royal Society of Canada, and the Chemical Institute of Canada.

Sections B and F of the *Canadian Journal of Research* have been chosen by the Chemical Institute of Canada as its medium of publication for scientific papers.

EDITORIAL BOARD

Representing NATIONAL RESEARCH COUNCIL

DR. G. H. HENDERSON, (*Chairman*), Professor of Mathematical Physics, Dalhousie University, Halifax.

DR. A. R. GORDON, Head, Department of Chemistry, University of Toronto, Toronto.

DR. ROBERT NEWTON, President, University of Alberta, Edmonton, Alta.

DR. C. H. BEST, The Banting and Best Department of Medical Research, University of Toronto, Toronto.

Representing ROYAL SOCIETY OF CANADA

DR. A. NORMAN SHAW, Chairman, Department of Physics, McGill University, Montreal.

DR. J. W. T. SPINKS, Department of Chemistry, University of Saskatchewan Saskatoon.

} Section III

DR. H. S. JACKSON, Head, Department of Botany, University of Toronto, Toronto.

DR. E. HORNE CRAIGIE, Department of Zoology, University of Toronto, Toronto.

} Section V

Ex officio

DR. LÉO MARION, Editor-in-Chief, Division of Chemistry, National Research Laboratories, Ottawa.

DR. H. H. SAUNDERSON, Director, Division of Information Services, National Research Council, Ottawa.

Representing THE CHEMICAL INSTITUTE OF CANADA

DR. H. G. THODE, Department of Chemistry, McMaster University, Hamilton.

EDITORIAL COMMITTEE

Editor-in-Chief, DR. LÉO MARION
Editor, Section A, DR. A. NORMAN SHAW
Editor, Section B, DR. J. W. T. SPINKS, DR. H. G. THODE
Editor, Section C, DR. H. S. JACKSON
Editor, Section D, DR. E. HORNE CRAIGIE
Editor, Section E, DR. J. B. COLLIP
Editor, Section F, DR. J. A. ANDERSON, DR. A. NORMAN SHAW, DR. H. G. THODE

Manuscripts should be addressed:

Editor-in-Chief,
Canadian Journal of Research,
National Research Council, Ottawa, Canada.

Canadian Journal of Research

Issued by THE NATIONAL RESEARCH COUNCIL OF CANADA

VOL. 27, SEC. A. JULY, 1949 NUMBER 4

CONTRIBUTIONS TO THE THEORY OF WAVE GUIDES[1]

BY W. Z. CHIEN[2], L. INFELD, J. R. POUNDER, A. F. STEVENSON, AND J. L. SYNGE[3]

Abstract

Part I deals with the problem of determining the field due to a source of radiation inside a semi-infinite rectangular wave guide closed at one end by a plug, the current distribution in the source being regarded as known. Both the walls of the guide and the plug are treated as being perfectly conducting. Three different methods of solving the problem are given. The radiation resistance is then deduced from energy considerations. In particular, an expression for the radiation resistance of a linear antenna perpendicular to the wider face of the plug, fed at the point of entry, is derived, it being assumed that the antenna current is sinusoidal and that only the fundamental *H*-wave is transmitted by the guide.

In Part II, one of the methods of paper I is extended to the case of a guide of *arbitrary* cross section, and the general problem of the calculation of radiation resistance and reactance is discussed.

In Part III, a number of formulae for the radiation resistance of antennae of various shapes, with various assumed current distributions, in rectangular and circular guides, are given.

In Part IV, explicit calculations for the impedance of a linear antenna in a rectangular wave guide are given. Further numerical calculations relating to the same problem, from the point of view of matching and sensitivity, have been made by Messrs. Chien and Pounder, but are not reproduced here.

General Introduction

The four parts of this paper are based on four of the reports which were issued by the Special Committee on Applied Mathematics of the National Research Council, the authors of which were, at the time, members of the Department of Applied Mathematics of the University of Toronto. The four parts deal with rather closely related topics in the field of wave guide theory which are all of a certain mathematical interest.

They have been reproduced with only slight alterations from their original form, and no attempt has been made to refer to more recent work, although, so far as the authors are aware, most of the results contained herein have not hitherto been published. References are given at the end of each part separately. The figures and equations are also numbered separately for each part.

The authors wish to acknowledge the help received from the Field Station of the National Research Council.

[1] *Manuscript received October 29, 1948.*
Contribution from the Department of Mathematics, University of Toronto, Toronto, Ont.

[2] *Formerly of the University of Toronto.*

[3] *Institute of Advanced Studies, Dublin.*

PART I. RADIATION FROM A SOURCE INSIDE A PERFECTLY CONDUCTING WAVE GUIDE OF RECTANGULAR SECTION

By L. Infeld, A. F. Stevenson, and J. L. Synge

1. Introduction

We consider a wave guide of rectangular section, extending to infinity in one direction and closed in the other direction by a plug. The guide and the plug are assumed to be perfect conductors.

A source of energy is placed inside the guide. First we take this source to be a dipole, arbitrary in position and direction. We find the field produced inside the guide by the dipole, particularly the field a long way down the guide. This gives the mean flux of energy at infinity in the guide. Since the walls and plug are perfectly conducting, no energy can pass into them or out of them, and so this flux of energy is the power output of the dipole. Dividing this output by the mean value of the square of the current in the dipole, we obtain the radiation resistance.

Once the field due to a dipole has been found, the field due to a finite antenna follows by integration. The power output of the antenna is obtained from the field a long way down the guide, and the radiation resistance of the antenna is given by dividing the output by the mean value of the square of the current entering the antenna. We thus find the resistance, but not the reactance. The Heaviside (or rational) system of units is used throughout, the final results being converted into ohms.

We have succeeded in solving our problem by three independent methods, all of them giving the same result. Since we do not know which of these methods will prove most useful in the calculation of reactance, we give all three of them here. The first two methods are included in the main body of the paper, the third in Appendix B.

These three different methods can be characterized as follows.

The first two methods are based on the idea of images. The first (Section 3) is the more intuitive one; it treats the dipoles as singularities throughout, and gives the field only at great distances from the lattice. The second (Section 4) is the more rigorous one; it gives the damped waves near the lattice as well as the field at great distances; it is characterized by a smoothing process which enables us to replace summations by integrations. Finally, the third method (Appendix B) avoids the use of images altogether (except for images in the end of the guide) and calculates the field not by means of the Hertzian vector, but directly from Maxwell's equations, assuming a known current distribution.

Our method is sufficiently general to cover any rectangular section for the guide and any form of antenna, assumed to be a very thin wire. Details are developed only for a guide which cuts off all radiation except the H_{10} wave;

for this case a general formula for radiation resistance is given, the antenna remaining arbitrary. In particular we take the antenna to be straight and perpendicular to the wider face of the guide, being fed at the point of entry. Then the radiation resistance is

$$R = \frac{60}{\pi}\frac{\lambda^2}{\gamma ab}\cos^2\frac{\pi x_0}{a}\sin^2\frac{2\pi\gamma z_0}{\lambda}\tan^2\frac{\pi l}{\lambda}\ \text{ohms}, \tag{1.1}$$

where a = longer edge of cross section in centimeters,

b = shorter edge of cross section in centimeters,

λ = wave length in centimeters (i.e., frequency = $3\times10^{10}/\lambda$ c.p.s.),

$$\gamma = \sqrt{1-\frac{\lambda^2}{4a^2}}, \tag{1.2}$$

l = length of antenna in centimeters,

x_0 = distance of antenna from the central line of the wider face of the guide in centimeters,

z_0 = distance of antenna in front of plug in centimeters.

The arrangement is shown in Fig. 1.

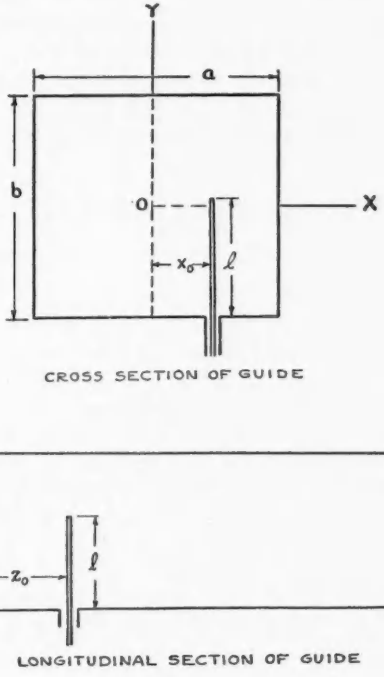

FIG. 1.

As a particular result, we place the antenna symmetrically ($x_0 = 0$) and take $l = \lambda/4$ and the following numerical values:

(1.3) $\qquad a = 5.5$ cm., $\qquad b = 4.5$ cm., $\qquad \lambda = 10$ cm.;

then the resistance is

(1.4) $\qquad R = 185 \sin^2 (0.262\, z_0)$ ohms.

To match such a guide to a coaxial line with an impedance of 70 ohms we should take

(1.5) $\qquad \sin (0.262\, z_0) = \sqrt{\frac{70}{185}} = 0.615, \quad z_0 = 2.53$ cm., 9.46 cm., . . .

This gives the possible positions at which the plug should be set.

2. The Lattice of Dipoles

We use the method of images. This method is available only for the following sections:

(i) Rectangle,

(ii) Equilateral triangle,

(iii) Isosceles right-angled triangle,

(iv) 30°—60°—90° triangle.

The rectangular section is the simplest, and the only one of these sections actually employed; we shall confine our attention to it.

The image of a dipole with respect to a perfectly conducting plane is well known. It is found by taking the geometrical image, and then reversing direction. The dipole and its image give a field which satisfies the condition

(2.1) $\qquad \vec{E_t} = 0,$

over the plane, $\vec{E_t}$ being the tangential component of electric intensity.

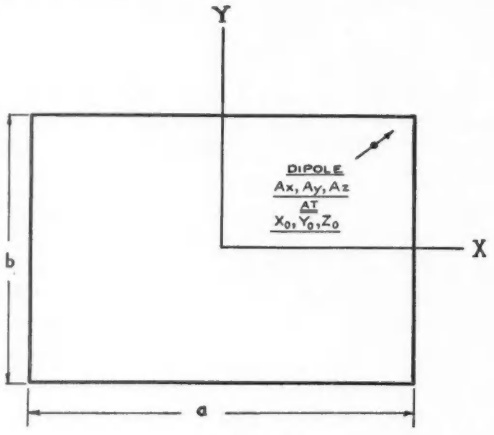

FIG. 2.

Let us first consider the case where the rectangular guide has no plug, so that it extends to infinity in both directions. Suppose that there is a dipole inside the guide. It is easy to find a doubly infinite system of images (all external to the guide) so that the lattice consisting of the dipole and its images gives a field satisfying the condition (2.1) over the walls of the guide. If we now add a plug, the condition (2.1) will be satisfied over it if we add to the above lattice its image in the plane of the plug.

Let us take the origin at the center of the plug (Fig. 2), the axes of x and y parallel to the edges of the rectangular section and the axis of z along the axis of the guide, pointing towards the open end. Let a and b be the lengths of the edges of the section of the guide.

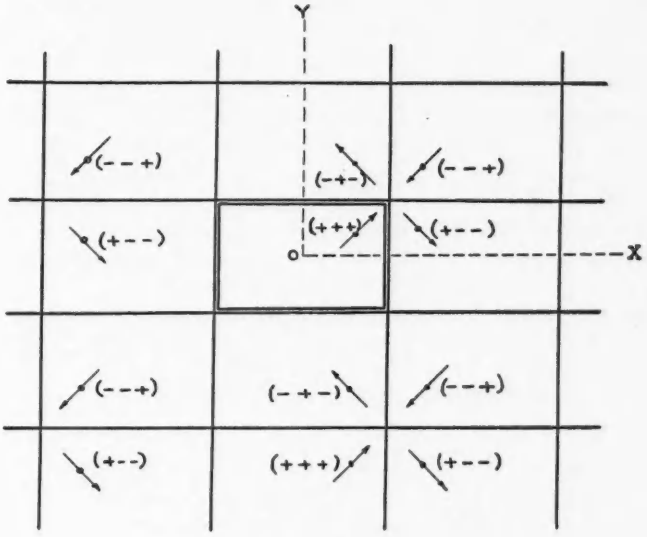

FIG. 3.

We place a dipole with components (A_x, A_y, A_z) at (x_0, y_0, z_0), these components being complex in general. Fig. 3 shows part of the lattice in the plane $z = z_0$. The arrows are to be regarded as oblique to the plane of the paper and equally inclined to it. The signs indicate the components: thus

$$(+, +, +) \quad \text{means} \quad (A_x, A_y, A_z),$$
$$(+, -, -) \quad \text{means} \quad (A_x, -A_y, -A_z).$$

If we let μ and ν take all integer values, positive, zero, and negative, we may represent the components and positions of all the dipoles in the plane $z = z_0$ as follows:

$$(2.2)\quad \begin{cases} (A_x,\ A_y,\ A_z) & \text{at } (x_0 + 2\mu a,\ y_0 + 2\nu b,\ z_0), \\ (A_x,\ -A_y,\ -A_z) & \text{at } (-x_0 + (2\mu + 1)a,\ y_0 + 2\nu b,\ z_0), \\ (-A_x,\ A_y,\ -A_z) & \text{at } (x_0 + 2\mu a,\ -y_0 + (2\nu + 1)b,\ z_0), \\ (-A_x,\ -A_y,\ A_z) & \text{at } (-x_0+(2\mu+1)a,\ -y_0+(2\nu+1)b,\ z_0). \end{cases}$$

The images with respect to the plane of the plug are given by this table on changing the signs of A_x, A_y, and z_0.

The lattice shown in (2.2) is a superposition of four *basic lattices*, in each of which all the dipoles are the same. The periods of all these basic lattices are $(2a, 2b)$. Instead of calculating at once the field due to the whole system of dipoles, we first calculate the field due to the basic lattice shown in the first line of (2.2). The fields of the other basic lattices then follow by simple substitutions; adding all four fields, we get the field due to the system (2.2). The field due to the plug is then easily obtained and added to the field already found.

The transformation by which we pass from the field of one basic lattice to that of another is given by the following table, read downwards:

$$(2.3)\quad \begin{cases} \text{I} & A_x,\ A_y,\ A_z & x_0,\ y_0,\ z_0 \\ \text{II} & A_x,\ -A_y,\ -A_z & -x_0 + a,\ y_0,\ z_0 \\ \text{III} & -A_x,\ A_y,\ -A_z & x_0,\ -y_0 + b,\ z_0 \\ \text{IV} & -A_x,\ -A_y,\ A_z & -x_0 + a,\ -y_0 + b,\ z_0, \end{cases}$$

(Basic lattice | Components | Base-point)

The co-ordinates of a general dipole in the basic lattice I are

$$(2.4)\qquad x_{\mu\nu} = x_0 + 2\mu a,\quad y_{\mu\nu} = y_0 + 2\nu b,\quad z = z_0,$$

where μ, ν take all integer values, positive, zero, and negative.

Let λ be the wave length of the radiation (i.e., frequency $= c/\lambda$), and let $k = 2\pi/\lambda$. The time factor is e^{-ikct}. We shall use an accent on a symbol containing the time factor, and drop the accent when the time factor is omitted. As usual, physical quantities are to be found by taking the real parts of the complex expressions.

The Hertz vector at the point (x, y, z) due to a dipole $\vec{A}$ at (x', y', z') is

$$(2.5)\qquad \vec{\phi}' = \vec{\phi}\, e^{-ikct}, \qquad \vec{\phi} = \frac{\vec{A}}{4\pi}\frac{e^{ikr}}{r},$$

where r is the distance between (x, y, z) and $x', y', z')$. Thus the Hertz vector due to the basic lattice I is

$$(2.6)\qquad \vec{\phi} = \frac{\vec{A}}{4\pi}\sum_{\mu=-\infty}^{\infty}\sum_{\nu=-\infty}^{\infty}\frac{e^{ikr_{\mu\nu}}}{r_{\mu\nu}},$$

where $r_{\mu\nu}$ is the distance between (x, y, z) and $x_{\mu\nu}, y_{\mu\nu}, z_{\mu\nu})$.

3. The Field Due to a Basic Lattice: Discontinuous Method

The idea used here is based on the familiar theory of a diffraction grating. It is known that a finite lattice composed of oscillating dipoles sends out pencils of radiation in a discrete number of directions. The field far from the lattice and very near to the center of a pencil of radiation can be represented by a plane wave; the field outside these pencils of radiation is practically nonexistent. Without going into mathematical details we can foresee what will happen if the lattice becomes larger and larger. All the discrete pencils of radiation become wider and wider, finally covering the whole space. The regions where the radiation was practically nonexistent shrink to nothing. The final radiation at a point, arbitrary but far enough from the lattice, can be obtained by taking into account all the plane waves traveling in all the *admitted* directions, given by the geometrical structure of the lattice. This is the principal idea which we shall work out here mathematically.

Let us consider first a *patch*, that is a finite basic lattice, consisting of dipoles whose co-ordinates are given by (2.4), where

$$-M \leqslant \mu \leqslant M, \qquad -N \leqslant \nu \leqslant N. \tag{3.1}$$

Let α, β, γ be the direction cosines of the line going through the center of a radiation pencil and x, y, z the co-ordinates along this line. Then, at distances great compared with the dimensions of the patch, we have, in the first approximation,

$$r_{\mu\nu} = r - 2\mu a\alpha - 2\nu b\beta, \tag{3.2}$$

r being the distance from the center of the patch; and the Hertz vector due to the patch is (to this approximation)

$$\vec{\phi}(M, N) = \frac{\vec{A}}{4\pi} \frac{e^{ikr}}{r} \left(\sum_{\mu=-M}^{M} e^{-2ik\mu a\alpha} \right) \left(\sum_{\nu=-N}^{N} e^{-2ik\nu\beta b} \right). \tag{3.3}$$

From (3.3) we obtain the possible direction cosines of the radiation pencils if M and N are large, which we shall assume throughout. These are:

$$\alpha = \alpha_m ; \qquad \beta = \beta_n ; \qquad \gamma = \gamma_{mn} , \tag{3.4}$$

where

$$\alpha_m = \frac{m\pi}{ka} , \qquad \beta_n = \frac{n\pi}{kb} , \quad \gamma_{mn} = \sqrt{1 - \frac{\pi^2}{k^2}\left(\frac{m^2}{a^2} + \frac{n^2}{b^2}\right)} , \tag{3.5}$$

m and n being integers, positive, negative, or zero. Since γ must be real, the condition for m, n is

$$\frac{m^2}{a^2} + \frac{n^2}{b^2} < \frac{4}{\lambda^2} , \tag{3.6}$$

the last inequality, together with (3.5), defining the directions of all the radiation pencils, or, in other words, all the (m, n) pencils. The Hertz vector along the center of the (m, n) pencil is

$$\vec{\phi}(M, N) = \frac{\vec{A}}{\pi} \frac{e^{ikr_{mn}}}{r_{mn}} MN. \tag{3.7}$$

This result is based on (3.2) which may be rewritten for the present choice of points of observation

$$r_{mn,\mu\nu} = r_{mn} - 2\mu a\alpha_m - 2\nu b\beta_n \tag{3.8}$$
$$= r_{mn} - \frac{2\mu m\pi}{k} - \frac{2\nu n\pi}{k}.$$

The result as expressed in (3.7) is not very satisfactory since it contains M and N characterizing the dimensions of the patch. We can improve (3.7) by taking instead of (3.8) the rigorous formula

$$r_{mn,\mu\nu} = (r_{mn}^2 + 4\mu^2a^2 + 4\nu^2b^2 - 4r_{mn}\mu a\alpha_m - 4r_{mn}\nu b\beta_n)^{\frac{1}{2}}. \tag{3.9}$$

We see that (3.8) is the first approximation to (3.9), the second approximation being:

$$r_{mn,\mu\nu} = r_{mn} - \frac{2\pi}{k}(\mu m + \nu n) \tag{3.10}$$
$$+ \frac{2}{r_{mn}}\left[\mu^2a^2\left(1 - \frac{m^2\pi^2}{a^2k^2}\right) + \nu^2b^2\left(1 - \frac{n^2\pi^2}{b^2k^2}\right) - \frac{2\mu\nu mn\pi^2}{k^2}\right].$$

When this is substituted in (2.6), we get for the Hertz vector along the center of the pencil:

$$\phi_{mn}(M, N) = \frac{\vec{A}}{4\pi}\frac{e^{ikr_{mn}}}{r_{mn}}\sum_{\mu=-M}^{M}\sum_{\nu=-N}^{N} \tag{3.11}$$
$$\exp\left\{\frac{2ik}{r_{mn}}\left[\mu^2a^2\left(1 - \frac{m^2\pi^2}{a^2k^2}\right) + \nu^2b^2\left(1 - \frac{n^2\pi^2}{b^2k^2}\right) - \frac{2\mu\nu mn\pi^2}{\mu k^2}\right]\right\},$$

which is more rigorous than (3.7).

Let us now increase M and N to infinity, that is, we spread the pencil over the whole space. But in this case the pencils overlap and $\vec{\phi}_{M,N}(M, N \to \infty)$ ceases to represent the Hertz vector inside the broadening pencil. It will represent only the (m, n) contribution to the total $\vec{\phi}$, where

$$\vec{\phi} = \sum_{m=-m_0}^{m_0}\sum_{n=-n_0}^{n_0}\vec{\phi}_{mn}(M, N \to \infty), \tag{3.12}$$

M_0 and N_0 being the greatest integers satisfying (3.6).

We turn now toward the calculation of

$$\vec{\phi}_{mn} = \vec{\phi}_{mn}(M, N \to \infty), \tag{3.13}$$

by replacing the summation in (3.11) by an integration. This leads us to an integral of the type;

$$\int_{-\infty}^{\infty}\int_{-\infty}^{\infty} e^{i(c\xi^2 + d\eta^2 + 2e\xi\eta)}d\xi d\eta, \tag{3.14}$$

which can be brought by a rotation of the co-ordinate system into the form

$$(3.15)\qquad \left(\int_{-\infty}^{\infty} e^{ic'\xi^2}d\xi\right)\left(\int_{-\infty}^{\infty} e^{id'\eta^2}d\eta\right) = 4(c'd')^{-\frac{1}{2}}\left[\sqrt{\frac{\pi}{8}}(1+i)\right]^2 = (c'd')^{-\frac{1}{2}}i\pi .$$

But

$$(3.16)\qquad c'd' = cd - g^2 .$$

Comparison with (3.11) gives:

$$(3.17)\qquad c = 2ka^2\left(1 - \frac{m^2\pi^2}{a^2k^2}\right), \quad d = 2kb^2\left(1 - \frac{n^2\pi^2}{b^2k^2}\right),$$

$$g = -\frac{2mn\pi^2}{k}, \quad \xi = \frac{\mu}{\sqrt{r_{mn}}}, \quad \eta = \frac{\nu}{\sqrt{r_{mn}}} .$$

The result is:

$$(3.18)\qquad \vec{\phi}_{mn} = \frac{i\vec{A}}{8kabr_{mn}}\, e^{ikr_{mn}},$$

where

$$(3.19)\qquad r_{mn} = (x - x_0)\,\alpha_m + (y - y_0)\,\beta_n + (z - z_0)\,\gamma_{mn} ,$$

and (x, y, z) represents an arbitrary point in space. The plane wave as represented by (3.18) has no physical meaning. To find the Hertz vector at a point, arbitrary but far enough from the basic lattice, we must perform the summation indicated in (3.12). Remembering that, according to (3.5)

$$(3.20)\qquad \alpha_{-m} = -\alpha_m , \qquad \beta_{-n} = -\beta_n ,$$

we have, because of (3.18), as our final result:

$$(3.21)\qquad \vec{\phi} = \frac{i\vec{A}}{8kab}\left\{e^{ik(z-z_0)} + 2\sum_{m=1}^{m_0}\frac{1}{\gamma_{m0}}\cos k\alpha_m(x - x_0)\, e^{ik\gamma_{m0}(z-z_0)}\right.$$

$$+ 2\sum_{n=1}^{n_0}\frac{1}{\gamma_{0n}}\cos k\beta_n(y - y_0)e^{ik\gamma_{0n}(z-z_0)}$$

$$\left. + 4\sum_{m=1}^{m_0}\sum_{n=1}^{n_0}\frac{1}{\gamma_{mn}}\cos k\alpha_m(x - x_0)\cos k\beta_n(y - y_0)e^{ik\gamma_{mn}(z-z_0)}\right\}$$

representing the Hertz vector due to the basic lattice I.

We can now find the Hertz vector of the lattices equivalent to that of the wave guide. We have to apply our formula (3.21) four times, changing the components of $\vec{A}$ and x_0, y_0, according to the table (2.3). In this way, we obtain the Hertz vector of the lattice in the plane $z = z_0$. The Hertz vector of the lattice in the plane $z = -z_0$ is obtained by changing z_0 into $-z_0$, and A_x, A_y into $-A_x$, $-A_y$ in this result. The final Hertz vector obtained in this way is a summation of the Hertz vector for *eight* properly chosen basic lattices. Denoting now by ϕ_x, ϕ_y, ϕ_z the components of this *resulting* Hertz vector we find because of (3.21) and (3.5):

$$
(3.22)\quad
\begin{cases}
\phi_x = \dfrac{2A_x}{kab}\left\{\displaystyle\sum_{n=1}^{n_0}\frac{1}{\gamma_{0n}}\sin n\chi\sin n\chi_0\sin(k\gamma_{0n}z_0)e^{ik\gamma_{0n}z}\right. \\
\qquad +2\displaystyle\sum_{m=1}^{m_0}\sum_{n=1}^{n_0}\frac{1}{\gamma_{mn}}\cos m\psi\cos m\psi_0\sin n\chi\sin n\chi_0 \\
\qquad \left.\sin(k\gamma_{mn}z_0)e^{ik\gamma_{mn}z}\right\}, \\
\phi_y = \dfrac{2A_y}{kab}\left\{\displaystyle\sum_{m=1}^{m_0}\frac{1}{\gamma_{m0}}\sin m\psi\sin m\psi_0\sin(k\gamma_{m0}z_0)e^{ik\gamma_{m0}z}\right. \\
\qquad +2\displaystyle\sum_{m=1}^{m_0}\sum_{n=1}^{n_0}\frac{1}{\gamma_{mn}}\sin m\psi\sin m\psi_0\cos n\chi\cos n\chi_0 \\
\qquad \left.\sin(k\gamma_{mn}z_0)e^{ik\gamma_{mn}z}\right\}, \\
\phi_z = \dfrac{4iA_z}{kab}\displaystyle\sum_{m=1}^{m_0}\sum_{n=1}^{n_0}\frac{1}{\gamma_{mn}}\sin m\psi\sin m\psi_0\sin n\chi\sin n\chi_0 \\
\qquad \cos(k\gamma_{mn}z_0)e^{ik\gamma_{mn}z}
\end{cases}
$$

where

$$
(3.23)\quad
\begin{cases}
\psi = \dfrac{\pi x}{a} - \dfrac{\pi}{2}, & \psi_0 = \dfrac{\pi x_0}{a} - \dfrac{\pi}{2}, \\
\chi = \dfrac{\pi y}{b} - \dfrac{\pi}{2}, & \chi_0 = \dfrac{\pi y_0}{b} - \dfrac{\pi}{2}.
\end{cases}
$$

Equations (3.22) represent the Hertz vector for great z inside the wave guide, i.e., for

$$-\tfrac{1}{2}a \leqslant x \leqslant \tfrac{1}{2}a, \qquad -\tfrac{1}{2}b \leqslant y \leqslant \tfrac{1}{2}b.$$

4. The Field Due to a Basic Lattice: Continuous Method

Let us consider the basic lattice I in the plane $z = z_0$, as in (2.3). Instead of discrete dipoles, let us take a continuous distribution over the plane with density $\vec{\sigma}$, so that a dipole $\vec{\sigma}\,dx'dy'$ is associated with the element $dx'dy'$, where x', y' are co-ordinates in the plane $z = z_0$. Let p be a large positive integer; consider the expression

$$(4.1)\qquad \vec{\sigma} = \vec{A}\frac{K(p)}{ab}\cos^{2p}X'\cos^{2p}Y',$$

where $K(p)$ is a constant and

$$(4.2)\qquad X' = \tfrac{1}{2}\pi(x' - x_0)/a, \qquad Y' = \tfrac{1}{2}\pi(y' - y_0)/b.$$

It is evident that this density will be very small except in the immediate neighborhood of the positions of the dipoles in the discrete lattice; the larger we make p, the more closely does this continuous distribution approach the discrete distribution. We choose the constant $K(p)$ so that the total dipole

strength inside the period rectangle $(2a, 2b)$ is the same in the continuous and discrete distributions, i.e., so that

$$\iint \vec{\sigma}\, dx'\, dy' = \vec{A}\,, \tag{4.3}$$

the ranges of the integral being

$$x_0 - a < x' < x_0 + a, \qquad y_0 - b < y' < y_0 + b.$$

Since

$$\int_{x_0 - a}^{x_0 + a} \cos^{2p} X'\, dx' = \frac{2a}{\pi} \int_{-\frac{1}{2}\pi}^{\frac{1}{2}\pi} \cos^{2p} X'\, dX'$$

$$= 2a\, \frac{(2p)!}{2^{2p}(p!)^2},$$

we take

$$K(p) = \frac{2^{4p}(p!)^4}{4(2p!)^2}. \tag{4.4}$$

By Stirling's formula this is approximately $\pi p/4$, but it is actually more convenient to retain the exact value (4.4).

The Hertz vector for the basic lattice, smoothed out as described above, is

$$\vec{\phi} = \frac{1}{4\pi} \iint \vec{\sigma}\, e^{ikr}/r\, .\, dx'dy', \tag{4.5}$$

where r is the distance from the point (x', y', z_0) to the point of observation (x, y, z). Let us drop a perpendicular from (x, y, z) on the plane $z = z_0$, and take polar co-ordinates (R, θ) relative to the foot of this perpendicular (Fig. 4). Then

$$x' = x + R\cos\theta, \qquad y' = y + R\sin\theta, \tag{4.6}$$

and (4.5) gives

$$\vec{\phi} = \frac{\vec{A}\, K(p)}{4\pi ab} \int_0^{\infty} e^{ikr} r^{-1} R\, dR \int_0^{2\pi} \cos^{2p} X' \cos^{2p} Y' d\theta\,. \tag{4.7}$$

On substituting

$$\cos^{2p} X' = \frac{1}{2^{2p}} \sum_{m=-p}^{p} \binom{2p}{p+m} e^{2imX'},$$

and a similar expression for $\cos^{2p} Y'$, we have

$$\int_0^{2\pi} \cos^{2p} X' \cos^{2p} Y'\, d\theta \tag{4.8}$$

$$= \frac{1}{2^{4p}} \sum_{m=-p}^{p} \sum_{n=-p}^{p} \binom{2p}{p+m} \binom{2p}{p+n} e^{2i(mX+nY)} \int_0^{2\pi} e^{i\pi R\left(\frac{m\cos\theta}{a} + \frac{n\sin\theta}{b}\right)} d\theta,$$

where X, Y are given by (4.2) on removing all accents. Since for any real constants k_1, k_2,

$$\int_0^{2\pi} e^{i(k_1\cos\theta + k_2\sin\theta)} d\theta = 2\pi J_0(\sqrt{k_1^2 + k_2^2}), \tag{4.9}$$

where J_0 is the Bessel function of order zero, (4.7) reduces to

$$\vec{\phi} = \frac{\vec{A}\,K(p)}{2^{4p+1}ab} \sum_{m=-p}^{p} \sum_{n=-p}^{p} \binom{2p}{p+m}\binom{2p}{p+n} e^{2i(mX+nY)} I_{mn}, \tag{4.10}$$

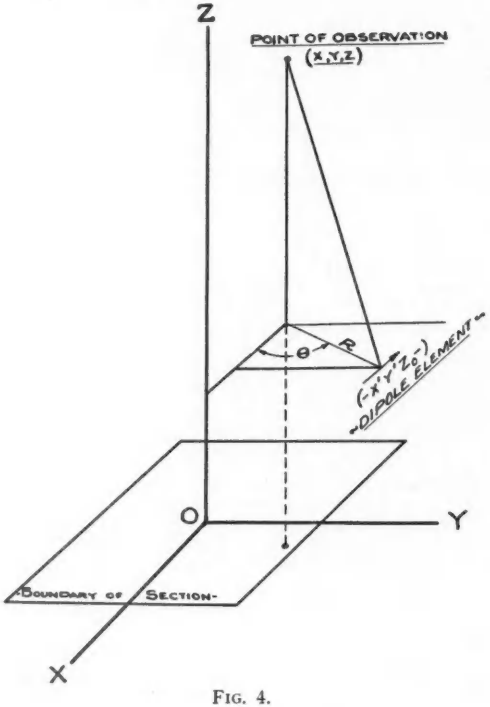

FIG. 4.

where

$$I_{mn} = \int_0^\infty e^{ikr} r^{-1} R J_0(C_{mn}R)\,dR, \tag{4.11}$$

$$C_{mn} = \pi\sqrt{m^2/a^2 + n^2/b^2}. \tag{4.12}$$

Now

$$R^2 = r^2 - (z - z_0)^2,$$

and so

$$I_{mn} = \int_{|z-z_0|}^\infty e^{ikr} J_0(C_{mn}\sqrt{r^2 - (z-z_0)^2})\,dr. \tag{4.13}$$

This integral is evaluated in Appendix A; we find

$$I_{mn} = \frac{i}{k\gamma_{mn}} e^{ik\gamma_{mn}|z-z_0|}, \tag{4.14}$$

where γ_{mn} is defined by

$$(4.15)\qquad \begin{cases} k\gamma_{mn} = |\sqrt{k^2 - C_{mn}^2}| & \text{if } C_{mn} < k, \\ k\gamma_{mn} = i|\sqrt{k^2 - C_{mn}^2}| & \text{if } C_{mn} > k. \end{cases}$$

When we substitute this in (4.10) we get for the Hertz vector of the smoothed basic lattice I

$$(4.16)\qquad \vec{\phi} = \frac{i\vec{A}K(p)}{2^{4p+1}kab} \sum_{m=-p}^{p} \sum_{n=-p}^{p} \binom{2p}{p+m}\binom{2p}{p+n} \frac{1}{\gamma_{mn}} e^{ik[\alpha_m(x-x_0)+\beta_n(y-y_0)+\gamma_{mn}|z-z_0|]},$$

where

$$k\alpha_m = m\pi/a, \qquad k\beta_n = n\pi/b.$$

If we go a long way down the guide, so that $z \to \infty$, only those terms in (4.16) survive for which γ_{mn} is real, i.e.,

$$(4.17)\qquad C_{mn} < k,$$

or equivalently

$$(4.18)\qquad \frac{m^2}{a^2} + \frac{n^2}{b^2} < \frac{4}{\lambda^2}.$$

This condition is the same as (3.6), and is in fact the cut-off condition given by the eigenvalue method for an empty guide. The condition limits the values of m and n to some finite ranges

$$-m_0 \leqslant m \leqslant m_0, \qquad -n_0 \leqslant n \leqslant n_0.$$

Thus in calculating $\vec{\phi}$ from (4.16) we have only a finite number of terms. We now proceed to the limit $p \to \infty$ in order to pass from the smoothed basic lattice to the discrete basic lattice. Since, for fixed values of m and n,

$$(4.19)\qquad \lim_{p\to\infty} \frac{K(p)}{2^{4p}}\binom{2p}{p+m}\binom{2p}{p+n} = \lim_{p\to\infty} \frac{1}{4} \frac{(p!)^4}{(p+m)!(p-m)!(p+n)!(p-n)!} = \frac{1}{4},$$

we get for the Hertz vector of the discrete basic lattice I a long way down the guide

$$(4.20)\qquad \vec{\phi} = \frac{i\vec{A}}{8kab} \sum_{m=-m_0}^{m_0} \sum_{n=-n_0}^{n_0} \frac{1}{\gamma_{mn}} e^{ik[\alpha_m(x-x_0)+\beta_n(y-y_0)+\gamma_{mn}(z-z_0)]},$$

where

$$(4.21)\qquad \gamma_{mn} = \sqrt{1 - \frac{C_{mn}^2}{k^2}} = \sqrt{1 - \frac{\lambda^2}{4}\left(\frac{m^2}{a^2} + \frac{n^2}{b^2}\right)}.$$

Equation (4.20) is the same as (3.21), and so the two methods lead to the same expression for the field at a great distance down the guide. From this point the argument proceeds in common.

However, before finally leaving the smoothed lattice, let us write down the Hertz vector at any point inside the guide. To do this, we have to superimpose on (4.16) the corresponding expressions for the other basic lattices in

(2.3), and then superimpose on the result the expression corresponding to the images with respect to the plane of the plug. A simple calculation gives

$$\vec{\phi} = \frac{iK(p)}{2^{4p+1}kab} \sum_{m=-p}^{p} \sum_{n=-p}^{p} \binom{2p}{p+m}\binom{2p}{p+n} \frac{1}{\gamma_{mn}} e^{ik(\alpha_m x + \beta_n y)} [\vec{F}_{(mn)} e^{ik\gamma_{mn}|z-z_0|} + \vec{G}_{(mn)} e^{ik\gamma_{mn}|z+z_0|}], \tag{4.22}$$

where

$$\begin{cases} F_{(mn)x} = -G_{(mn)x} = A_x[e^{-ik\alpha_m x_0} + (-1)^m e^{ik\alpha_m x_0}][e^{-ik\beta_n y_0} - (-1)^n e^{ik\beta_n y_0}], \\ F_{(mn)y} = -G_{(mn)y} = A_y[e^{-ik\alpha_m x_0} - (-1)^m e^{ik\alpha_m x_0}][e^{-ik\beta_n y_0} + (-1)^n e^{ik\beta_n y_0}], \\ F_{(mn)z} = G_{(mn)z} = A_z[e^{-ik\alpha_m x_0} - (-1)^m e^{ik\alpha_m x_0}][e^{-ik\beta_n y_0} - (-1)^n e^{ik\beta_n y_0}]. \end{cases} \tag{4.23}$$

5. The H_{10} Wave

Let us suppose that the dimensions of the guide and the frequency are such that

$$\frac{1}{a^2} < \frac{4}{\lambda^2} < \frac{1}{a^2} + \frac{1}{b^2}. \tag{5.1}$$

These conditions are satisfied for example by the numerical values given in (1.3). Then the condition (3.6) or (4.18) is satisfied only by

$$m = -1, 0, 1, \qquad n = 0. \tag{5.2}$$

Putting $m_0 = 1$, $n_0 = 0$ in (3.22) and writing

$$\gamma = \gamma_{10} = \gamma_{-10} = \sqrt{1 - \frac{\lambda^2}{4a^2}}, \tag{5.3}$$

we get for the Hertz vector a long way down the guide

$$\begin{cases} \phi_x = \phi_z = 0, \\ \phi_y = \dfrac{2A_y}{k\gamma ab} \cos\frac{\pi x_0}{a} \sin k\gamma z_0 \cos\frac{\pi x}{a} e^{ik\gamma z}. \end{cases} \tag{5.4}$$

The corresponding field is

$$\begin{cases} E_x = \dfrac{\partial^2 \phi_y}{\partial x \partial y} = 0, \\ E_y = \dfrac{\partial^2 \phi_y}{\partial y^2} + k^2 \phi_y \\ \qquad = \dfrac{2kA_y}{\gamma ab} \cos\frac{\pi x_0}{a} \sin k\gamma z_0 \cos\frac{\pi x}{a} e^{ik\gamma z}, \\ E_z = \dfrac{\partial^2 \phi_y}{\partial z \partial y} = 0, \\ H_x = ik \dfrac{\partial \phi_y}{\partial z} = -\dfrac{2kA_y}{ab} \cos\frac{\pi x_0}{a} \sin k\gamma z_0 \cos\frac{\pi x}{a} e^{ik\gamma z}, \\ H_y = 0, \\ H_z = -ik \dfrac{\partial \phi_y}{\partial x} = \dfrac{2i\pi A_y}{\gamma a^2 b} \cos\frac{\pi x_0}{a} \sin k\gamma z_0 \sin\frac{\pi x}{a} e^{ik\gamma z}. \end{cases} \tag{5.5}$$

The time-mean of the flux of energy across a section of the guide is

$$F = \text{real part of } \tfrac{1}{2}c \int_{-\frac{1}{2}a}^{\frac{1}{2}a} \int_{-\frac{1}{2}b}^{\frac{1}{2}b} (E_x\overline{H}_y - E_y\overline{H}_x)\, dx\, dy \tag{5.6}$$

$$= \frac{k^2 c A_y \overline{A}_y}{\gamma ab} \cos^2 \frac{\pi x_0}{a} \sin^2 k\gamma z_0 .$$

The transmitted wave is the H_{10} wave, as indeed we know otherwise by the eigenvalue method. It is the quantitative character of the present result that is new. We note that:

(i) The radiation depends only on the component A_y of the dipole, i.e., on the component parallel to the shorter edge of the cross section.

(ii) The radiation depends only on two (x_0, z_0) of the co-ordinates of the dipole.

A current $I' = I \exp(-ikct)$ flowing in an element $\overrightarrow{ds_0}$ (dx_0, dy_0, dz_0) of wire with direction cosines L, M, N is equivalent to a dipole with components

$$A_x = \frac{iIL}{kc} ds_0 , \quad A_y = \frac{iIM}{kc} ds_0 , \quad A_z = \frac{iIN}{kc} ds_0 . \tag{5.7}$$

If the current element belongs to an antenna in a rectangular wave guide with a plug, the field a long way down the guide is given by (5.5) when we substitute from (5.7).

If the antenna is very short (length l) compared with the wave length, and the current I is regarded as constant along it the output is by (5.6)

$$F = \frac{M^2 l^2 I\overline{I}}{c\gamma ab} \cos^2 \frac{\pi x_0}{a} \sin^2 k\gamma z_0 . \tag{5.8}$$

Since the time-average of the square of the current is $\frac{1}{2}I\overline{I}$, the radiation resistance is

$$R = \frac{F}{\frac{1}{2}I\overline{I}} = \frac{2M^2 l^2}{c\gamma ab} \cos^2 \frac{\pi x_0}{a} \sin^2 k\gamma z_0 \tag{5.9}$$

in Heaviside units. Since

$$1 \text{ Heaviside unit of resistance} = 4\pi \times 9 \times 10^{11} \text{ ohms}, \tag{5.10}$$

the radiation resistance of the short antenna is

$$R = 240\pi \frac{M^2 l^2}{\gamma ab} \cos^2 \frac{\pi x_0}{a} \sin^2 k\gamma z_0 \text{ ohms}, \tag{5.11}$$

the lengths being measured in centimeters.

For a finite antenna the surviving parts of the field are by (5.5)

$$E_y = \frac{2iJ}{c\gamma ab} \cos \frac{\pi x}{a} e^{ik\gamma z},$$

$$H_x = -\frac{2iJ}{cab} \cos \frac{\pi x}{a} e^{ik\gamma z}, \tag{5.12}$$

$$H_z = -\frac{2\pi J}{ck\gamma a^2 b} \sin \frac{\pi x}{a} e^{ik\gamma z},$$

where

$$J = \int I \cos \frac{\pi x_0}{a} \sin k\gamma z_0 \, dy_0 , \tag{5.13}$$

the integral being taken along the antenna. Accordingly the output is

$$F = \frac{J\bar{J}}{c\gamma ab} . \tag{5.14}$$

If I_0 is the current entering the antenna, the radiation resistance is

$$R = \frac{F}{\frac{1}{2}I_0\bar{I}_0} = \frac{2J\bar{J}}{c\gamma ab I_0\bar{I}_0} \text{ Heaviside units} \tag{5.15}$$

$$= 240\pi \frac{1}{\gamma ab} \frac{J\bar{J}}{I_0\bar{I}_0} \text{ ohms.}$$

When this is calculated in any particular case the current I_0 cancels out, and the result depends only on the shape and position of the antenna and the point at which it is fed.

6. Straight Antenna Parallel to the Shorter Side of the Cross Section

When the condition (5.1) is satisfied, the only radiation transmitted by the guide is the H_{10} wave. Any form of antenna will transmit this wave, except an antenna lying entirely in a plane perpendicular to the y-axis. But it is only the component of current parallel to the y-axis that contributes to the radiation, and the simplest plan is to use a straight antenna parallel to the y-axis.

Let us consider the arrangement shown in Fig. 1, where the length of the antenna is l and it is fed at the point where it enters the guide. Let I_0 be the current entering; then according to the usual rule of sine-distribution the current along the antenna is

$$I = I_0 \frac{\sin k(l - \frac{1}{2}b - y_0)}{\sin kl} . \tag{6.1}$$

Then (5.13) gives

$$J = I_0 \cos \frac{\pi x_0}{a} \sin k\gamma z_0 \int_{-\frac{1}{2}b}^{l-\frac{1}{2}b} \frac{\sin k(l - \frac{1}{2}b - y_0)}{\sin kl} \, dy_0 \tag{6.2}$$

$$= I_0 \cos \frac{\pi x_0}{a} \sin k\gamma z_0 \frac{1}{k} \tan \tfrac{1}{2}kl,$$

and so by (5.15)

$$R = 240\,\pi \frac{1}{k^2\gamma ab} \cos^2 \frac{\pi x_0}{a} \sin^2 k\gamma z_0 \tan^2 \tfrac{1}{2}kl \text{ ohms} \tag{6.3}$$

$$= \frac{60}{\pi} \frac{\lambda^2}{\gamma ab} \cos^2 \frac{\pi x_0}{a} \sin^2 \frac{2\pi\gamma z_0}{\lambda} \tan^2 \frac{\pi l}{\lambda} \text{ ohms.}$$

Let us now place the antenna centrally, so that $x_0 = 0$, and at the same time put $l = \lambda/4$; we get

$$R = \frac{60}{\pi} \frac{\lambda^2}{\gamma ab} \sin^2 \frac{2\pi\gamma z_0}{\lambda} \text{ ohms.} \tag{6.4}$$

Finally we take the numerical values given in (1.3) and obtain (1.4); the matching condition (1.5) follows at once.

It is clear from (6.3) that there are three different ways of matching the radiation resistance of the antenna to the impedance of a given line:

(i) By adjusting the position of the antenna relative to the central line, i.e., by changing x_0;

(ii) By adjusting the position of the plug, i.e., by changing z_0;

(iii) By adjusting the length of the antenna, i.e., by changing l.

Until such time as reactance has been calculated, it is not possible to decide which of these methods is the best.

Acknowledgment

We wish to thank Professors B. de F. Bayly and V. G. Smith of the Department of Electrical Engineering, University of Toronto, for useful advice during the accomplishment of this work.

APPENDIX A

We shall now evaluate the integral occurring in (4.13), namely

$$I(\zeta) = \int_\zeta^\infty e^{ikr} J_0 (C\sqrt{r^2 - \zeta^2})\, dr, \tag{A1}$$

where ζ, k, C are real and positive.

Differentiation with respect to ζ gives

$$\frac{dI}{d\zeta} = -e^{ik\zeta} - C\zeta \int_\zeta^\infty e^{ikr} \frac{J_0'(C\sqrt{r^2 - \zeta^2})}{\sqrt{r^2 - \zeta^2}}\, dr. \tag{A2}$$

We integrate by parts, writing $\sqrt{r^2 - \zeta^2} = R$;

$$C \int_\zeta^\infty e^{ikr} \frac{J_0'(CR)}{R}\, dr = \int_{r=\zeta}^\infty \frac{e^{ikr}}{r} J_0'(CR) d(CR) \tag{A3}$$

$$= \left[\frac{e^{ikr}}{r} J_0(CR)\right]_\zeta^\infty - \int_\zeta^\infty \frac{d}{dr}\left(\frac{e^{ikr}}{r}\right) J_0(CR) dr.$$

The first term here is $-e^{ik\zeta}/\zeta$. Hence (A2) becomes

$$\frac{1}{\zeta}\frac{dI}{d\zeta} = \int_\zeta^\infty \frac{d}{dr}\left(\frac{e^{ikr}}{r}\right) J_0(CR) dr. \tag{A4}$$

Comparing this with (A1), we observe that the application of the operator

$$\frac{1}{\zeta}\frac{d}{d\zeta}$$

to the integral has the effect of inserting the operator

$$\frac{d}{dr}\frac{1}{r}$$

in front of the first part of the integrand. The fact that that part is actually e^{ikr} is not involved in the argument, except in so far as it secures convergence. Thus, applying the same operator to (A4), we get

$$\frac{1}{\zeta}\frac{d}{d\zeta}\left(\frac{1}{\zeta}\frac{dI}{d\zeta}\right) = \int_{\zeta}^{\infty}\frac{d}{dr}\left\{\frac{1}{r}\frac{d}{dr}\left(\frac{e^{ikr}}{r}\right)\right\}J_0(CR)dr. \tag{A5}$$

Let us now go back to (A1) and put, by virtue of the Bessel differential equation,

$$J_0(CR) = -J_0''(CR) - J_0'(CR)/CR. \tag{A6}$$

Thus

$$I(\zeta) = -C^{-1}\int_{r=\zeta}^{\infty}e^{ikr}(R/r)J_0''(CR)d(CR) - C^{-1}\int_{\zeta}^{\infty}e^{ikr}J_0(CR)/R.dr. \tag{A7}$$

On integrating the first integral by parts, we obtain

$$\begin{aligned} I(\zeta) &= C^{-1}\int_{\zeta}^{\infty}\left\{\frac{d}{dr}\left(e^{ikr}\frac{R}{r}\right) - \frac{e^{ikr}}{R}\right\}J_0'(CR)dr \\ &= C^{-1}\int_{\zeta}^{\infty}e^{ikr}\left(\frac{ik}{r} - \frac{1}{r^2}\right)RJ_0'(CR)dr \\ &= C^{-2}\int_{r=\zeta}^{\infty}e^{ikr}\left(\frac{ik}{r^2} - \frac{1}{r^3}\right)R^2J_0'(CR)d(CR), \end{aligned} \tag{A8}$$

and further integration by parts gives

$$C^2I(\zeta) = \int_{\zeta}^{\infty}\frac{d}{dr}\left\{e^{ikr}\left(-\frac{ik}{r^2} + \frac{1}{r^3}\right)(r^2 - \zeta^2)\right\}J_0(CR)dr. \tag{A9}$$

This integral splits into two parts. The first is

$$\begin{aligned} &\int_{\zeta}^{\infty}\frac{d}{dr}\left\{e^{ikr}\left(-ik + \frac{1}{r}\right)\right\}J_0(CR)dr \\ &\quad = k^2\int_{\zeta}^{\infty}e^{ikr}J_0(CR)dr + \int_{\zeta}^{\infty}\frac{d}{dr}\left(\frac{e^{ikr}}{r}\right)J_0(CR)dr \\ &\quad = k^2I + \frac{1}{\zeta}\frac{dI}{d\zeta}, \end{aligned} \tag{A10}$$

by (A1) and (A4). The second part of the integral is

$$\text{(A11)} \qquad -\zeta^2 \int_\zeta^\infty \frac{d}{dr}\left\{e^{ikr}\left(-\frac{ik}{r^2}+\frac{1}{r^3}\right)\right\} J_0(CR)dr$$

$$= \zeta^2 \int_\zeta^\infty \frac{d}{dr}\left\{\frac{1}{r}\frac{d}{dr}\left(\frac{e^{ikr}}{r}\right)\right\} J_0(CR)dr$$

$$= \zeta \frac{d}{d\zeta}\left(\frac{1}{\zeta}\frac{dI}{d\zeta}\right),$$

by (A5). Thus (A9) becomes

$$\text{(A12)} \qquad C^2 I = k^2 I + \frac{1}{\zeta}\frac{dI}{d\zeta} + \zeta \frac{d}{d\zeta}\left(\frac{1}{\zeta}\frac{dI}{d\zeta}\right),$$

or

$$\text{(A13)} \qquad \frac{d^2 I}{d\zeta^2} + (k^2 - C^2)I = 0.$$

Hence

$$\text{(A14)} \qquad I(\zeta) = Ae^{i\zeta\sqrt{k^2-C^2}} + Be^{-i\zeta\sqrt{k^2-C^2}},$$

where A and B are independent of ζ. For definiteness, and without loss of generality, we interpret the radical in the following sense:

$$\text{(A15)} \qquad \begin{aligned} \sqrt{k^2 - C^2} &= \left|\sqrt{k^2 - C^2}\right| \quad \text{if} \quad k > C, \\ \sqrt{k^2 - C^2} &= i\left|\sqrt{k^2 - C^2}\right| \quad \text{if} \quad k < C. \end{aligned}$$

Now putting $\zeta = 0$ in (A1), we have a well known formula (Gray, Mathews, and Macrobert, Bessel Functions, p. 65)

$$\text{(A16)} \qquad I_{\zeta=0} = \int_0^\infty e^{ikr} J_0(Cr)\, dr$$

$$= \frac{i}{\sqrt{k^2 - C^2}},$$

the radical being interpreted as in (A15). Also by (A4)

$$\text{(A17)} \qquad \left(\frac{dI}{d\zeta}\right)_{\zeta=0} = \lim_{\zeta\to 0} \zeta \int_\zeta^\infty \frac{d}{dr}\left(\frac{e^{ikr}}{r}\right) J_0(C\sqrt{r^2 - \zeta^2})dr$$

$$= \lim_{\zeta\to 0} \zeta \int_\zeta^\infty \frac{d}{dr}\left(\frac{e^{ikr}}{r}\right) J_0(Cr)dr$$

$$= \lim_{\zeta\to 0} \zeta \left\{-\frac{e^{ik\zeta}}{\zeta} J_0(C\zeta) - C\int_\zeta^\infty \frac{e^{ikr}}{r} J_0'(Cr)dr\right\}.$$

Since the last integral has a finite limit for $\zeta \to 0$,

we get

$$\text{(A18)} \qquad \left(\frac{dI}{d\zeta}\right)_{\zeta=0} = -1.$$

The values (A16), (A18) enable us to determine A and B in (A14). We obtain

$$\text{(A19)} \qquad I(\zeta) = \int_{\zeta}^{\infty} e^{ikr} J_0(C\sqrt{r^2 - \zeta^2})dr = \frac{i}{\sqrt{k^2 - C^2}}\, e^{i\zeta\sqrt{k^2-C^2}},$$

the required result; the interpretation of the radicals on the right hand side is as in (A15), which agrees with (4.15).

We may remark that our result may be obtained formally by changing reals into imaginaries in a known formula; cf. Riemann–Weber, Differentialgleichungen der Physik, vol. 2(1927), p. 546. Such a procedure is not, of course, mathematically valid. We have not been able to find our result in the literature of Bessel functions.

APPENDIX B

The following treatment of the problem considered in this paper does not make use of the method of images, and offers interesting possibilities of generalization. In this, we find the steady-state solution corresponding to an assigned *volume* distribution of current throughout the wave guide, and deduce the field due to a current element (dipole) as a limiting case.

We use the same notation as before, except that it is now rather more convenient to take the origin at a corner of the plug-face than at its center. In Fig. 2, the origin must therefore be supposed transferred to the bottom left-hand corner, so that the equations of the faces of the guide are $x = 0$, $x = a$, $y = 0$, $y = b$.

Maxwell's equations for a volume current density $\vec{j}$ may be written, in Heaviside units,

$$\text{(B1)} \qquad \text{curl } \vec{E} = ik\vec{H}, \quad \text{curl } \vec{H} = -ik\vec{E} + \frac{1}{c}\vec{j}.$$

We shall, for the purposes of calculation, suppose that the wave guide extends to infinity in *both* directions along the z-axis, and eliminate the plug. We then assume that j_z, j_y are odd functions of z, and that j_x is an even function of z. It is then evident that the boundary condition (2.1) will be satisfied over the plug-face (as may be verified from the solution to be obtained).

We now make the following assumptions for the field components, which obviously satisfy the boundary conditions (2.1) on the faces of the guide:

$$
\begin{aligned}
E_x &= \sum_{m,n} A^{(1)}_{mn}(z)\cos(C_m x)\sin(D_n y),\\
E_y &= \sum_{m,n} A^{(2)}_{mn}(z)\sin(C_m x)\cos(D_n y),\\
E_z &= \sum_{m,n} A^{(3)}_{mn}(z)\sin(C_m x)\sin(D_n y),\\
H_x &= \sum_{m,n} B^{(1)}_{mn}(z)\sin(C_m x)\cos(D_n y),\\
H_y &= \sum_{m,n} B^{(2)}_{mn}(z)\cos(C_m x)\sin(D_n y),\\
H_z &= \sum_{m,n} B^{(3)}_{mn}(z)\cos(C_m x)\cos(D_n y),
\end{aligned}
\tag{B2}
$$

where $C_m = m\pi/a$, $D_n = n\pi/b$, the summations running from zero to infinity. For the components of $\vec{j}$ we now assume

$$
\begin{aligned}
j_x &= \sum_{m,n} j^{(1)}_{mn}(z)\cos(C_m x)\sin(D_n y),\\
j_y &= \sum_{m,n} j^{(2)}_{mn}(z)\sin(C_m x)\cos(D_n y),\\
j_z &= \sum_{m,n} j^{(3)}_{mn}(z)\sin(C_m x)\sin(D_n y).
\end{aligned}
\tag{B3}
$$

Substituting (B2) and (B3) in the Maxwell equations (B1), we have six linear equations of the first order to determine the six functions $A^{(1)}_{mn}(z), \ldots, B^{(3)}_{mn}(z)$ in terms of the functions $j^{(1)}_{mn}, j^{(2)}_{mn}, j^{(3)}_{mn}$. The solution of these equations is facilitated by noting that from (B1) follows

$$
(\nabla^2 + k^2)\vec{H} = -\frac{1}{c}\,\mathrm{curl}\,\vec{j}. \tag{B4}
$$

Taking say, the x-component of this equation, and using (B2), (B3), we find

$$
\frac{d^2B^{(1)}_{mn}}{dz^2} + u^2_{mn}B^{(1)}_{mn} = \frac{1}{c}\left(\frac{dj^{(2)}_{mn}}{dz} - D_n j^{(3)}_{mn}\right), \tag{B5}
$$

where

$$
u^2_{mn} = k^2 - C^2_m - D^2_n\,. \tag{B6}
$$

For definiteness, we suppose the positive root of (B6) is taken for u_{mn} if $u^2_{mn} > 0$ and the positive-imaginary root if $u^2_{mn} < 0$. The solution of (B5) which represents outgoing waves, or damped waves, for large positive or negative z is readily found, by the method of variation of constants, to be

$$
B^{(1)}_{mn} = \frac{e^{iu_{mn}z}}{2icu_{mn}}\int_{-\infty}^{z} f^{(1)}_{mn}(z)dz + \frac{e^{-iu_{mn}z}}{2icu_{mn}}\int_{z}^{\infty} \bar{f}^{(1)}_{mn}(z)dz, \tag{B7}
$$

where

$$
f^{(1)}_{mn} = e^{-iu_{mn}z}\,(iu_{mn}j^{(2)}_{mn} - D_n j^{(3)}_{mn}),
$$

and the bar denotes, here and in what follows, the complex conjugate (the functions $j^{(1,2,3)}_{mn}$ being treated as *real*). This gives outgoing waves at infinity if u_{mn} is real, and damped waves if u_{mn} is positive imaginary.

In a similar manner, the y- and z-components of (B4) give us $B^{(2)}_{mn}$ and $B^{(3)}_{mn}$, and the second of (B1) then gives us $A^{(1)}_{mn}$, $A^{(2)}_{mn}$, $A^{(3)}_{mn}$. We thus find:

$$B^{(\alpha)}_{mn} = \frac{e^{iu_{mn}z}}{2icu_{mn}} \int_{-\infty}^{z} f^{(\alpha)}_{mn}(z)dz + \frac{e^{-iu_{mn}z}}{2icu_{mn}} \int_{z}^{\infty} \bar{f}^{(\alpha)}_{mn}(z)dz, \ (\alpha = 2,3),$$

(B8)
$$A^{(\beta)}_{mn} = \frac{e^{iu_{mn}z}}{2kcu_{mn}} \int_{-\infty}^{z} g^{(\beta)}_{mn}(z)dz + \frac{e^{-iu_{mn}z}}{2kcu_{mn}} \int_{z}^{\infty} \bar{g}^{(\beta)}_{mn}(z)dz - \frac{i}{kc} j^{(3)}_{mn}\, \delta_{\beta 3}$$

$$(\beta = 1,2,3;\ \delta_{\beta 3} = 0 \text{ unless } \beta = 3,\ \delta_{33} = 1),$$

where

$$f^{(2)}_{mn} = e^{-iu_{mn}z}\ (C_m j^{(3)}_{mn} - iu_{mn} j^{(1)}_{mn}),$$
$$f^{(3)}_{mn} = e^{-iu_{mn}z}\ (D_n j^{(1)}_{mn} - C_m j^{(2)}_{mn}),$$
$$g^{(1)}_{mn} = e^{-iu_{mn}z}\ [(C_m^2 - k^2) j^{(1)}_{mn} + C_m D_n j^{(2)}_{mn} - iC_m u_{mn} j^{(3)}_{mn}],$$
$$g^{(2)}_{mn} = e^{-iu_{mn}z}\ [C_m D_n j^{(1)}_{mn} + (D_n^2 - k^2) j^{(2)}_{mn} - iD_n u_{mn} j^{(3)}_{mn}],$$
$$g^{(3)}_{mn} = e^{-iu_{mn}z}\ [iC_m u_{mn} j^{(1)}_{mn} + iD_n u_{mn} j^{(2)}_{mn} + (u^{(2)}_{mn} - k^2)\, j^{(3)}_{mn}].$$

In deriving (B7), (B8), it has been assumed that $\vec{j}$, and hence the functions $j^{(1,2,3)}_{mn}$, tends to zero at infinity sufficiently rapidly, and also that j_z, j_y, and hence $j^{(1,2)}_{mn}$, vanish for $z = 0$, so that these functions are continuous for $z = 0$ If this latter condition is not satisfied, other terms appear; but we can evidently suppose it satisfied, since we are going to proceed to the limiting case of a current *element*.

(B2), together with (B7) and (B8), now gives a solution of the equations (B1), as may be verified by direct substitution, and all conditions are satisfied.

Suppose now that the guide transmits only the H_{10} wave; then from (B6) we see that all the u_{mn} are pure imaginary except u_{10}. From what has been said above, it then follows that all the functions $A^{(1)}_{mn}, \ldots, B^{(3)}_{mn}$ represent damped waves except those with $m = 1, n = 0$. Hence, from (B2), (B7), (B8), and since the $j^{(\beta)}_{mn} \to 0$ as $z \to \infty$, we find for the field, for z large and positive

$$E_y = \frac{-k}{2cu_{10}} e^{iu_{10}z} \int_{-\infty}^{\infty} j^{(2)}_{10} e^{-iu_{10}z}\, dz \,.\, \sin \frac{\pi x}{a},$$

(B9)
$$H_x = -\frac{u_{10}}{k} E_y,$$

$$H_z = \frac{\pi i}{2acu_{10}} e^{iu_{10}z} \int_{-\infty}^{\infty} j^{(2)}_{10} e^{-iu_{10}z}\, dz \,.\, \cos \frac{\pi x}{a},$$

$$E_x = E_z = H_y = 0.$$

This represents an H_{10} wave. From (B3) we have

(B10)
$$j^{(2)}_{10}(z) = \frac{2}{ab} \int_0^a dx \int_0^b dy.\ \ j_y(x, y, z) \sin \frac{\pi x}{a}.$$

To obtain the field due to a current element of components ($ILds_0$, $IMds_0$, $INds_0$) situated at the point (x_0, y_0, z_0), we now suppose that $\vec{j}$ tends to zero everywhere except in the immediate neighborhood of the points (x_0, y_0, z_0) and (x_0, y_0, $-z_0$). At these points $\vec{j}$ is to tend to infinity in such a way that the total components of current in any small region surrounding (x_0, y_0, z_0) are ($ILds_0$, $IMds_0$, $INds_0$), and the total components of current in any small region surrounding (x_0, y_0, $-z_0$) are ($-ILds_0$, $-IMds_0$, $+INds_0$). The introduction of the singularity at (x_0, y_0, $-z_0$) is, of course, necessary in order to preserve the odd or even character of the components of $\vec{j}$. This case can be represented symbolically in terms of δ-functions by putting, in our final results,

$$\text{(B11)} \qquad \begin{cases} j_x = ILds_0\,\delta(x - x_0)\delta(y - y_0)\,[\delta(z - z_0) - \delta(z + z_0)], \\ j_y = IMds_0\delta(x - x_0)\delta(y - y_0)\,[\delta(z - z_0) - \delta(z + z_0)], \\ j_z = INds_0\,\delta(x - x_0)\delta(y - y_0)\,[\delta(z - z_0) + \delta(z + z_0)]. \end{cases}$$

Using (B_{10}), we then find, for this case,

$$\text{(B12)} \qquad \int_{-\infty}^{\infty} j_{10}^{(2)}\, e^{-iu_{10}z}\, dz = \frac{-4i}{ab} \sin\frac{\pi x_0}{a} \sin\,(u_{10}z_0)\, IM\, ds_0\,.$$

Inserting this in (B9), and putting $u_{10} = \gamma k$, where γ is as defined in (5.3), we finally have for the field at a large distance down the guide

$$\text{(B13)} \qquad \begin{cases} E_y = \dfrac{2iIMds_0}{\gamma abc} \sin\dfrac{\pi x_0}{a} \sin\,\gamma k z_0 \sin\dfrac{\pi x}{a}\, e^{i\gamma kz}\,, \\ H_x = -\gamma E_y\,, \\ H_z = \dfrac{2\pi IMds_0}{\gamma ka^2bc} \sin\dfrac{\pi x_0}{a} \sin\,\gamma k z_0 \sin\dfrac{\pi x}{a}\, e^{i\gamma kz}\,. \end{cases}$$

Comparing with (5.5) and (5.7) and allowing for the change of origin, we see that this field is identical with that given by the method of images. The rest of the calculation now proceeds as before.

It may be remarked that use of (B11) in the general formulae (B2), (B7), (B8) gives the field at *any* point in the guide, expressed as a double Fourier series (except in the plane $z = z_0$, where the representation obviously fails).

PART II. A GENERAL METHOD FOR CALCULATING THE IMPEDANCE OF AN ANTENNA IN A WAVE GUIDE OF ARBITRARY CROSS SECTION

BY A. F. STEVENSON

1. Introduction

In this part, it is shown that the problem of finding the radiation resistance and reactance of an antenna of arbitrary shape in a wave guide of arbitrary cross section can be solved if the current distribution in the antenna is known, and if the eigenfunctions which determine the free propagation in the guide

can be found. In the case where only a single E- or H-wave is transmitted, a simple closed expression for the resistance results. The reactance, on the other hand, requires the summation of an infinite series, the calculation of which would be somewhat tedious, though quite feasible, in any given case. The reactance is discussed in Section 4. Incidentally, the field at any point in the guide is obtained in the course of the work.

The method used is a generalization of one of the three methods previously given for calculating the field due to a dipole in a rectangular wave guide in Part I. Its great advantage, as compared with previous special methods for rectangular and circular guides, is its generality and comparative simplicity.

In a recent report, Chu (2) has given formulae for the resistance of antennae in rectangular and circular guides in particular cases, and has stated that the method used is applicable to guides of any cross section. He gives no indication of the method, however, beyond stating that it involves the use of orthogonal functions. Actually, some of Chu's formulae are not correct.

2. Calculation of the Field

We consider a cyclindrical wave guide closed by a plug, both guide and plug being perfectly conducting. We take origin in the plane of the plug-face, with the z-axis along the length of the guide (Fig. 1). We use Heaviside

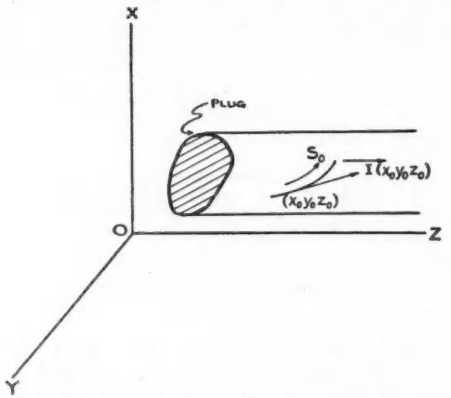

FIG. 1. *Wave guide with antenna of arbitrary shape and current distribution.*

units, and suppose a steady state in which all quantities vary with the time according to the factor $e^{-i\omega t}$, this factor being omitted (the electric field is thus the real part of $\vec{E}e^{-i\omega t}$, etc.).

We first recall the solutions which give the *free* propagation in a guide extending to infinity in both directions. For E-waves, we have to solve the eigenvalue problem

$$(1) \qquad \begin{cases} \dfrac{\partial^2 \psi}{\partial x^2} + \dfrac{\partial^2 \psi}{\partial y^2} + \mu^2 \psi = 0 \quad \text{inside } S, \\ \psi = 0 \text{ on } C, \end{cases}$$

where S denotes the interior of the cross section of the guide, and C denotes the boundary of S (Fig. 2). Let the eigenvalues of this problem, arranged

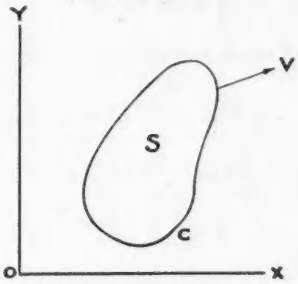

FIG. 2. *Cross section of guide.*

in ascending order of magnitude, and the corresponding orthogonal eigenfunctions, be

$$\mu = \mu_1, \mu_2, \ldots,$$
$$\psi = \psi_1, \psi_2, \ldots.$$

We suppose the eigenfunctions normalized so that

$$\int_S \psi_n^2 \, dx \, dy = 1.$$

The case of degeneracy can be included by supposing that some of the μ's may be equal. The field for an E_n-wave, propagated (or damped) in the positive z-direction, is then given, apart from an arbitrary constant factor, by

$$(2) \quad \begin{cases} E_x = f_n'(z) \dfrac{\partial \psi_n}{\partial x}, \quad E_y = f_n'(z) \dfrac{\partial \psi_n}{\partial y}, \quad E_z = \mu_n^2 f_n(z) \psi_n, \\ H_x = -ikf_n(z) \dfrac{\partial \psi_n}{\partial y}, \quad H_y = ikf_n(z) \dfrac{\partial \psi_n}{\partial x}, \quad H_z = 0, \end{cases}$$

where

$$k = \omega/c = 2\pi/\lambda, \quad f_n(z) = e^{iu_n z},$$

and

$$(2') \qquad u_n = \sqrt{k^2 - \mu_n^2}.$$

In (2'), the positive square-root is to be taken if u_n is real (propagation), and the positive-imaginary if u_n is pure imaginary (damping).

For the H-waves, we have to solve the eigenvalue problem

$$(3) \quad \begin{cases} \dfrac{\partial^2 \Psi}{\partial x^2} + \dfrac{\partial^2 \Psi}{\partial y^2} + M^2 \Psi = 0 \quad \text{inside } S, \\ \dfrac{\partial \Psi}{\partial \nu} = 0 \text{ on } C, \end{cases}$$

where ν denotes the outward normal to C (Fig. 2). Let the eigenvalues, arranged in ascending order of magnitude, and corresponding eigenfunctions, be

$$M = M_1, M_2, \ldots\ldots,$$
$$\Psi = \Psi_1, \Psi_2, \ldots\ldots.$$

As before, we suppose the eigenfunctions normalized so that

$$\int_S \Psi_n^2 \, dx \, dy = 1 ,$$

and degeneracy can be included as before. Then the field for an H-wave is given by

$$(4) \quad \begin{cases} E_x = ik F_n(z) \dfrac{\partial \Psi_n}{\partial y}, \quad E_y = -ik F_n(z) \dfrac{\partial \Psi_n}{\partial x}, \quad E_z = 0 \\ H_x = F_n'(z) \dfrac{\partial \Psi_n}{\partial x}, \quad H_y = F_n'(z) \dfrac{\partial \Psi_n}{\partial y}, \quad H_z = M_n^2 F_n(z) \Psi_n , \end{cases}$$

where

$$F_n(z) = e^{iU_n z} ,$$

and

$$(5) \qquad U_n = \sqrt{k^2 - M_n^2} ,$$

the same convention as to the sign of the square root being used in (5) as in (2′).

We now consider the problem of finding the field due to a current element in the wave guide. For this purpose, we suppose the guide extends to infinity in *both* directions, and eliminate the plug. We then suppose that there is an assigned volume distribution of current, of density $\vec{j}$, throughout the guide and find the field due to it. We then find the field due to a current element by proceeding to the limiting case where $\vec{j}$ vanishes except at the element and its electrical image in the plug-face.

The Maxwell equations for the case considered are

$$(6) \qquad ik \vec{H} = \text{curl } \vec{E}, \quad ik \vec{E} = -\text{curl } \vec{H} + \frac{1}{c} \vec{j} .$$

We suppose that $\vec{j}$ is continuous and vanishes at infinity sufficiently rapidly. Bearing (2) and (4) in mind, we now assume for the field a superposition of E- and H-waves of the form

$$(7) \quad \begin{cases} E_x = \sum_n \left[a_n(z) \dfrac{\partial \psi_n}{\partial x} + ik A_n(z) \dfrac{\partial \Psi_n}{\partial y} \right] , \\ E_y = \sum_n \left[a_n(z) \dfrac{\partial \psi_n}{\partial y} - ik A_n(z) \dfrac{\partial \Psi_n}{\partial x} \right] , \\ E_z = \sum_n b_n(z) \psi_n , \\ H_x = \sum_n \left[-ik c_n(z) \dfrac{\partial \psi_n}{\partial y} + C_n(z) \dfrac{\partial \Psi_n}{\partial x} \right] , \\ H_y = \sum_n \left[ik c_n(z) \dfrac{\partial \psi_n}{\partial x} + C_n(z) \dfrac{\partial \Psi_n}{\partial y} \right] , \\ H_z = \sum_n D_n(z) \Psi_n , \end{cases}$$

where the summations run from 1 to ∞, and where $a_n(z)$, ---, $D_n(z)$ are six functions to be determined. The field (7) satisfies the boundary conditions of the problem, and it can be proved that the most general such field can be expressed in this way.

For the components of $\vec{j}$, we assume analogously

$$(8)\qquad \begin{cases} \frac{1}{c} j_x = \sum_n \left[p_n(z) \frac{\partial \psi_n}{\partial x} + ik\, q_n(z) \frac{\partial \Psi_n}{\partial y} \right], \\ \frac{1}{c} j_y = \sum_n \left[p_n(z) \frac{\partial \psi_n}{\partial y} - ik\, q_n(z) \frac{\partial \Psi_n}{\partial x} \right], \\ \frac{1}{c} j_z = \sum_n r_n(z)\, \psi_n . \end{cases}$$

We now note that by differentiating the first two of (8) with respect to x and y, and combining, and using the differential equations (1), (3) satisfied by the functions ψ_n, Ψ_n, we can replace (8) by

$$(8')\qquad \begin{cases} \frac{1}{c} j_1 = -\sum_n \mu_n^2\, p_n(z)\, \psi_n , \\ \frac{1}{c} j_2 = -ik \sum_n M_n^2\, q_n(z)\, \Psi_n , \\ \frac{1}{c} j_z = \sum_n r_n(z)\, \psi_n , \end{cases}$$

where

$$j_1 = \frac{\partial j_x}{\partial x} + \frac{\partial j_y}{\partial y}, \quad j_2 = \frac{\partial j_x}{\partial y} - \frac{\partial j_y}{\partial x}.$$

We shall refer to (8′) as the transform of (8). In a similar way (by differentiation and combination of the x- and y-component equations), we construct the transforms of (7) and (6).

We now substitute the transforms of (7) and (8) in the transform of (6). We then obtain six equations, in each of which only one of the sets of functions ψ_1, ψ_2, --- or Ψ_1, Ψ_2, --- occurs. We can then equate coefficients of each ψ_n or Ψ_n on both sides of the equations. We obtain in this manner three differential equations of the first order for the functions a_n, b_n, c_n and three for the functions A_n, C_n, D_n, the functions p_n, q_n, r_n being regarded as known. These differential equations are quite simple and are easily solved by the method of variation of constants, the arbitrary constants in the solution being determined so that only outgoing, or damped, waves exist at $z = \pm\infty$. We thus obtain

$$(9)\qquad \begin{cases} a_n(z) = c_n'(z) - \frac{i}{k} p_n(z), \quad b_n(z) = \mu_n^2\, c_n(z) - \frac{i}{k} r_n(z) , \\ c_n(z) = \frac{e^{iu_n z}}{2k\, u_n} \int_{-\infty}^{z} e^{-iu_n z} (iu_n p_n - r_n) dz - \frac{e^{-iu_n z}}{2k\, u_n} \times \\ \qquad\qquad \int_{z}^{\infty} e^{iu_n z} (iu_n p_n + r_n) dz , \\ A_n(z) = \frac{1}{M_n^2} D_n(z), \quad C_n(z) = \frac{1}{M_n^2} D_n'(z) , \\ D_n(z) = -\frac{k\, M_n^2}{2U_n} e^{iU_n z} \int_{-\infty}^{z} e^{-iU_n z} q_n\, dz - \frac{k\, M_n^2}{2U_n} e^{-iU_n z} \int_{z}^{\infty} e^{iU_n z} q_n\, dz . \end{cases}$$

The constants u_n, U_n are those defined in (2′), (5) with the same convention as to the sign of the square root.

The functions p_n, q_n, r_n are found in terms of the components of $\vec{j}$ by applying to (8′) the usual process for determining the coefficients in expansions in orthogonal normalized functions. We thus have the field due to any continuous distribution of current $\vec{j}$. We pass to the case of a current element of strength $\vec{I}ds_0$ situated at the point (x_0, y_0, z_0), in the presence of the plug, by putting, in accordance with the principle outlined previously,

$$(10)\qquad \begin{cases} j_x = I_x\, ds_0\, \delta(x-x_0)\, \delta(y-y_0)\, [\delta(z-z_0) - \delta(z+z_0)], \\ j_y = I_y\, ds_0\, \delta(x-x_0)\, \delta(y-y_0)\, [\delta(z-z_0) - \delta(z+z_0)], \\ j_z = I_z\, ds_0\, \delta(x-x_0)\, \delta(y-y_0)\, [\delta(z-z_0) + \delta(z+z_0)], \end{cases}$$

the notation of "delta-functions" being used. Finding first the functions p_n, q_n, r_n by means of (8′), substituting in (9), and then using (10), we thus find, for $z > 0$ and $z \neq z_0$,

$$(11)\qquad \begin{cases} a_n(z) = \dfrac{iu_n}{kc\mu_n^2} P_n(x_0, y_0) f_1(u_n, z, z_0) - \dfrac{i}{kc} R_n(x_0, y_0) f_2(u_n, z, z_0), \\ b_n(z) = -\dfrac{i}{kc} P_n(x_0, y_0) f_3(u_n, z, z_0) - \dfrac{\mu_n^2}{kcu_n} R_n(x_0, y_0) f_4(u_n, z, z_0), \\ c_n(z) = \dfrac{1}{\mu_n^2} b_n(z), \\ A_n(z) = \dfrac{1}{cU_nM_n^2} Q_n(x_0, y_0) f_1(U_n, z, z_0), \\ C_n(z) = \dfrac{1}{cM_n^2} Q_n(x_0, y_0) f_3(U_n, z, z_0), \\ D_n(z) = M_n^2 A_n(z), \end{cases}$$

where

$$(12)\qquad \begin{cases} P_n(x_0, y_0) = \left[I_x \dfrac{\partial \psi_n(x_0, y_0)}{\partial x_0} + I_y \dfrac{\partial \psi_n(x_0, y_0)}{\partial y_0} \right] ds_0, \\ Q_n(x_0, y_0) = \left[I_x \dfrac{\partial \Psi_n(x_0, y_0)}{\partial y_0} - I_y \dfrac{\partial \Psi_n(x_0, y_0)}{\partial x_0} \right] ds_0, \\ R_n(x_0, y_0) = I_z \psi_n(x_0, y_0) ds_0, \end{cases}$$

and

$$(13)\qquad \begin{cases} f_1(u, z, z_0) = e^{iuz} \sin uz_0, z > z_0, \\ \qquad\qquad = e^{iuz_0} \sin uz, z < z_0, \\ f_2(u, z, z_0) = e^{iuz} \cos uz_0, z > z_0, \\ \qquad\qquad = ie^{iuz_0} \sin uz, z < z_0, \\ f_3(u, z, z_0) = ie^{iuz} \sin uz_0, z > z_0, \\ \qquad\qquad = e^{iuz_0} \cos uz, z < z_0, \\ f_4(u, z, z_0) = e^{iuz} \cos uz_0, z > z_0, \\ \qquad\qquad = e^{iuz_0} \cos uz, z < z_0. \end{cases}$$

Equations (7), (11), (12), (13) now give the field at any point in the guide due to a current element $\vec{I}\,ds_0$ at (x_0, y_0, z_0) in the presence of the plug. It will be observed that the functions f_2, f_3 are discontinuous at $z = z_0$. This is due to the nature of the field in the immediate neighborhood of the element; *in* the plane $z = z_0$, the series (7) are not valid in general. But this is of no practical consequence.

To find the field due to a thin antenna with a given distribution of current of linear density $\vec{I}(x_0, y_0, z_0)$ (Fig. 1), we have merely to write $\vec{I} = \vec{I}(x_0, y_0, z_0)$ and integrate the expressions for $a_n(z)$, ---, $D_n(z)$ given by (11), (12), (13) with respect to s_0 along the antenna, ds_0 being an element of length. We can draw the following two general conclusions:

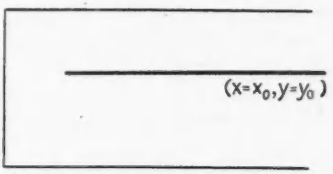

FIG. 3. *Longitudinal antenna.*

(1) A longitudinal antenna (Fig. 3) can only generate E-waves, whereas a transverse antenna (Fig. 4) can generate both E- and H-waves. This fact is already doubtless well known to experimental workers.

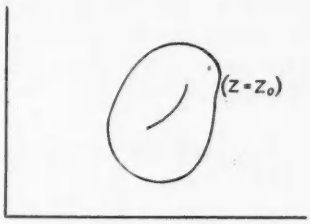

FIG. 4. *Transverse antenna.*

(2) When a transverse antenna is used for generating an E_n-wave, the effect is a maximum, other things being equal, when the antenna coincides with one of the orthogonal trajectories of the curves ψ_n = constant. The effect is zero when the antenna coincides with one of the curves ψ_n = constant.

(3) When a transverse antenna is used for generating an H_n-wave, the effect is a maximum when the antenna coincides with one of the curves Ψ_n = constant. The effect is zero when the antenna coincides with one of the orthogonal trajectories of the curves Ψ_n = constant.

3. The Formulae for Radiation Resistance

To find the resistance, we need merely calculate the mean flux of energy at $z = +\infty$ by Poynting's theorem, and equate this to the mean rate of working of the applied voltage. The method is sufficiently well known, and we omit the details of calculation. In considering the field at infinity, only a few terms (usually only one) of the infinite series in (7) survive, all the other terms being damped out. We consider the following two cases:

(1) The dimensions of the guide (and manner of excitation) are such that only the E_n-wave is generated. We find

$$(14) \qquad (R)_{\text{ohms}} = 120\pi\alpha_n \left| \frac{1}{k}\int\left(I_x \frac{\partial\psi_n}{\partial x} + I_y \frac{\partial\psi_n}{\partial y}\right) \sin(u_n z)\, ds \right.$$
$$\left. - \frac{1}{\alpha_n}\int I_z\psi_n \cos(u_n z)\, ds \right|^2 \frac{1}{|I_0|^2},$$

where $\psi_n = \psi_n(x, y)$, I_0 is the current at the feeding point, and

$$\alpha_n = \frac{ku_n}{\mu_n^2} = \frac{u_n/k}{1 - (u_n/k)^2}.$$

We note that $u_n = 2\pi/\lambda'$, where λ' is the wave length *in the guide*, so that $u_n/k = \lambda/\lambda'$. The integral in (14) is extended over the length of the antenna (we have dropped the suffix 0). We recall that ψ_n is a *normalized* eigenfunction (for definition of μ_n, ψ_n see beginning of Section 2). If μ_n is a degenerate eigenvalue of (1), (14) must be replaced by the sum of such expressions for each independent and orthogonal eigenfunction ψ_n.

(2) The dimensions of the guide (and manner of excitation) are such that only the H_n-wave is generated. We find

$$(15) \quad (R)_{\text{ohms}} = 120\pi\beta_n \left| \frac{1}{k}\int\left(I_z \frac{\partial\Psi_n}{\partial y} - I_y \frac{\partial\Psi_n}{\partial x}\right) \sin(U_n z)\, ds \right|^2 \cdot \frac{1}{|I_0|^2},$$

where

$$\beta_n = \frac{k^3}{U_n M_n^2} = \frac{k/U_n}{1 - (U_n/k)^2}.$$

The same remarks apply to the case of degeneracy as in (14). (For definition of M_n, U_n, Ψ_n see beginning of Section 2.)

We conclude that for a longitudinal antenna lying along the line $x = x_0$, $y = y_0$, and generating an E_n-wave, R varies as $[\psi_n(x_0, y_0)]^2$; while for a transverse antenna lying at a distance z_0 from the plug, and generating either an E_n- or an H_n-wave, R varies as $\sin^2 \frac{2\pi z_0}{\lambda'}$, where λ' is the wave length in the guide. These results are true, of course, for a guide of *any* cross section, and for any assumed current distribution.

4. Calculation of Reactance

The e.m.f. method of calculating reactance uses the formula (3)

$$R - iX = -\frac{1}{I_0^2}\int I(s)E(s)ds,^* \tag{16}$$

where the integral is extended along the antenna, and $E(s)$ denotes the electric field along the surface of the antenna calculated for a current concentrated on the axis of the antenna. This procedure can be justified when the gap is along the length of the antenna, but it seems rather questionable to the writer whether it holds when the gap is *across* the antenna, as is usually the case in a wave guide (for the *resistance*, which can be calculated by means of the *distant* field, the procedure is less open to doubt). Assuming, however, that (16) holds, the reactance can evidently be calculated by means of the formulae in Section 2 giving the field. But as there will now be an infinite number of terms surviving in the series (7), the result will be expressed by means of an infinite series. Formula (16) assumes that the field is symmetrical about the axis of the antenna. This is evidently approximately the case if the radius of the antenna is small compared with its distance from the walls of the guide (except at the point of entry), and if it enters the guide normally (taking account of the image effect in the tangent plane). Otherwise an *average* of $E(s)$ over the cross section of the antenna must be used in (16).

We shall not give an explicit formula for reactance in the general case. Without detailed calculation, however, we can draw a rather interesting conclusion regarding the way the reactance of a transverse antenna, generating only an E_n- or H_n-wave, varies with the distance of the antenna from the plug, other factors being kept constant. Let the axis of the antenna be any curve lying in the plane $z = z_0$, and let us take the integral in (16) along a parallel curve lying in the plane $z = z_0 + r$, where r is the radius of the antenna. Then use of (7), (11), (13) shows that the integral in (16) is, in its dependence on z_0, r, of the form

$$\sum_m [A_m e^{iu_m(2z_0+r)} + B_m e^{iu_m r} + C_m e^{iU_m(2z_0+r)} + D_m e^{iU_m r}], \tag{17}$$

where $A_m, \ldots, D_m$ are independent of z_0, r. In the first and third terms of the summand in (17), r can be neglected.

Suppose now, for definiteness, that only the E_n-wave is generated. Then u_n is real, but all the other u's and *all* the U's (except possibly those for which the corresponding coefficient $A_m, \ldots, D_m$ is zero) are pure imaginary. Then (17) can be written

$$A_n e^{2iu_n z_0} + \sum_{m \neq n} A_m e^{-2|u_m|z_0} + \sum_m C_m e^{-2|U_m|z_0} + D, \tag{18}$$

where $A_n, \ldots, D$ are independent of z_0. The 2nd and 3rd terms in (18) will evidently be small compared with the other terms unless z_0 is small,

* *Formula (16) is a little different from that given by Labus, but is more compact and is easily deducible from his formula. The negative sign appears here before iX on account of the time factor being taken as* $e^{-i\omega t}$.

i.e., unless the antenna is near the plug (when the above method would, in any case, break down). Excluding this case, therefore, we see from (16) that X is approximately of the form

$$X = C_1 \cos (2u_n z_0 + \epsilon) + C_2 ,$$

where C_1 , C_2 , ϵ are independent of z_0 . An exactly similar result is obtained if only the H_n-wave is generated, with U_n in place of u_n .

Hence if the distance from the plug to the antenna varies, other factors being kept constant, the reactance should vary approximately sinusoidally (except near the plug), the period being half the wave length in the guide. This is the same behavior as in the case of the resistance (see end of Section 3), though the phase will of course be different. Some experiments of Chipman and Burr (1) support this conclusion for the case of a straight transverse antenna in a rectangular guide.

References

1. Chipman, R. A. and Burr, A. C. Queen's University, Department of Physics. Rept. No. 2. *Revised* March 25, 1942.
2. Chu, L. J. Massachusetts Institute of Technology, Radiation Laboratory. Rept. No. 43–4.
3. Labus, J. Hochfrequenztech. u. Elektroakust. 41 : 17. 1933.

PART III. THE RESISTANCES OF ANTENNAE OF VARIOUS SHAPES AND POSITIONS IN RECTANGULAR AND CIRCULAR WAVE GUIDES

By W. Z. Chien

1. Introduction and Summary

The radiation resistance of an antenna inside a wave guide is defined as the ratio of the total power radiated to the mean square value of the feeding current. If the current distribution along the antenna is given, the first step is to calculate the field at the far end of the guide. When this has been done, the calculation of the total power radiated is just a straightforward integration.

In the following section, we give a list of formulae for the resistance of various antennae inside rectangular and circular wave guides. These formulae are divided into four general cases according to the cross section of the wave guide and the type of wave transmitted. For each general case, we have a general formula for the resistance in terms of integrals depending on the shape and position of the antenna and its current distribution. The general formula (1), quoted from Part I, gives the resistance of an arbitrary antenna in a rectangular wave guide transmitting the H_{10} wave only. The formulae (2), (3), (4) give the resistance of various antennae in circular wave guides. These formulae are calculated from the field distributions given by H. Buchholz (1). The purpose of keeping these general formulae in the list is that they offer a simple means of calculating those special cases missing in this list without knowing the actual field distribution. It should be noted that these formulae are but special forms of two more general formulae, which have been given by A. F. Stevenson in Part II.

2. Results

The Resistance of an Arbitrary Antenna in a Rectangular Wave Guide Transmitting only the H_{10} Wave

General formula:

(1) $$R = \frac{240\pi\varphi^2}{ab\gamma} \text{ ohms,}$$

where

(1a) $$\varphi = \int \frac{I}{I_0} \sin\left(\frac{2\pi}{\lambda}\gamma z_0\right) \cos\left(\frac{\pi}{a}x_0\right) dy_0 \text{ (taken along the antenna).}$$

The conditions for transmitting the H_{10} wave only in a rectangular wave guide are in general:

(1b) $$\frac{1}{a} < \frac{2}{\lambda} < \frac{1}{b}, \qquad \frac{1}{a} < \frac{2}{\lambda} < \frac{2}{a}.$$

The notation is as follows:

x, y, z = the rectangular co-ordinate system, origin at the center of the plug face,

a = the longer side of the guide along the x-axis.

b = the shorter side of the guide along the y-axis,

λ = the wave length,

$\gamma = \sqrt{1 - \left(\frac{\lambda}{2a}\right)^2}$, $\frac{2\pi}{\lambda}\gamma$ = the phase constant of the H_{10} wave.

x_0, y_0, z_0 = the co-ordinates of a point on the antenna,

I = the current along the antenna,

I_0 = current at the feeding point of the antenna.

Special cases:

1*a*. A straight antenna of length l parallel to the y-axis, running from $y = -b/2$ to $y = l - b/2$ (Fig. 1). Assuming sinusoidal current distribution,

$$R = \frac{60\lambda^2}{\pi ab\gamma}\left[\cos\left(\frac{\pi}{a}x_0\right)\sin\left(\frac{2\pi\gamma}{\lambda}z_0\right)\tan\left(\frac{\pi l}{\lambda}\right)\right]^2 \text{ ohms,}$$

where x_0 = the off-center distance from the y-axis to the antenna,

z_0 = the distance from the plug to the antenna.

1*b*. The same antenna as in case 1*a*. Assuming uniform current distribution,

$$R = \frac{240l^2}{ab\gamma}\left[\cos\left(\frac{\pi}{a}x_0\right)\sin\left(\frac{2\pi\gamma}{\lambda}z_0\right)\right]^2 \text{ ohms.}$$

1*c*. A circular loop, the axis of which is parallel to the x-axis, radius r_0, center at (x_0, y_0, z_0) (see Fig. 2).

Assuming uniform current distribution,

$$R = \frac{960\pi^3 r_0^2}{ab\gamma}\left[\cos\left(\frac{\pi}{a}x_0\right)\cos\left(\frac{2\pi\gamma}{\lambda}z_0\right)J_1\left(\frac{2\pi\gamma}{\lambda}r_0\right)\right]^2 \text{ ohms.}$$

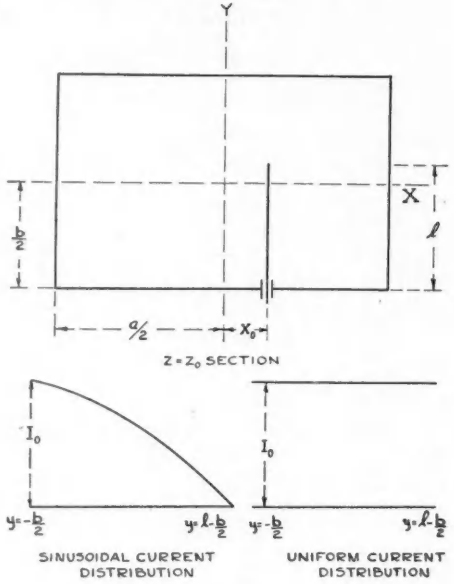
Y
X
$\frac{b}{2}$
l
$a/2$
X_0
$Z = Z_0$ SECTION
I_0
$y=-\frac{b}{2}$
$y=l-\frac{b}{2}$
SINUSOIDAL CURRENT DISTRIBUTION
I_0
$y=-\frac{b}{2}$
$y=l-\frac{b}{2}$
UNIFORM CURRENT DISTRIBUTION

FIG. 1.

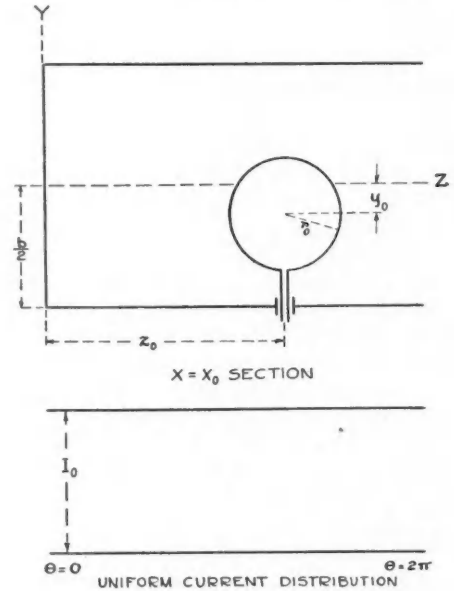
Y
Z
y_0
δ
$\frac{b}{2}$
z_0
$X = X_0$ SECTION
I_0
$\theta=0$
$\theta=2\pi$
UNIFORM CURRENT DISTRIBUTION

FIG. 2.

1*d*. A circular loop, the axis of which is parallel to the z-axis, radius r_0, center at (x_0, y_0, z_0) (see Fig. 3).

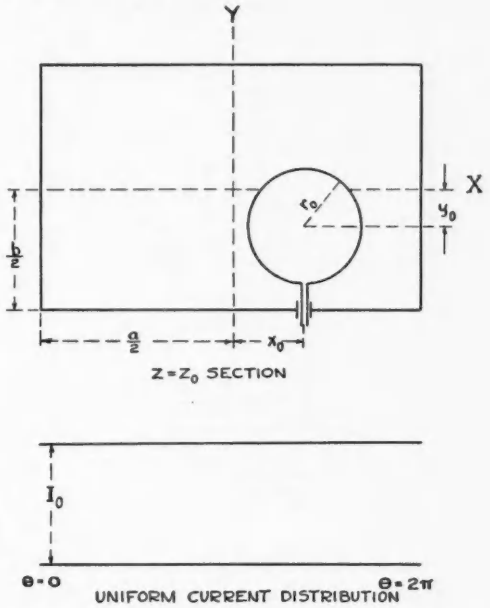

FIG. 3.

Assuming uniform current distribution,

$$R = \frac{960\pi^3 r_0^2}{ab\gamma}\left[\sin\left(\frac{\pi}{a}x_0\right)\sin\left(\frac{2\pi\gamma}{\lambda}z_0\right)J_1\left(\frac{\pi}{a}r_0\right)\right]^2 \text{ ohms.}$$

1*e*. An American antenna of circular shape in the yz plane, being divided into four sections, radius r_0 and center at (x_0, y_0, z_0) (see Fig. 4). Assuming sinusoidal current distribution in each section so that $\pi r_0 = \lambda$,

$$R = \frac{61440\pi r_0^2}{\gamma ab}\left[\cos\left(\frac{\pi}{a}x_0\right)\cos\left(\frac{2\pi}{\lambda}\gamma z_0\right)F(2\gamma)\right]^2 \text{ ohms,}$$

where

$$F(x) = \frac{d^2}{dx^2}\left(\frac{\sin^2\frac{x}{2}}{x}\right), \quad \pi r_0 = \lambda.$$

1*f*. An American antenna of the circular shape in the XY plane, being divided into four sections, radius r_0 and center at (x_0, y_0, z_0) (see Fig. 5). Assuming sinusoidal current distribution in each section so that $\pi r_0 = \lambda$,

$$R = \frac{61440\pi r_0^2}{ab\gamma}\left[\sin\left(\frac{\pi}{a}x_0\right)\sin\left(\frac{2\pi}{\lambda}\gamma z_0\right)F\left(\frac{\lambda}{a}\right)\right]^2 \text{ ohms.}$$

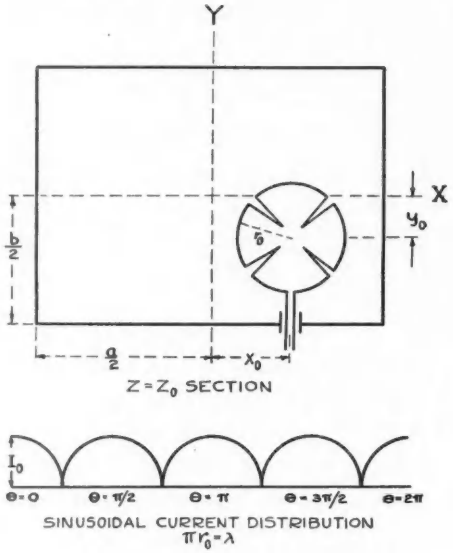
Y
X
y_0
r_0
$\frac{b}{2}$
$\frac{a}{2}$
x_0
$Z = Z_0$ SECTION
I_0
$\theta = 0$
$\theta = \pi/2$
$\theta = \pi$
$\theta = 3\pi/2$
$\theta = 2\pi$
SINUSOIDAL CURRENT DISTRIBUTION
$\pi r_0 = \lambda$

FIG. 4.

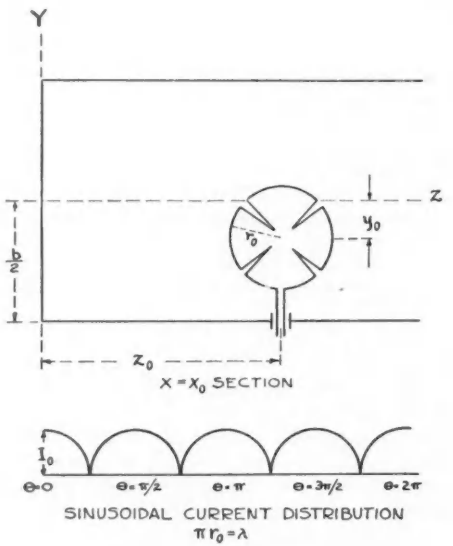
Y
Z
y_0
r_0
$\frac{b}{2}$
z_0
$X = X_0$ SECTION
I_0
$\theta = 0$
$\theta = \pi/2$
$\theta = \pi$
$\theta = 3\pi/2$
$\theta = 2\pi$
SINUSOIDAL CURRENT DISTRIBUTION
$\pi r_0 = \lambda$

FIG. 5.

The resistance of an Antenna Parallel to the Axis in a Circular Wave Guide Transmitting the E_{01} Wave Only

General Formula:

$$(2) \qquad R = \frac{30}{\pi^2 J_1^2(j_{01})} \frac{\lambda^2}{\gamma_{01} a^4} \left[\varphi_0 J_0\left(j_{01} \frac{r_0}{a}\right)\right]^2 \text{ ohms,}$$

where

$$(2a) \qquad \text{the numerical factor} = \frac{30}{\pi^2 J_1^2(j_{01})} = 11.28,$$

$$(2b) \qquad \varphi_0 = \int \frac{I}{I_0} \cos\left(\frac{2\pi}{\lambda} \gamma_{01} z_0\right) dz_0 \text{ (taken along the antenna).}$$

The conditions for transmitting the E_{01} wave only in a circular wave guide are:

(2c) antenna parallel to the axis,

$$(2d) \qquad j_{01} = 2.405 < \frac{2\pi a}{\lambda} < 5.520 = j_{02}.$$

The notation is as follows:

a = radius of the wave guide,

$j_{01} = 2.405$ = the first root of $J_0(x)$,

$$\gamma_{01} = \sqrt{1 - \left(\frac{j_{01}\lambda}{2\pi a}\right)^2} = \sqrt{1 - \left(0.3827 \frac{\lambda}{a}\right)^2},$$

$\frac{2\pi}{\lambda} \gamma_{01}$ = the phase constant of the E_{01} wave,

r_0, z_0 = the co-ordinates of the antenna, r_0 = the off-center distance,

z_0 = the distance from the plug,

I = current along the antenna,

I_0 = current at the feeding point.

Special cases:

2a. A straight antenna of length l parallel to the z-axis, running from $z = 0$ to $z = l$. Assuming sinusoidal current distribution (Fig. 6),

$$R = \frac{308.0}{\gamma_{01}} \left\{ \frac{\sin\left[\frac{\pi l}{\lambda}(1 + \gamma_{01})\right] \sin\left[\frac{\pi l}{\lambda}(1 - \gamma_{01})\right]}{\sin\left(\frac{2\pi l}{\lambda}\right)} J_0\left(j_{01} \frac{r_0}{a}\right) \right\}^2 \text{ ohms.}$$

$$\left[\frac{480}{[j_{01} J_1(j_{01})]^2} = 308.0.\right]$$

2b. The same antenna as in the case 2a. Assuming uniform current distribution,

$$R = 1.652 \frac{\lambda^4}{a^4 \gamma^3} \left[\sin\left(\frac{2\pi}{\lambda} \gamma_{01} l\right) J_0\left(j_{01} \frac{r_0}{a}\right)\right]^2 \text{ ohms.}$$

$$\left[\frac{15}{2}\left[\frac{j_{01}}{\pi^2 J_1(j_{01})}\right]^2 = 1.652.\right]$$

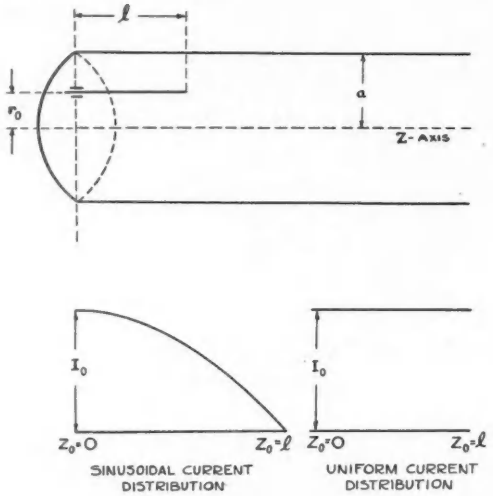

FIG. 6.

The Resistance of a Circular Loop Antenna Coaxially Placed in a Circular Wave Guide Transmitting the H_{01} Wave Only, Assuming Uniform Current Distribution (Fig. 7)

$$R = \frac{480\pi^2}{J_0^2(j'_{01})} \frac{r_0^2}{\gamma'_{01}a^2} \left[J_1\left(\frac{r_0}{a} j'_{01}\right) \sin\left(\frac{2\pi}{\lambda} \gamma'_{01} z_0\right)\right]^2 \text{ ohms}, \tag{3}$$

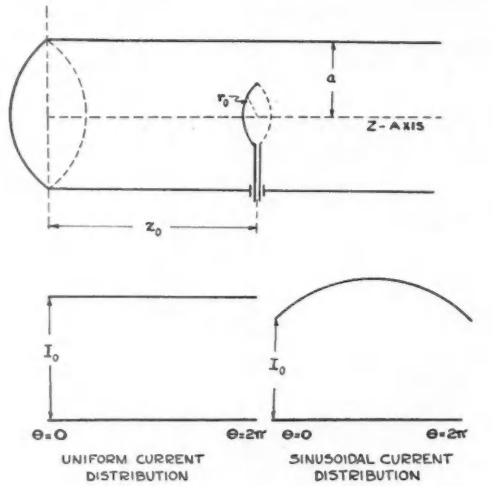

FIG. 7.

where the numerical factor is

$$(3a) \qquad \frac{480\pi^2}{J_0^2(j'_{01})} = 2.921 \times 10^4.$$

The conditions for transmitting the H_{01} wave only in a circular waveguide are:
(3*b*) symmetrically placed loop antenna with uniform current distribution,

$$(3c) \qquad j'_{01} = 3.832 < \frac{2\pi a}{\lambda} < 7.016 = j'_{02}.$$

The notation is as follows:

$j'_{01} = 3.832$ = the first root of $J'_0(x)$,

r_0 = the radius of the loop,

a = the radius of the wave guide,

$$\gamma'_{01} = \sqrt{1 - \left(\frac{\lambda j'_{01}}{2\pi a}\right)^2} = \sqrt{1 - \left(0.6098 \frac{\lambda}{a}\right)^2},$$

$\frac{2\pi}{\lambda}\gamma'_{01}$ = the phase constant of the H_{01} wave.

The Resistance of an Arbitrary Antenna in a Circular Wave Guide Transmitting the H_{11} Wave Only

General formula

$$(4) \qquad R = \frac{240}{J_1^2(j'_{11})\,(j'^2_{11} - 1)} \frac{1}{\gamma'_{11}} \left(\varphi_{1r} - \frac{j'_{11}}{a}\varphi_{1\theta}\right)^2 \text{ ohms},$$

where

$$(4a) \qquad \text{the numerical factor} = \frac{240}{J_1^2(j'_{11})\,(j'^2_{11} - 1)} = 296.6,$$

$$(4b) \qquad \varphi_{1r} = \int \frac{I}{I_0} J_1\left(j'_{11}\frac{r_0}{a}\right) \cos\theta_0 \sin\left(\frac{2\pi}{\lambda}\gamma'_{11} z_0\right) \frac{dr_0}{r_0} \text{ (taken along the antenna)},$$

$$(4c) \qquad \varphi_{1\theta} = \int \frac{I}{I_0} J'_1\left(j'_{11}\frac{r_0}{a}\right) \sin\theta_0 \sin\left(\frac{2\pi}{\lambda}\gamma'_{11} z_0\right) r_0\, d\theta_0.$$

The conditions for transmitting the H_{11} wave only in a circular wave guide are:
(4*d*) for an antenna having a component in the axial direction:

$$j'_{11} = 1.841 < \frac{2\pi a}{\lambda} < 2.405 = j_{01},$$

(4*e*) for an antenna having no component in the axial direction:

$$j'_{11} = 1.841 < \frac{2\pi a}{\lambda} < 3.054 = j'_{21}.$$

The notation is as follows:

a = the radius of the wave guide,

r_0, θ_0, z_0 = the co-ordinates of a point on the antenna,

$$j'_{11} = 1.841 = \text{the first root of } J'_1(x),$$

$$\gamma'_{11} = \sqrt{1 - \left(\frac{j'_{11}\lambda}{2\pi a}\right)^2} = \sqrt{1 - \left(0.2930\,\frac{\lambda}{a}\right)^2},$$

$$\frac{2\pi}{\lambda}\gamma'_{11} = \text{the phase constant of the } H_{11} \text{ wave.}$$

Special cases:

4*a*. A straight antenna of length l placed along a diameter of the wave guide with one end at the surface of the guide. Assuming uniform current distribution (Fig. 8),

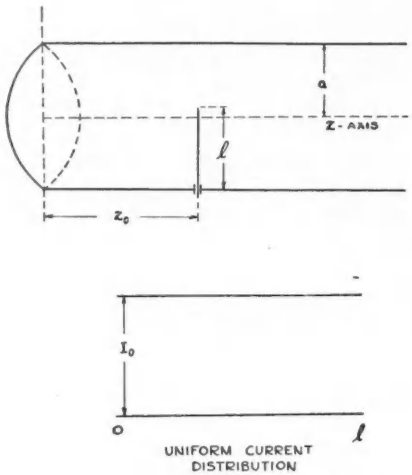

FIG. 8.

$$R = 296.6\,\frac{1}{\gamma'_{11}}\left[\sin\frac{2\pi}{\lambda}\gamma'_{11}\,z_0\right]^2\left\{B(j'_{11}) - B\left((a-l)\frac{j'_{11}}{a}\right)\right\}^2 \text{ ohms,}$$

where

$$B(x) = J'_0(x) + \int_0^x J_0(\alpha)\,d\alpha, \quad B(j'_{11}) = 1.382.$$

For the special case $l = 2a$: $R = 2259\,\frac{1}{\gamma'_{11}}\left[\sin\left(\frac{2\pi}{\lambda}\gamma'_{11}z_0\right)\right]^2$ ohms.

4*b*. A circular loop of radius r_0 placed coaxially in the guide at a distance z_0 from the plug. Assuming sinusoidal current distribution (Fig. 7),

$$R = 1.588 \times 10^5\,\frac{r_0^4}{a^2\lambda^2\gamma'_{11}\left(1 - \frac{4\pi^2}{\lambda^2}r_0^2\right)^2} \times$$

$$\left[\sin\left(\frac{2\pi}{\lambda}\gamma'_{11}z_0\right)\tan\left(\frac{2\pi^2}{\lambda}r_0\right)J'_1\left(j'_{11}\frac{r_0}{a}\right)\right]^2 \text{ ohms,}$$

where the numerical factor is

$$\frac{240\, j_{11}''^2}{(j_{11}''^2 - 1)J_1^2(j_{11}'')}\, 16\pi^2 = 1.588 \times 10^5 .$$

Reference

1. BUCHHOLZ, H. Ann. Physik, 39 : 81. 1941.

PART IV. THE IMPEDANCE OF A RECTANGULAR WAVE GUIDE WITH A THIN ANTENNA

BY L. INFELD

WITH APPENDICES BY J. R. POUNDER AND A. F. STEVENSON

1. Introduction

A wave guide of rectangular section extends to infinity in one direction and is closed in the other direction by a plug. The guide and the plug are assumed to be perfect conductors.

A thin, cylindrical antenna is placed inside the guide. To make our argument simple, we place this antenna parallel to the plug and parallel to the two other (shorter) walls of the guide, midway between them. Fig. 1 shows the choice of our co-ordinate system. In it, the lower end of the antenna has the co-ordinates (0, 0, 0) and the upper end has the co-ordinates (0, l, 0) where l is the length of the antenna. The z-axis is perpendicular to the plug, and points toward the open end.

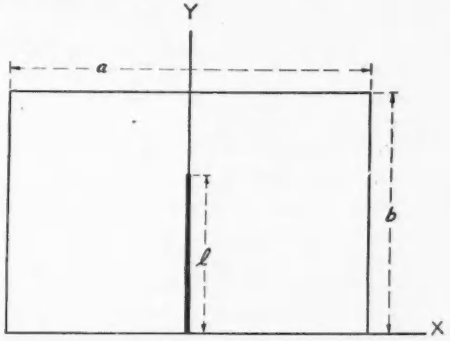

FIG. 1.

The parameters characterizing our problem are:

a, b, the dimensions of the guide,

$k = \frac{2\pi}{\lambda}$ (λ = wave length),

l = the length of the antenna,

ρ_0 = the radius of the antenna, (we assume $\rho_0 k \ll 1$),

z_0 = the distance between the plug and the antenna.

Our problem is to find the impedance of this wave guide under the assumption that the current distribution is sinusoidal. In this respect this paper is a continuation of Part I, in which the problem of the resistance of a rectangular wave guide was solved. However, the method of finding the impedance, and therefore both the resistance and the reactance, has turned out to be so simple that I intend to formulate this part independently, briefly repeating the reasoning concerning the images.

Our particular assumption about the position of the antenna is not essential. It would be easy to generalize our argument in this respect, as was done in Part I for the case of the resistance (see Appendix A). However, the assumption that the antenna is of cylindrical shape and that the current distribution is *given* is essential for our argument. Again, the assumption that the current distribution is sinusoidal is not necessary and the argument in the case of a constant current distribution and small antenna would be even simpler (see Appendix B).

Some of the results found here are valid for a wave guide of arbitrary shape as long as the antenna is parallel to the plug. This is shown by Stevenson in Appendix C. Especially the conclusions formulated in Section 8 are general and may be of interest to someone who does not care about the detailed calculations. Therefore, I tried to write Section 8 so that its contents may be understood without reading the previous parts.

2. The Lattice of Dipoles

We use the method of images. The image of a dipole with respect to a perfectly conducting plane is obtained by taking the geometrical image and then reversing the direction. The dipole and its image give a field satisfying the condition

$$\vec{E}_t = 0 \tag{2.1}$$

over the plane, $\vec{E}_t$ being the tangential component of the electric field.

Let us first consider the case where the rectangular wave guide has no plug, so that it extends to infinity in both directions. Suppose there is a dipole, inside the guide, placed along the y-axis. It is easy to find a doubly infinite system of images (all external to the guide) such that the lattice consisting of the dipole and its images gives a field satisfying the condition (2.1) over the walls of the guide. If we now add a plug, the condition (2.1) will be satisfied over it if we add to the above lattice its image in the plane of the plug.

We place a dipole with components $(0, A_y, 0)$ at $(0, y_0, 0)$. Fig. 2 shows part of the lattice in the plane $z = 0$.

If we let m and n take all integral values, positive, zero, and negative, we may represent the components and positions of all the dipoles in the plane $z = 0$ as follows:

$$\begin{aligned} &(0, A_y, 0) \quad \text{at} \quad (2ma, \pm y_0 + 2nb, 0) \quad — \quad \text{two basic lattices,} \\ &(0, -A_y, 0) \quad \text{at} \quad (\overline{2m+1}\, a, \pm y_0 + 2nb, 0) — \text{two basic lattices.} \end{aligned} \tag{2.2}$$

The images with respect to the plane of the plug are given by this table by changing the sign of A_y and replacing $z = 0$ by $z = -2z_0$. Thus we have eight "basic" lattices determining the field in the guide.

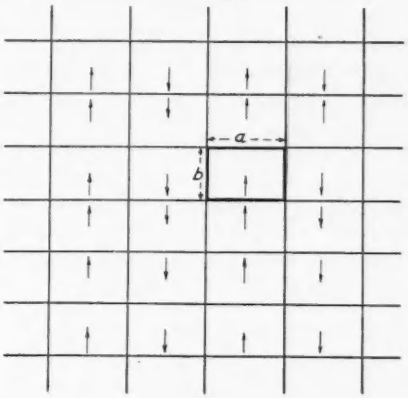

FIG. 2.

3. The Impedance of a Free Antenna

Before we return to our subject of the wave guide, we shall derive an expression for the impedance of a free antenna driven at the lower end. We assume the antenna to be as in Fig. 1, but we shall ignore the wave guide.

We shall now use Sommerfeld's formula (4), which allows us to write the Hertz vector (in Heaviside units) of a dipole at $(0, y_0, 0)$in the form of an integral:*

$$\frac{A_y}{4\pi}\frac{e^{ikr}}{r} = \frac{iA_y}{8\pi}\int_{-\infty}^{+\infty} e^{i\alpha y}\, e^{-i\alpha y_0}\, H_0^{(1)}\left(\rho\sqrt{k^2-\alpha^2}\right) d\alpha, \tag{3.1}$$

$$\rho^2 = x^2 + z^2, \quad r^2 = \rho^2 + (y - y_0)^2,$$

$$\sqrt{k^2 - \alpha^2} = \text{positive imaginary for } \alpha^2 > k^2,$$

$H_0^{(1)}$ = Hankel's function of the first kind and order zero.

We omit here and later the time-factor $e^{-i\omega t}$.

If we have, instead of a dipole, a finite antenna, then the Hertz vector of this antenna can be found by replacing A_y in (3.1) by

$$\frac{i}{kc}\, I_0 \frac{\sin k(l - y_0)}{\sin kl}\, dy_0, \tag{3.2}$$

and integrating over dy_0 from 0 to l. Here I_0 is the current at the driving point ($y_0 = 0$), and the expression (3.2) means the assumption of a sinusoidal current distribution.

* *Our formula follows from Equation (3) on p. 416 in Watson's book by putting* $\mu = -\frac{1}{2}$, $\nu = 0$.

It is convenient to introduce

$$(3.3)\quad f(\alpha) = \int_0^l e^{i\alpha\zeta} \sin k(l-\zeta)\,d\zeta$$

$$= \frac{1}{k\left(1-\left(\frac{\alpha}{k}\right)^2\right)}\left\{e^{i\alpha l} - \cos kl - \frac{i\alpha}{k}\sin kl\right\}.$$

Using (3.3), we have for the Hertz vector Φ_y of the finite antenna:

$$(3.4)\qquad \Phi_y = -\frac{I_0}{8\pi ck \sin kl}\int_{-\infty}^{\infty} f(\alpha)\, e^{i\alpha y} H_0^{(1)}\left(\rho\sqrt{k^2-\alpha^2}\right) d\alpha\,.$$

The next step is to introduce the y-component of the electric field, the only one in which we are interested:

$$E_y = k^2\,\Phi_y + \frac{\partial^2\Phi_y}{\partial y^2}$$

$$(3.5)$$

$$= \frac{-I_0}{8\pi ck \sin kl}\int_{-\infty}^{\infty}(k^2-\alpha^2)\, f(\alpha)\, e^{i\alpha y} H_0^{(1)}\left(\rho\sqrt{k^2-\alpha^2}\right) d\alpha\,.$$

Our last step is to calculate the impedance (Z_{00}) of this free antenna by the e.m.f. method:

$$(3.6)\qquad Z_{00} = -\frac{1}{I_0^2}\int_0^l E_y(\rho_0)\, I\, dy = -\frac{1}{I_0 \sin kl}\int_0^l E_y(\rho_0)\sin k(l-y)\,dy.$$

From (3.5), (3.6), (3.3), we obtain:

$$(3.7)\qquad Z_{00} = \frac{1}{8\pi ck\,\sin^2 kl}\int_{-\infty}^{\infty} f(\alpha)\,\overline{f(\alpha)}\,(k^2-\alpha^2)\, H_0^{(1)}\left(\rho_0\sqrt{k^2-\alpha^2}\right) d\alpha\,,$$

where $\overline{f(\alpha)}$ is the complex conjugate of $f(\alpha)$.

Equation (3.7) represents the impedance of a free antenna.

4. The Mutual Impedance of Two Antennae

Before we return to the wave guide we must solve the problem of the mutual impedance of two antennae.

Let us assume that the two antennae are parallel to each other and of the same length l. Let ρ be the distance between them. Then:

$$(4.1)\qquad Z_{AB} = -\frac{1}{(I_0^{(A)})^2}\int_0^l E_y^{(B)}(\rho)\, I^{(A)}\, dy\,.$$

Here Z_{AB} is the contribution to the impedance of antenna (A) coming from antenna (B). The indices (A) and (B) denote the current and the field

belonging to antennae (A) and (B) respectively. Finally we may remark that our formula assumes $\rho_0 \ll \rho$ and therefore it is immaterial whether ρ means the distance between the axes of these antennae or between lines parallel to them and lying on their surfaces.

We shall now consider two cases:

Case a: Each point of antenna (B) is obtained from a point of antenna (A) by replacing

$$0, y_0, 0 \quad \text{by} \quad a_0, y_0 + b_0, c_0, \tag{4.2}$$

a_0, b_0, c_0, being constants.

The calculation of $Z_{AB}^{(a)}$ is very similar to that of Z_{00}. Where we had $y - y_0$ before, we shall now have $y - y_0 - b_0$. Secondly, where we had ρ_0 before, we shall now have

$$\rho = \sqrt{a_0^2 + c_0^2}. \tag{4.3}$$

Thus, instead of (3.7), we now have:

$$Z_{AB}^{(a)} = \frac{1}{8\pi ck \sin^2 kl} \int_{-\infty}^{+\infty} e^{-i\alpha b_0} f(\alpha) \overline{f(\alpha)} (k^2 - \alpha^2) H_0^{(1)} (\rho\sqrt{k^2 - \alpha^2}) \, d\alpha . \tag{4.4}$$

Case b: Each point of antenna (B) is obtained from a point of autenna (A) by replacing

$$0, y_0, 0 \quad \text{by} \quad a_0, -y_0 + b_0, c_0 .$$

The calculation of $Z_{AB}^{(b)}$ will differ from that of $Z_{AB}^{(a)}$ in one respect: in the integration with respect to y_0 we shall have

$$\int_0^l e^{i\alpha y_0} \sin k(l - y_0) \, dy_0 = \overline{f(\alpha)}, \tag{4.5}$$

instead of

$$\int_0^l e^{-i\alpha y_0} \sin k(l - y_0) \, dy_0 = f(\alpha)$$

as before.

Thus we have for $Z_{AB}^{(b)}$:

$$Z_{AB}^{(b)} = \frac{1}{8\pi ck \sin^2 kl} \int_{-\infty}^{+\infty} e^{-i\alpha b_0} (\overline{f(\alpha)})^2 (k^2 - \alpha^2) H_0^{(1)} (\rho\sqrt{k^2 - \alpha^2}) \, d\alpha . \tag{4.6}$$

Both results, (4.4) and (4.6), will be needed in our later argument.

5. The Impedance of a Wave Guide

We summarize the result of our previous section: The mutual impedance of two "parallel", identical antennae (case a) is:

$$Z_{AB}^{(a)} = \int_{-\infty}^{+\infty} e^{-i\alpha b_0} \varphi(\rho, \alpha) \, d\alpha . \tag{5.1}$$

The mutual impedance of two "antiparallel", identical antennae (case b) is:

$$Z_{AB}^{(b)} = \int_{-\infty}^{\infty} e^{-i\alpha b_0}\, \psi(\rho, \alpha)\, d\alpha\,. \tag{5.2}$$

Here we have, according to (4.4) and (4.6):

$$\varphi(\rho, \alpha) = \frac{1}{8\pi ck \sin^2 kl} f(\alpha)\, \overline{f(\alpha)}\, (k^2 - \alpha^2)\, H_0^{(1)}\, (\rho\sqrt{k^2 - \alpha^2})\,,$$

$$\psi(\rho, \alpha) = \frac{1}{8\pi ck \sin^2 kl}\, (\overline{f(\alpha)})^2\, (k^2 - \alpha^2)\, H_0^{(1)}\, (\rho\sqrt{k^2 - \alpha^2})\,, \tag{5.3}$$

and according to (3.3)

$$f(\alpha) = \frac{1}{k\left(1 - \left(\frac{\alpha}{k}\right)^2\right)} \left\{ e^{-i\alpha l} - \cos kl + i\,\frac{\alpha}{k} \sin kl \right\}. \tag{5.4}$$

The self-impedance of an antenna is obtained from (5.1) by putting there:

$$b_0 = 0, \qquad \rho = \rho_0\,. \tag{5.5}$$

Now we know that the impedance of a wave guide is equivalent to the impedance of an antenna surrounded by *eight* basic lattices. In (2.2) we wrote down the co-ordinates of the dipoles of four basic lattices. If the dipoles become finite antennae, the four antenna-lattices consist of "parallel" or "antiparallel" antennae. The remaining four lattices are opposite in direction and placed in the plane $z = -2z_0$. Thus we have, because of (5.1), (5.3), and (2.2) for the impedance of an antenna in a wave guide:

$$\begin{aligned} Z = \sum_{m=-\infty}^{\infty} \sum_{n=-\infty}^{\infty} \int_{\infty}^{\infty} e^{i2nb\alpha} \Big[& \varphi(\rho_0 + 2ma, \alpha) + \psi(\rho_0 + 2ma, \alpha) \\ & - \varphi(\,(2ma + 1)a, \alpha) - \psi(\,(2m + 1)a, \alpha) \\ & - \varphi(\sqrt{(2ma)^2 + (2z_0)^2}, \alpha) - \psi(\sqrt{(2ma)^2 + (2z_0)^2}, \alpha) \\ & + \varphi(\sqrt{(\,(2m+1)a)^2 + (2z_0)^2}, \alpha) + \psi(\sqrt{(\,(2m+1)a)^2 + (2z_0)^2}, \alpha) \Big]\, d\alpha. \end{aligned} \tag{5.6}$$

We have here, in square brackets, eight expressions, each corresponding to one of the basic lattices. The terms with ρ_0, for $m = 0$, give the self-reactance, and in them ρ_0 must not be omitted. Otherwise, for $m \neq 0$, it is immaterial whether ρ_0 is omitted or not.

Our expression for the impedance, (5.6), though representing the solution of our problem, is too complicated to be used in actual calculations. Our aim is to change (5.6) in such a way that it will be applicable for practical purposes. We shall do it in detail for the first expression:

$$\sum_{-\infty}^{\infty} \sum_{-\infty}^{\infty} \int_{-\infty}^{+\infty} e^{-i2nb\alpha}\, \varphi(\rho_0 + 2ma, \alpha)\, d\alpha\,. \tag{5.7}$$

We introduce a new variable

$$\sigma = \frac{b}{\pi}\alpha .$$

Then instead of (5.7) we have

$$\frac{\pi}{b}\sum_{m=-\infty}^{\infty}\sum_{n=-\infty}^{\infty}\int_{-\infty}^{\infty} e^{-i2\pi n\sigma}\,\varphi\left(\rho_0 + 2ma, \frac{\pi}{b}\sigma\right)d\sigma . \tag{5.8}$$

We can now apply Poisson's formula (1), replacing (5.8) by

$$\frac{\pi}{b}\sum_{m=-\infty}^{\infty}\sum_{n=-\infty}^{\infty}\varphi\left(\rho_0 + 2ma, \frac{n\pi}{b}\right). \tag{5.9}$$

For $m \neq 0$, we have $\rho = \sqrt{4m^2a^2} = 2|m|a$. Therefore, the summation from $m = -\infty$ to $m = +\infty$ can be replaced by a summation from $m = 0$ to $m = \infty$. If we look back at (5.3), we see that $\varphi(-\alpha) = \varphi(\alpha)$; therefore $\varphi(-n) = \varphi(n)$. Again the summation from $n = -\infty$ to $n = \infty$ can be replaced by summation from 0 to ∞. Thus (5.9) takes the form

$$\frac{\pi}{b}\sum_{m=0}^{\infty}\sum_{n=0}^{\infty}\delta_m\delta_n\,\varphi\left(\rho_0 + 2ma, \frac{n\pi}{b}\right), \tag{5.10}$$

where

$$\delta_s = 2 \text{ for } s \neq 0, \quad \delta_0 = 1.$$

We have to repeat the same reasoning for the remaining seven expressions in (5.6), each time using Poisson's formula. Having done this and having introduced for φ and ψ expressions (5.3) and (5.4), we obtain for the total impedance:

$$Z = \frac{1}{4bck\sin^2 kl}\sum_{m=0}^{\infty}\sum_{n=0}^{\infty}(-1)^m\,\delta_m\delta_n\,\frac{\left(\cos kl - \cos\frac{n\pi l}{b}\right)^2}{1 - \left(\frac{n\pi}{bk}\right)^2}\times \tag{5.11}$$

$$\left[H_0^{(1)}\left[(\rho_0 + ma)\sqrt{k^2 - \left(\frac{\pi n}{b}\right)^2}\right] - H_0^{(1)}\left[\sqrt{\left((ma)^2 + (2z_0)^2\right)\left(k^2 - \left(\frac{\pi n}{b}\right)^2\right)}\right]\right].$$

This is the final result. If expressed in ohms, instead of Heaviside units, it must be multiplied by $120\pi c$.

6. Discussion of (5.11)

The great virtue of (5.11) is its quick convergence. Let us assume

$$\frac{\pi n}{bk} = \nu \gg 1, \quad mak = \mu \gg 1 . \tag{6.1}$$

Then

$$|H_0^{(1)}(i\mu\nu)| \sim \frac{e^{-\mu\nu}}{\sqrt{\mu\nu}}, \tag{6.2}$$

which shows that the evaluation of (5.11) will be comparatively easy to handle.

Let us imagine a point lattice (Fig. 3), where each point corresponds to one expression in the sum (5.11). Let us further assume that the dimensions of

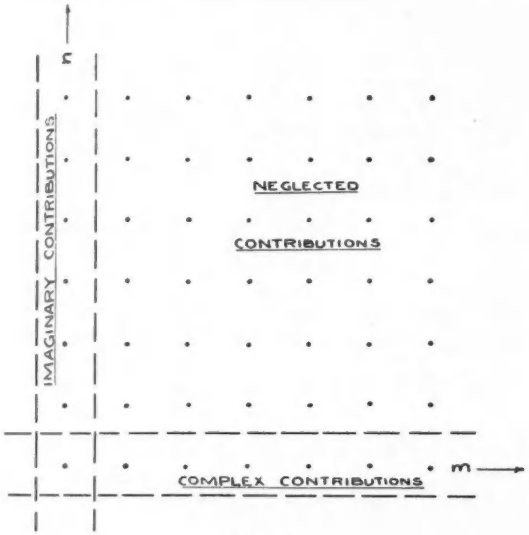

FIG. 3.

the wave guide are such that it lets through only the H_{01} wave, and that

$$\sqrt{1-\left(\frac{\pi m}{ak}\right)^2} = \sqrt{1-\left(\frac{\lambda m}{2a}\right)^2} \text{ is imaginary for } m = 2,3,\text{- - - -},$$
$$\text{and real for } m = 1,$$

(6.3)

$$\sqrt{1-\left(\frac{\pi n}{bk}\right)^2} = \sqrt{1-\left(\frac{\lambda n}{2b}\right)^2} \text{ is imaginary for } n = 1,2,\text{- - - -}.$$

Because $H_0^{(1)}$ of an imaginary argument is imaginary, we see that the contribution to the impedance is purely imaginary if $n \geqslant 1$. Only the points along the m-axis give a complex contribution. Because of (6.2), the most important contribution will come from the points on the m- and n-axes. It was found that all others can be ignored in practical applications. Therefore, we shall now focus our attention upon the contributions to (5.11) from these points, which are as follows:

(a) $m = 0, \quad n = 0$:

(6.4) $$\frac{\tan^2\frac{kl}{2}}{4bck}\left(H_0^{(1)}(\rho_0 k) - H_0^{(1)}(2z_0 k)\right),$$

(6.4) (Cont'd)

$$(b)\ m = 0,\quad n = 1,2,\text{----}:$$

$$\frac{1}{2bck\sin^2 kl}\sum_{n=1}^{\infty}\frac{\left(\cos kl - \cos\frac{\pi nl}{b}\right)^2}{1-\left(\frac{\pi n}{bk}\right)^2}\left[H_0^{(1)}\left(\rho_0 k\sqrt{1-\left(\frac{\pi n}{bk}\right)^2}\right) - H_0^{(1)}\left(2z_0 k\sqrt{1-\left(\frac{\pi n}{bk}\right)^2}\right)\right],$$

$$(c)\ n = 0,\quad m = 1,2,\text{----}:$$

$$\frac{\tan^2 kl/2}{2bck}\sum_{m=1}^{\infty}(-1)^m\left[H_0^{(1)}(mak) - H_0^{(1)}(k\sqrt{(ma)^2+(2z_0)^2})\right].$$

As $H_0^{(1)}(x)$ behaves like $\log x$ for small x, the (a) part gives the logarithmic term which appears in all calculations of impedance. In the (b) part, we shall have to sum a few expressions only, if $\rho_0 k$ is of the order of, say, $1/10$. Finally (c), that is the summation along the m-axis, is very simple, although it does not converge exponentially. However, even (c) converges as $\sum \frac{e^{imz}}{m^{3/2}}$, since for great m we can write

$$(-1)^m\left(H_0^{(1)}(mak) - H_0^{(1)}(k\sqrt{(ma)^2+(2z_0)^2})\right) \sim e^{-im\pi}\frac{2z_0^2}{mak}\,H_1^{(1)}(mak) \sim \frac{e^{im(ak-\pi)}}{m^{3/2}}.$$

We shall see later how to deal with part (c) in actual calculations.

If we are looking for reactance only, we shall have to replace $H_0^{(1)}$ by iY_0 in (6.4) (a) and (c).

7. The Resistance

The resistance is the real part of (6.4) (a) and (c) for $\rho_0 \to 0$.

$$(7.1)\qquad R = \frac{\tan^2\frac{kl}{2}}{4bck}\sum_{m=-\infty}^{\infty}\left(J_0(mak) - J_0(k\sqrt{(ma)^2+(2z_0)^2})\right)e^{i\pi m},$$

where R denotes the resistance.

We shall again use Poisson's formula, this time replacing summation by integration. Then we have:

$$(7.2)\qquad R = \frac{\tan^2\frac{kl}{2}}{4bck}\sum_{h=-\infty}^{\infty}\int_{-\infty}^{\infty}e^{-i2\pi(h-1/2)\alpha}\left[J_0(\alpha ak) - J_0(k\sqrt{(\alpha a)^2+(2z_0)^2})\right]d\alpha.$$

We can replace the J_0's by $H_0^{(1)}$'s and calculate R as the *real* part of

$$(7.3)\qquad \frac{\tan^2\frac{kl}{2}}{4bck}\sum_{h=-\infty}^{\infty}\int_{-\infty}^{\infty}e^{-i2\pi(h-1/2)\alpha}\left[H_0^{(1)}(\alpha ak) - H_0^{(1)}\left(k\sqrt{(\alpha a)^2+(2z_0)^2}\right)\right]d\alpha.$$

Now we can use Sommerfeld's formula (3.1) with

$$y_0 \to 2\pi(h - 1/2),\ \rho \to iak,\ y \to 0,\ k \to \frac{2iz_0}{a}.$$

We have, according to this formula:

$$\int_{-\infty}^{+\infty} e^{-i2\pi(h-1/2)\alpha} H_0^{(1)}(\alpha ak)d\alpha - \int_{-\infty}^{+\infty} e^{-i2\pi(h-1/2)\alpha} H_0^{(1)}\left(k\sqrt{(\alpha a)^2 + (2z_0)^2}\right)d\alpha$$

(7.5)

$$= \frac{2}{i\sqrt{-(ak)^2 + 4\pi^2(h-1/2)^2}} - \frac{2e^{\frac{-2z_0}{a}\sqrt{-(ak)^2+4\pi^2(h-1/2)^2}}}{i\sqrt{-(ak)^2 + 4\pi^2(h-1/2)^2}}.$$

We see that this expression will be real only if

(7.6) $$h = 0 \quad \text{or} \quad h = 1.$$

In this case we have for the above integrals (for $h = 0$ and $h = 1$):

(7.7) $$\frac{4}{ak\sqrt{1 - \left(\frac{\pi}{ak}\right)^2}} - \frac{4\cos\left(2z_0k\sqrt{1 - \left(\frac{\pi}{ak}\right)^2}\right)}{ak\sqrt{1 - \left(\frac{\pi}{ak}\right)^2}}.$$

The result is

(7.8) $$R = \frac{2\tan^2\frac{kl}{2}\sin^2\left(z_0k\sqrt{1 - \left(\frac{\pi}{ak}\right)^2}\right)}{abck^2\sqrt{1 - \left(\frac{\pi}{ak}\right)^2}},$$

which is in perfect agreement with the result obtained in Part I.

8. The Impedance Circle

We shall present our reasoning here in the form of theorems, so that the reader interested in their formulation only can omit the proofs.

We assume the dimensions of the wave guide (a, b) and the wave length (λ) and the thickness of the antenna ($2\rho_0$) as known and kept constant. The characteristic impedance of the line (Z_0) is also known. Our problem is to find l_0 (the matching length of the antenna) and z_0 (the distance of the antenna from the plug) so that the resistance will be that of the line and the reactance will be zero. It is convenient to take as the unit of impedance that of the line (Z_0). In this unit our problem is to find l_0, z_0, such that

(8.1) $$R = 1, X = 0, \text{ where } Z = R - iX.$$

This we shall refer to as the *matching* problem.

Theorem I

The resistance can be expressed in the form

(8.2) $$R = A(l) - A(l)\cos\left(\frac{4\pi}{\lambda}\gamma z_0\right),$$

where

$$(8.3)\qquad \begin{cases} A(l) = \dfrac{30\lambda^2}{ab\pi\gamma Z_0}\tan^2\left(\dfrac{\pi l}{\lambda}\right), \\ \gamma = \sqrt{1-\left(\dfrac{\lambda}{2a}\right)^2}. \end{cases}$$

The proof follows immediately from (7.8), if we assume that the impedence of the line (Z_0) is expressed in ohms.

Theorem II

If z_0 is *not* small compared with λ, then we can express the reactance in the form

$$(8.4)\qquad X = A'(l) + A(l)\sin\left(\frac{4\pi}{\lambda}\gamma z_0\right), \text{ to a very good approximation,}$$

where $A'(l)$ is a certain complicated function given explicitly in the course of the proof. But—this is essential—neither A nor A' depends on z_0.

Proof

The reactance X is the imaginary part of $-Z$. From (5.11) we see that $-Z$ can be split into two parts, one which does not depend on z_0 and the other which does. The part of Z which does not depend on z_0 is

$$(8.5)\qquad \frac{30\pi}{Z_0 bk\sin^2 kl}\sum_{m=0}^{\infty}\sum_{n=0}^{\infty}(-1)^m\delta_m\delta_n\frac{\left(\cos\dfrac{n\pi l}{b}-\cos kl\right)^2}{1-\left(\dfrac{n\pi}{bk}\right)^2}\times$$

$$H_0^{(1)}\left[(\rho_0+ma)\sqrt{k^2-\left(\frac{\pi n}{b}\right)^2}\right].$$

It was shown in Section 7 that the real part of this is A, as defined in (8.3). We shall therefore denote the expression (8.5) by

$$A - iA',$$

where A' is real. Thus we can write:

$$(8.6)\qquad X = A' - Im(C),$$

$$(8.7)\qquad C = \frac{30\pi}{Z_0 bk\sin^2 kl}\sum_{m=0}^{\infty}\sum_{n=0}^{\infty}(-1)^m\delta_m\delta_n\frac{\left(\cos kl-\cos\dfrac{n\pi l}{b}\right)^2}{1-\left(\dfrac{n\pi}{bk}\right)^2}\times$$

$$H_0^{(1)}\left[k_n\sqrt{(ma)^2+(2z_0)^2}\right],$$

where

$$k_n^2 = k^2 - \left(\frac{\pi n}{b}\right)^2.$$

Before, in Section 7, we calculated the *real* part of C. We shall now calculate in a very similar manner the imaginary part of C.

Using Poisson's formula (1) we can write for C

$$C = \frac{30\pi}{Z_0 bk \sin^2 kl} \sum_{n=0}^{\infty} \delta_n \frac{\left(\cos kl - \cos \frac{n\pi l}{b}\right)^2}{1 - \left(\frac{n\pi}{bk}\right)^2} \sum_{h=-\infty}^{\infty} \int_{-\infty}^{\infty} e^{-i2\pi(h-1/2)\alpha} \times H_0^{(1)}\left[k_n \sqrt{(ma)^2 + (2z_0)^2}\right] d\alpha . \tag{8.8}$$

Now we proceed exactly as in Section 7, (7.4), (7.5), using Sommerfeld's formula (4). Therefore:

$$C = \frac{30\pi}{bkZ_0 \sin^2 kl} \sum_{n=0}^{\infty} \delta_n \frac{\left(\cos kl - \cos \frac{n\pi l}{b}\right)^2}{1 - \left(\frac{n\pi}{bk}\right)^2} \sum_{h=-\infty}^{\infty} \frac{2e^{-\frac{2z_0}{a}\sqrt{-(ak_n)^2 + 4\pi^2(h-1/2)^2}}}{i\sqrt{-(ak_n)^2 + 4\pi^2(h-1/2)^2}} . \tag{8.9}$$

For $n > 0$ the exponent of e is real and negative. If the antenna is not too near the plug, then the only contributions to C which have to be taken into account are those coming from $n = 0$:

$$C = \frac{60\pi \tan^2 \frac{kl}{2}}{bkZ_0} \sum_{h=-\infty}^{\infty} \frac{e^{-\frac{2z_0}{a}\sqrt{-(ak)^2 + 4\pi^2(h-1/2)^2}}}{i\sqrt{-(ak)^2 + 4\pi^2(h-1/2)^2}} . \tag{8.10}$$

For the same reason we can neglect all expressions in this sum with the exception of those for which

$$h = 0, \text{ or } h = 1. \tag{8.11}$$

Therefore:

$$Im(C) = -A \sin\left(\frac{4\pi\gamma z_0}{\lambda}\right), \tag{8.12}$$

and finally

$$X = A' + A \sin\left(\frac{4\pi\gamma z_0}{\lambda}\right), \tag{8.13}$$

which proves our theorem.

Theorem III

If we change z_0 and keep all other parameters (a, b, λ, ρ_0, l) constant, then the points characterized by the corresponding pairs (R, X) lie on a circle, called the *impedance circle*. This circle is tangent to the X (reactance)-axis and the co-ordinates of its center are (A, A').

This can easily be seen from (8.2) and (8.4). Indeed, eliminating z_0 from these equations, we have

$$(R - A)^2 + (X - A')^2 = A^2, \tag{8.14}$$

which proves our theorem. (See Fig. 4).

What is the physical significance of the symbols appearing in (8.14)? R and X are the resistance and reactance corresponding to given values of l and z_0. As z_0 changes, the point (R, X) moves along the impedance circle. $2A$ is the

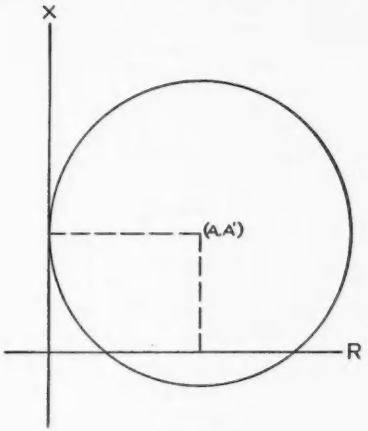

FIG. 4.

maximum resistance for a given l and variable z_0. A' can be interpreted as the reactance at the point for which the resistance vanishes; indeed for

$$\frac{2\pi\gamma}{\lambda} z_0 = s\pi; \quad s = 1,2,3, \text{----},$$

we have $R = 0, X = A'$.

9. The Matching Problem

We can now turn toward the solution of the matching problem. We have to find a circle, and a point on the circle, for which

$$R = 1, \quad X = 0. \tag{9.1}$$

Putting these values into (8.14) we have

$$A = \frac{A'^2}{2} + \frac{1}{2}. \tag{9.2}$$

Therefore the center of the impedance circle must lie on the parabola (9.2) for the matching problem to be solved (Fig. 5). The remaining problem is: how to find the right point on the parabola? Theoretically speaking, we ought to regard (9.2) as an equation for the determination of l_0, as A and A' are known functions of l.

If we look at (9.2) we see that the difficulty is to find A' as a function of l, as the other expression, A, is very simple. But A' is a part of Z; more explicitly the imaginary part of that part of $-Z$ which does not depend on z_0. Let

us rewrite from (6.4) the part of $-Z$ in which we are interested, that is, the part which does not depend on z_0. This is:

$$
\begin{aligned}
&-A' = \\
&\left\{
\begin{aligned}
&(a)\ \frac{30\pi \tan^2 \frac{kl}{2}}{bkZ_0}\ Y_0(\rho_0 k) \\
&+ \\
&(b)\ \frac{60\pi}{ibkZ_0 \sin^2 kl} \sum_{n=1}^{\infty} \frac{\left(\cos kl - \cos \frac{\pi n l}{b}\right)^2}{1 - \left(\frac{\pi n}{bk}\right)^2}\ H_0^{(1)}\left(\rho_0 k \sqrt{1 - \left(\frac{\pi n}{bk}\right)^2}\right) \\
&+ \\
&(c)\ \frac{60\pi \tan^2 \frac{kl}{2}}{bkZ_0} \sum_{m=1}^{\infty} (-1)^m\ Y_0(mak).
\end{aligned}
\right\}
\end{aligned}
\tag{9.3}
$$

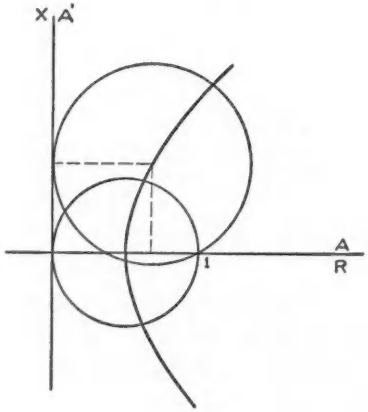

FIG. 5.

Thus we have here the explicit expression for A' which was used in all further calculations. In computing, the only difficulty encountered was to calculate (c):

$$\sum_{m=1}^{\infty} (-1)^m\ Y_0(mak), \tag{9.4}$$

which converges very slowly. This mathematical problem is treated elsewhere (2), where a table and graph of (9.4) is given.

To make our procedure clear we shall take the following special example:

$$
\begin{aligned}
(9.5) \qquad a &= 7.213 \text{ cm.}, \quad b = 3.404 \text{ cm.}, \quad \lambda = 10.0 \text{ cm.}, \\
\rho_0 &= 0.397 \text{ cm.}, \quad Z_0 = 80 \text{ ohms.}
\end{aligned}
$$

Then A' is a function of l only. Putting different values of l, we have $\frac{1}{2}(1 + A'(l)^2)$ as represented by Fig. 6. Next we draw A (which is much

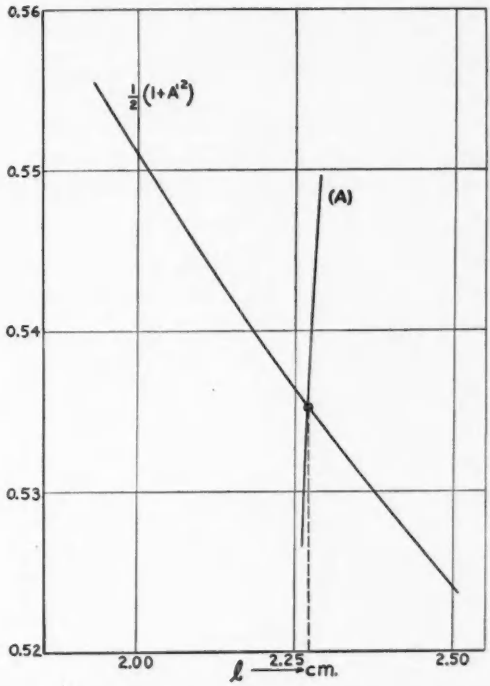

FIG. 6. *A and* $\frac{1}{2}(1 + A'^2)$ *as functions of* l. $\lambda = 10.0$ *cm.*, $a = 7.213$ *cm.*, $b = 3.404$ *cm.*, $\rho = 0.397$ *cm.*

simpler) as a function of l. The intersection of these two curves has the co-ordinate l_0, satisfying

$$\frac{1}{2}(1 + A'(l_0)^2) = A(l_0). \tag{9.6}$$

Once we have found l_0, we can easily find the set of z_0's from (8.2) and (8.3):

$$R = 1 = \frac{30\lambda^2}{ab\pi\gamma Z_0} \tan^2 \frac{\pi l_0}{\lambda} \left(1 - \cos \frac{4\pi\gamma Z_0}{\lambda}\right).$$

Thus the method allows us to find l_0, z_0, for which $R = 1, X = 0$. In our particular case (9.5) we have

$$l_0 = 2.316; \quad z_0 = 9.839 \pm \frac{\lambda s}{2\gamma}; \quad s = 0, 1, 2, \cdots.$$

In this way l_0, z_0 were calculated for two wave guides, for different λ's, ρ_0's, Z_0's. The calculations were made by Chien and Pounder. It proved that the omission of all the terms for which $m, n > 0$ was justified. In the expression (b) of (9.3) it was sufficient to take some six terms.

References

1. BOCHNER, S. Vorlesungen uber Fourierische Integrale, p. 33. Akademische Verlagsgesellschaft M.B.H., Leipzig. 1932.
2. INFELD, L., SMITH, V. G., and CHIEN, W. Z. J. Math. Phys. 26 : 22. 1947.
3. SCHELKUNOFF, S. A. Impedance of a transverse wire in a rectangular waveguide. Bell Telephone System, Lab. Rept. April, 1940.
4. WATSON, G. N. Theory of Bessel functions, pp. 415–416. Cambridge University Press 1922.

APPENDIX A

Generalization of the Impedance Formula for an Unsymmetrical Position of the Antenna Relative to the Sides of the Guide

BY J. R. POUNDER

We assume now that the antenna is placed at a distance x_0 from the center of the guide (Fig. 7). Let us generalize the previous reasoning step by step. We have four lattices of dipoles in the plane $z = 0$,

$$\text{(A1)} \qquad \begin{aligned} &0,\ A_y,\ 0 \quad \text{at} \quad x_0 + 2ma,\ \pm y_0 + 2nb,\ 0 \\ &0,\ -A_y,\ 0 \quad \text{at} \quad \overline{2m+1}\ a - x_0,\ \pm y_0 + 2nb,\ 0 \end{aligned}$$

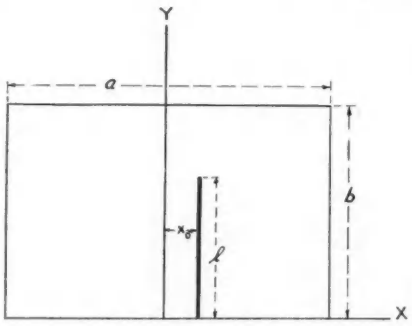

FIG. 7.

and four other lattices in the plane $z = -2z_0$ obtained by reflection in the plug and by changing A_y into $-A_y$. (Fig. 8)

The impedance of the antenna, corresponding to formula (5.6), is now by exactly the same method as before:

$$\begin{aligned} Z = \sum_{m=-\infty}^{\infty} \sum_{n=-\infty}^{\infty} \int_{-\infty}^{\infty} e^{-i2nb\alpha}\, d\alpha \Big[&\varphi(\rho_0 + 2ma, \alpha) + \psi(\rho_0 + 2ma, \alpha) \\ &- \varphi(\rho_0 + \overline{2m+1}\, a - 2x_0, \alpha) - \psi(\rho_0 + \overline{2m+1}\, a - 2x_0, \alpha) \\ &- \varphi\left(\sqrt{(2ma)^2 + (2z_0)^2}, \alpha\right) - \psi\left(\sqrt{(2ma)^2 + (2z_0)^2}, \alpha\right) \\ &+ \varphi\left(\sqrt{\overline{2m+1}\, a - 2x_0)^2 + (2z_0)^2}, \alpha\right) \\ &+ \psi\left(\sqrt{\overline{2m+1}\, a - 2x_0)^2 + (2z_0)^2}, \alpha\right) \Big] \cdot \end{aligned} \qquad \text{(A2)}$$

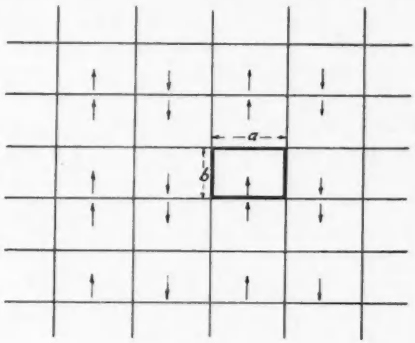

FIG. 8.

Again by the use of Poisson's formula (1) we obtain:

$$Z \text{ (in ohms)} = \frac{30\pi}{bk \sin^2 kl} \sum_{n=-\infty}^{\infty} \sum_{m=-\infty}^{\infty} \frac{\left(\cos kl - \cos \frac{n\pi l}{b}\right)^2}{1 - \left(\frac{\pi n}{bk}\right)^2} \times$$

$$\left\{ H_0^{(1)} \left[(\rho_0 + 2ma) \sqrt{k^2 - \left(\frac{\pi n}{b}\right)^2} \right] \right.$$

$$- H_0^{(1)} \left[(\rho_0 + \overline{2m+1}\, a - 2x_0) \sqrt{k^2 - \left(\frac{\pi n}{b}\right)^2} \right]$$

(A3)

$$- H_0^{(1)} \left[\sqrt{((2ma)^2 + (2z_0)^2) \left(k^2 - \left(\frac{\pi n}{b}\right)^2\right)} \right]$$

$$\left. + H_0^{(1)} \left[\sqrt{((\overline{2m+1}\, a - 2x_0)^2 + (2z_0)^2) \left(k^2 - \left(\frac{\pi n}{b}\right)^2\right)} \right] \right\} .$$

As can be shown by computation very similar to that of Section 7, but somewhat more complicated, the real part of (A3) is:

$$\text{(A5)} \qquad R = 2A \cos^2 \left(\frac{\pi x_0}{a}\right) \sin^2 \left(\frac{2\pi\gamma z_0}{\lambda}\right) = 2B \sin^2 \left(\frac{2\pi\gamma z_0}{\lambda}\right),$$

where A is defined by (8.3), and

$$\text{(A6)} \qquad B = A \cos^2 \frac{\pi x_0}{a} .$$

This formula agrees with the corresponding one in Part I. It is obvious that for $x_0 = 0$ this expression for the resistance reduces to that given in (7.8).

It can be shown (with the same assumption as before, namely, that z_0 is not small compared with λ) that the reactance can be written:

$$\text{(A7)} \qquad X = B' + B \sin \frac{4\pi\gamma z_0}{\lambda}, \text{ where}$$

$$(A8)\quad B - iB' = \frac{15\lambda}{Z_0 b \sin^2 kl} \sum_{n=0}^{\infty} \sum_{m=-\infty}^{\infty} \delta_n \frac{\left(\cos kl - \cos \frac{n\pi l}{b}\right)^2}{1 - \left(\frac{\pi n}{bk}\right)^2} \times$$

$$\left\{ H_0^{(1)} \left[(\rho_0 + 2ma)k \sqrt{1 - \left(\frac{\pi n}{bk}\right)^2} \right] \right.$$

$$\left. - H_0^{(1)} \left[(\rho_0 + \overline{2m+1}\, a - 2x_0)k \sqrt{1 - \left(\frac{\pi n}{bk}\right)^2} \right] \right\}.$$

Now (A5) can be written

$$(A9)\quad R = B\left(1 - \cos \frac{4\pi\gamma z_0}{\lambda}\right), \qquad B = \frac{30\lambda^2}{ab\pi\gamma Z_0} \cos^2 \frac{\pi x_0}{a} \tan^2 \frac{kl}{2}.$$

It is evident from (A9) and (A7) that all that was said before about the impedance circle is true also in this more general case.

APPENDIX B

Antenna of Length $l = b$

By J. R. Pounder

In the case in which the length of the antenna $= b$, one usually assumes uniform current distribution (see Fig. 9). The problem is not new, having been solved by Schelkunoff for a infinite guide without a plug (3). One of the two methods used by Schelkunoff seems to correspond to that presented in this paper.

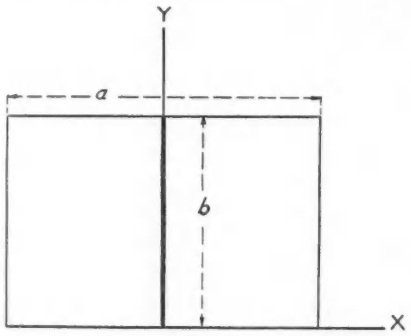

Fig. 9.

The same argument may be used here as before, or a slightly different treatment may be given which replaces the separate antenna-images by infinitely long antennae. The essential point of either method is that the double-sum is replaced by a simple summation. Here we shall outline the argument of the first method.

Because of the assumed uniform current distribution, we obtain instead of formula (3.3),

$$f(\alpha) = \frac{1 - e^{-i\alpha b}}{i\alpha}. \tag{B1}$$

By the same argument as before we arrive at formula (5.6), but the next step (the use of Poisson's formula) gives us an infinite series corresponding to (5.11) in which all terms involving $n \neq 0$ vanish. What remains is:

$$\begin{aligned} Z = \frac{bk}{4c} \sum_{m=-\infty}^{\infty} \{ & H_0^{(1)}[(\rho_0 + 2ma)k] \\ & - H_0^{(1)}[(\overline{2m+1}\, a + \rho_0 - 2x_0)k] - H_0^{(1)}[k\sqrt{(2ma)^2 + (2z_0)^2}] \\ & + H_0^{(1)}[k\sqrt{(\overline{2m+1}\, a - 2x_0)^2 + (2z_0)^2}]\}. \end{aligned} \tag{B2}$$

From this we can compute, just as before (using Poisson's and Sommerfeld's formulae), the resistance and the reactance. We obtain

$$R = \frac{b}{ac\gamma} \cos^2 \frac{\pi x_0}{a} \left(1 - \cos \frac{4\pi\gamma z_0}{\lambda}\right), \quad \gamma = \sqrt{1 - \left(\frac{\lambda}{2a}\right)^2}, \tag{B3}$$

$$\begin{aligned} X = \frac{b}{ac\gamma} \cos^2 \frac{\pi x_0}{a} \sin \frac{4\pi\gamma z_0}{\lambda} - Im \frac{bk}{4c} \sum_{m=-\infty}^{\infty} \{ & H_0^{(1)}[k(\rho_0 + 2ma)] \\ & - H_0^{(1)}[k(\rho_0 + \overline{2m+1}\, a - 2x_0)]\}. \end{aligned} \tag{B4}$$

If we consider only the special case in which $x_0 = 0$, and at the same time change from Heaviside units to ohms, these expressions become:

$$R = \frac{120\pi b}{a\gamma} \left(1 - \cos \frac{4\pi\gamma z_0}{\lambda}\right) = Z_0 \left(D - D \cos \frac{4\pi\gamma z_0}{\lambda}\right), \tag{B5}$$

$$\begin{aligned} X &= \frac{120\pi b}{a\gamma} \sin \frac{4\pi\gamma z_0}{\lambda} - \frac{60\pi^2 b}{\lambda} \sum_{m=-\infty}^{\infty} (-1)^m Y_0(k(\rho_0 + ma)) \\ &= Z_0 \left(D' + D \sin \frac{4\pi\gamma z_0}{\lambda}\right), \end{aligned} \tag{B6}$$

where Z_0 is the impedance of the line, and $D = \dfrac{120\pi b}{a\gamma Z_0}$.

Obviously, the theorems about the impedance circle hold as before.

The matching problem can be stated as before: How shall we make

$$R = Z_0 \quad \text{and} \quad X = 0\,? \tag{B7}$$

We eliminate z_0 as in Section 9, getting

$$D'^2 + 1 = 2D. \tag{B8}$$

We cannot now satisfy (B8) by choosing l, since l has been chosen as equal to b, but perhaps we can find some other parameter instead. Assuming a *given* wave guide, that is, given a, b, and λ, we may ask:

Having adjusted z_0 so that $R = Z_0$, can we adjust ρ_0, the thickness of the antenna, so that $X = 0$, that is, so that (B8) is satisfied?

It turns out that it is quite easy to match the line by choosing ρ_0. Here we shall give the matching conditions for the guide described in (9.5), that is,

$$\lambda = 10.0 \text{ cm.}, \quad a = 7.213 \text{ cm.}, \quad b = 3.404 \text{ cm.}$$

ρ_0 and z_0, giving the matching conditions, are represented as functions of Z_0 by Fig. 10. As an example, imagine that $\rho_0 = 0.1985$ cm.; then we see from Fig. 10 that the matching requires $Z_0 = 60$ ohms and $z_0 = 6.15$ cm.

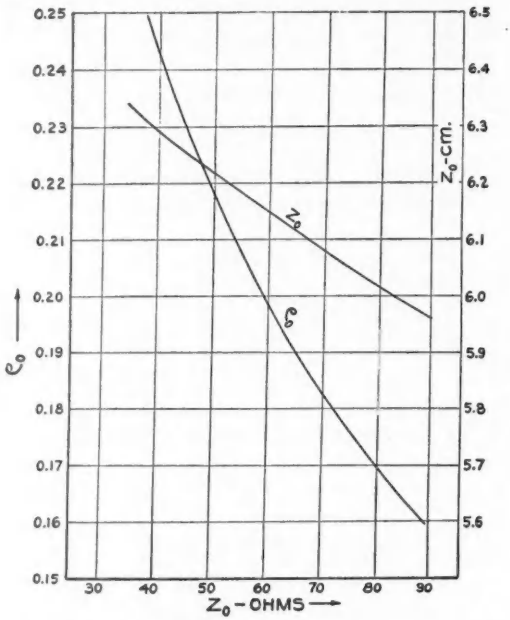

FIG. 10. *ρ_0 and z_0 as functions of Z_0. $\lambda = 10.0$ cm., $a = 7.213$ cm., $b = 3.404$ cm.*

If experiment were to verify these results, it would mean that the current distribution *is* uniform.

APPENDIX C

Resistance and Reactance as Functions of Distance between Antenna and Plug for a Wave Guide of Arbitrary Cross Section

BY A. F. STEVENSON

The results (8.2) and (8.4) for resistance and reactance can be written

$$R = A(1 - \cos 2uz_0), \tag{C1}$$

$$X = A' + A \sin 2uz_0, \tag{C2}$$

where z_0 is the distance of the antenna from the plug, $u = 2\pi/\lambda'$, λ' being the wave length in the guide, and A, A' are independent of z_0. We wish to point

out that the results (C1), (C2) hold for a wave guide of arbitrary cross section and an antenna of any shape which lies wholly in a plane distant z_0 from the plug, provided that the antenna is not too near the plug, and provided that the dimensions of the guide and manner of excitation are such that only a single E- or H-wave is transmitted. The current distribution in the antenna (provided it is independent of z_0) is immaterial.

In Part II, it was, in fact, shown that, under the conditions stated, R is proportional to $\sin^2 uz_0$, which is equivalent to (C1), but (C2) was only established in the less precise form

$$X = C_1 \cos (2uz_0 + \epsilon) + C_2 .$$

The result (C2) follows easily, however, from (16) and (18) of Part II. For, disregarding unimportant terms, these give for the impedance in the case considered

(C3) $$R - iX = Be^{2iuz_0} + C ,$$

where B, C are (real or complex) constants independent of z_0. Put

(C4) $$B = B_1 + iB_2 , \quad C = C_1 + iC_2 .$$

Then equating the real parts of each side of (C3) we obtain

$$R = B_1 \cos 2uz_0 - B_2 \sin 2uz_0 + C_1 .$$

Comparing this with (C1) (already established), we see that we must have

(C5) $$C_1 = -B_1 = A, \quad B_2 = 0 .$$

Substituting (C5), (C4) in (C3), and equating the imaginary parts of each side, we obtain

$$X = A \sin 2uz_0 - C_2 ,$$

which is equivalent to (C2). The result regarding the "impedance circle" follows as in Section 8.

VEILING GLARE IN AERIAL PHOTOGRAPHY[1]

By K. M. Baird[2]

Abstract

In this paper veiling glare is defined and its general aspects in aerial photography are discussed. Experimental results showing the effect of glare on the resolving power of a standard aerial film are presented in the form of graphs. A method of measurement is described and typical amounts encountered in widely used aerial cameras are given. From the results it is shown that veiling glare commonly causes a loss of photographic speed of as much as 100% where resolving power is the primary consideration. Recommendations are made for minimizing flare in cameras.

Introduction

Veiling glare is that scattered light which causes reduction of image contrast in an optical system. It may be conveniently expressed mathematically in different ways, depending on the particular aspect studied. For example, L. A. Jones (3) has used a "flare factor", defined as the ratio of the luminance scale of the scene to the luminance scale of the image. This factor, representing the compression of the luminance range caused by flare, was useful in studying tone reproduction. On the other hand, in the present paper, which is primarily concerned with resolving power, it has been found more convenient to use "per cent veiling glare", defined as the ratio of the amount of flare light in the image plane to the amount of pure image forming light, the ratio expressed as a per cent.

According to the definition given above, any light scattered outside the geometrical image, even that caused by diffraction or residual aberrations of the lens, might be called veiling glare; although the term is generally used only to describe light scattered over a relatively large area. The latter distinction is arbitrary and there is no sharp division either with respect to areas involved or effects on resolving power. Indeed, it is probable that the results given below could be used to predict in lines per millimeter the resolving power of a lens used in combination with Aero Super XX, if the energy distribution in the image formed by the lens were determined by use of the same film. Such a method is that used by Jones and Wolfe (4). The dependence of the amount of veiling glare found to be present on the area considered is discussed in the section on measurement of veiling glare.

In an exact study of the effect of veiling glare on the resolving power of film, the cause as well as the amount must be taken into account. This will be clear from a consideration of such typical causes as light scattered from the walls of the camera, reflections between lens surfaces, haze, etc. In the first example quoted, light that would not otherwise reach the image plane has been thrown on to the film, thereby increasing the illumination. In the second

[1] *Manuscript received February 25, 1949.*

Contribution from the Division of Physics, National Research Council, Ottawa, Canada. Issued as N.R.C. No. 1952.

example, on the other hand, the veiling glare arises from the redistribution of what was originally image forming light, and the illumination of the film is not increased in general, although the shadow areas gain light at the expense of the highlights. Thus there are two general types of veiling glare, that which increases the amount of light reaching the film and that which does not. For convenience these will be designated "Type I" and "Type II", respectively. Haze does not clearly fall into one or other of these types but will be shown later to be more conveniently considered of Type II. The difference in effect of these two types will be considered in the next section.

Of the various causes of veiling glare those due to the camera or lens are usually easy to classify as one or the other of the above two types. In the case of haze the classification is a little more difficult since in considering the difference between conditions when haze does and does not exist the effect of decreased ground illumination caused by haze must be taken into account.

If it is assumed that an exposure meter is used as a guide to the camera aperture and shutter settings, it seems logical to consider the haze as veiling glare of Type II, i.e., it reduces contrast but does not greatly affect the average image luminance, since the meter reads the luminance of ground plus haze. Haze could be measured as a per cent veiling glare by determining the loss of contrast of objects that were of known contrasts on the ground. In this paper only measurements of veiling glare caused in the camera or lens are described.

Effect of Veiling Glare

The effects of the two types of veiling glare are indicated in Figs. 1 and 2 as a modification of the characteristic curve of the film. The characteristics

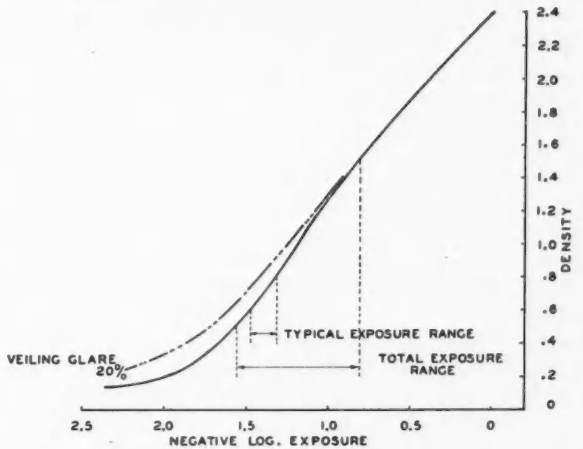

FIG. 1. *Characteristic curve of Super XX Aero Film showing modification caused by 20% veiling glare in the case where glare consists entirely of added light. The range of typical exposures and the total exposure range are taken from a British report (5).*

of the film itself are unchanged of course but the reproduction of tones under the given conditions of veiling glare is equivalent to that by a film having the modified characteristic curve under conditions of no glare. For the following

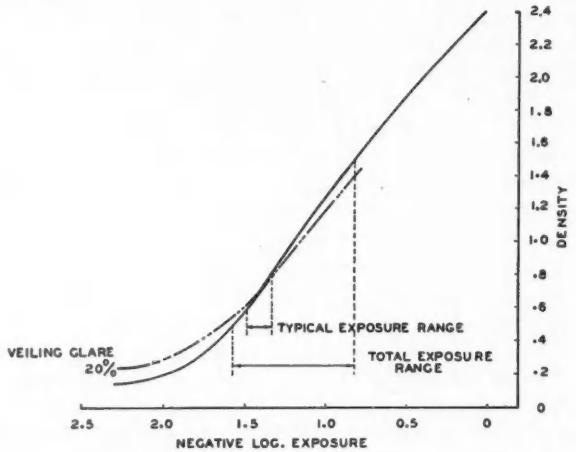

FIG. 2. *Same as Fig. 1 except that the veiling glare arises from what was originally image forming light.*

discussion it is convenient to define "object exposure" as the exposure that would result if the causes of veiling glare were absent, as distinguished from the "image exposure", which the film receives in the image plane. The corresponding terms "log object luminance ratio" and "log image luminance ratio" will also be used.

The broken lines of Figs. 1 and 2 are graphs of the densities on an Aero Super XX film, plotted as ordinates, that result from the log object exposures that are plotted on the abscissa. The solid lines of both figures are characteristic curves of Aero Super XX film and therefore identical. The broken line of Fig. 1 was obtained by finding the density that resulted from the object exposure plus 20% of the typical object exposure in aerial photography. This density was then plotted against the log object exposure. The densities on this curve are of course always greater than the Super XX densities owing to the added light, but the two curves approach each other asymptotically at large exposures.

The broken line of Fig. 2, which represents veiling glare of Type II, was obtained by finding the density that resulted from the object exposure less 1/6 (i.e., 5/6 of the object exposure) plus 1/6 of the typical object exposure. It is clear that this corresponds to 20% veiling glare as it is defined above. This curve has the same shape as that of Type I but differs in that it crosses the Super XX curve at the typical log object exposure, namely -1.4 log meter candle seconds.

It should be understood that the log exposure values along the abscissa do not represent for the modified curves the actual log exposure on the film but rather the exposure that would result under conditions of no glare, i.e., they are log object exposures. The log image exposure corresponding to a given point on the modified curve is given by considering the point on the solid curve representing the same density as the given point.

It is pointed out that using 20% of the exposure at the middle of the typical exposure range as the added light is equivalent to assuming that the average exposure is the same as the typical exposure. This does not exactly represent conditions in an aerial photograph but it is felt that the inexactness does not affect the conclusions drawn except when there are unusually bright sources in the field of view.

The range of typical exposures and the total range of exposures shown in the figures were taken from a British report based on statistical findings in reconnaissance photography over Europe during the war (5).

The figures show that the two types of glare have different effects. In the case shown in Fig. 2, at the region of typical exposures, the glare reduces the optical contrast without affecting the exposure, with the result that the photographic contrast is reduced. In Fig. 1, on the other hand, the exposure is increased, resulting in the use of a different part of the Super XX curve. Since the slope of the curve is increasing, the loss of optical contrast tends to be compensated photographically in the lower part of the exposure range. It is noteworthy that in Fig. 1 the contrast on the film is actually increased at the toe of the curve although obviously the contrast of the optical image is always reduced by veiling glare. This is caused by the rapid change in slope at the toe of the true characteristic curve of the film. The effects on resolving power will be discussed in detail in a later section.

Determination of Effect on Resolving Power

The effect of various amounts of veiling glare on the resolving power of a camera–film combination was found by calculating the resulting change in contrast and making use of experimental curves relating resolving power to log exposure and contrast. A set of such curves for Super XX Aero Film processed in D-19*b* to a gamma of 1.34 is shown in Fig. 3.

These curves were obtained by printing sets of resolution charts on strips of film, the charts being illuminated through a calibrated optical step wedge. One of the films so obtained is reproduced in Fig. 4. Resolving power readings from such a film, together with the calibration of the wedge, gave one of the curves. (Each curve in Fig. 3 represents the average of several films.) The different curves were obtained by using charts of different contrasts. Processing was done with the accurate control that is usual in sensitometry. From the H and D curve, which also has been plotted in Fig. 3, it is seen that the range of typical densities recommended in the British paper (5), quoted above, lies in the region of maximum resolving power for a log luminance ratio of 0.2.

This value is given as the typical object contrast by the same report. In these curves and throughout this paper, contrast is expressed as the log of the luminance ratio of the two target areas. The log exposure is given for the brighter target area so that when the log exposure is such that the density resulting on the film is zero, the resolving power is also zero.

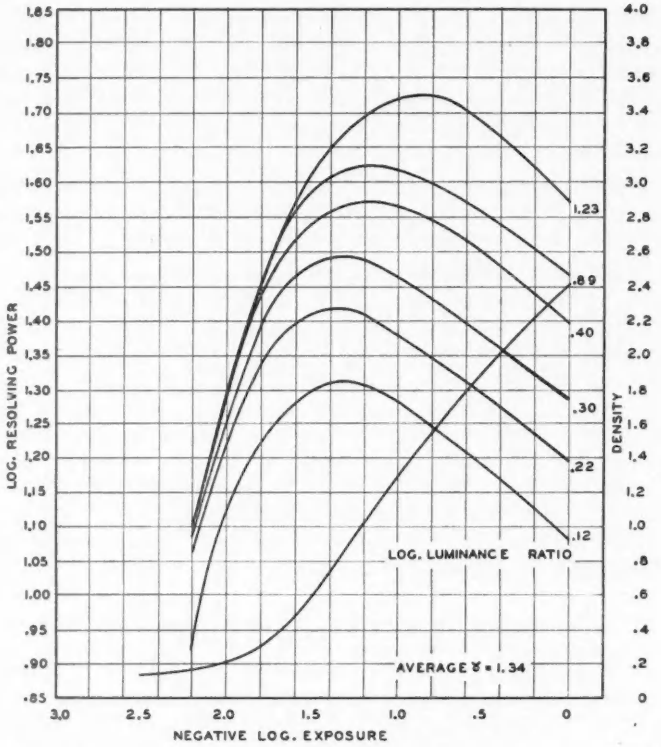

FIG. 3. *Curves showing the variation of resolving power with log exposure for various log luminance ratios of the test target for Super XX Aero Film developed in D-19b. The densities along the right-hand side of the graph refer only to the H and D curve. The log resolving power values refer to the other curves.*

The solid curves in Figs. 5, 6, and 7 were obtained from Fig. 3 by interpolation and have been plotted on a larger scale for convenience. These graphs show three variables, giving the resolving power for any log exposure or contrast in the range covered. Thus by calculating the change in log exposure and contrast caused by a given amount of veiling glare, the change in resolving power can be obtained. This has been done for values of 10, 20, and 40% veiling glare of Type I in Figs. 5, 6, and 7 respectively. The change in resolving power is indicated by the arrows and by the broken curves, which

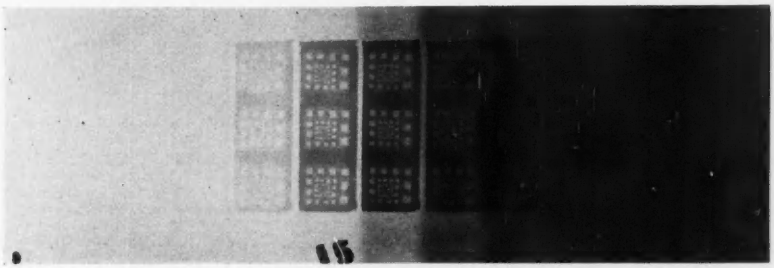

FIG. 4. *A reproduction of one of the films used to obtain the curves in Fig. 3.*

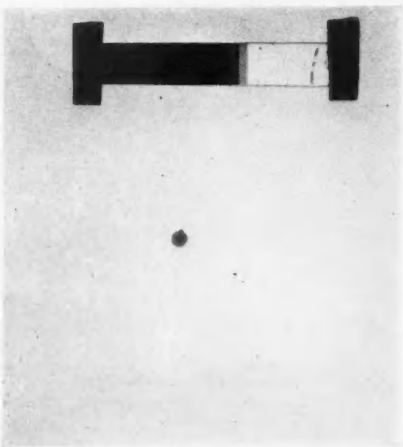

FIG. 9. *Shows a picture taken in the tunnel in Fig. 8 for the determination of per cent veiling glare in an aerial camera. Note the grayness of the image of the black hole.*

were obtained by calculating the modified log exposure and modified contrast for the given amounts of veiling glare. The modified log exposure was calculated by adding to the corresponding original exposure value a certain per cent of the typical exposure. By doing this for a given log exposure value and also for that value decreased by the log luminance ratio, two modified

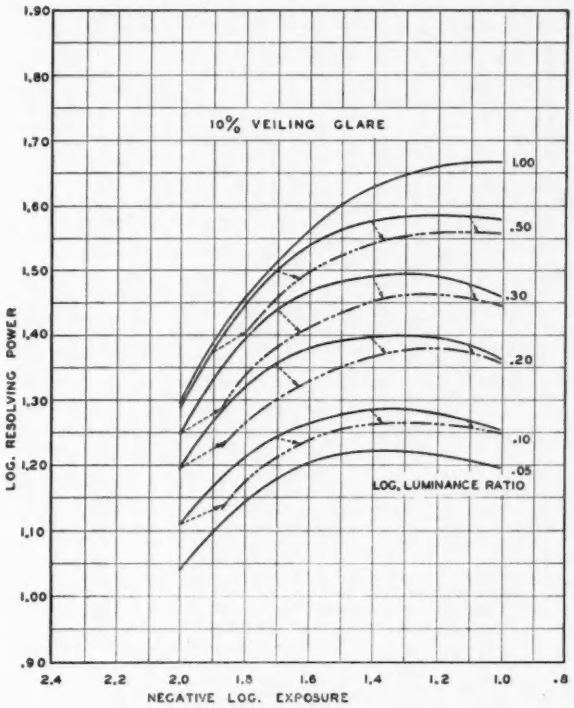

FIG. 5. *Curves showing the effect of 10% veiling glare on the resolving power of Super XX Aero Film. The solid curves, obtained from Fig. 3, show the variation of resolving power with log exposure when there is no glare. The arrows show the change in position on the graph caused by 10% veiling glare. The broken curves show the modification of the film characteristic that results.*

log exposure values were obtained, the difference of which gave the modified log luminance ratio contrast.

From the modified log exposure and contrast the resolving power is given by the appropriate point on the graphs. Corresponding points on curves without veiling glare (solid) and curves with veiling glare (broken) are represented by the tail and the head of an arrow respectively. Hence the change in resolving power due to a certain per cent veiling glare may be found by reading the head and tail of an arrow. For example log object exposure

$= -1.4$ and log object luminance ratio $= 0.2$ gives a log resolving power of 1.4 if there is no veiling glare. In the presence of 20% veiling glare of Type I this is changed to 1.35.

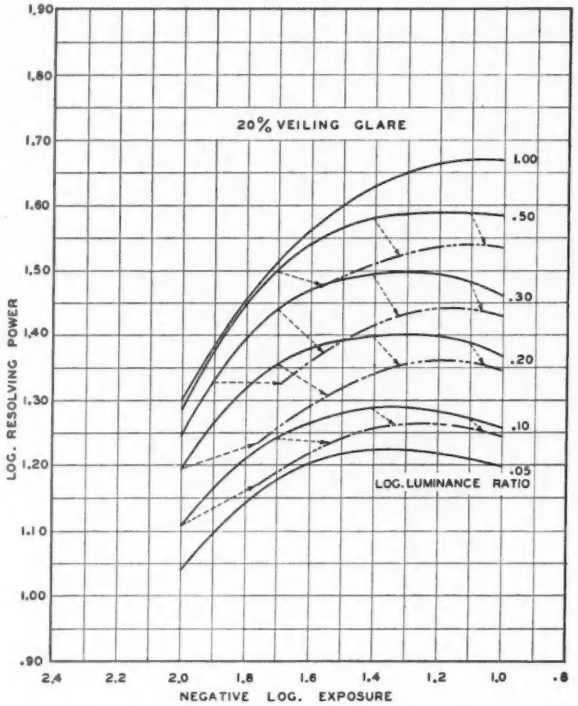

FIG. 6. *Same as Fig. 5 for 20% veiling glare.*

The effect of Type II veiling glare can also be obtained from the graphs. It can be shown that in this case the modified contrast is the same as for Type I but the modified log exposure is less than for the latter by an amount log $(1 + V/100)$, where V signifies the per cent veiling glare. Thus for the point considered in the preceding example the modified log exposure is the same as the original (as would be expected at the middle of the typical exposure range) and the modified resolving power is therefore again about 1.35 (given by a point slightly above the broken curve).

The graphs show that Type II veiling glare caused greater loss of resolving power at low exposures but less loss at high exposures than Type I. However, as the above example shows, the difference is not great for the log exposure range of -1.3 to -1.5, i.e., in the range of typical exposures in aerial photography. In fact the difference is not significant for the arguments in this

paper, and therefore the two types will not be considered separately hereafter. In any case, in practice both types exist simultaneously.

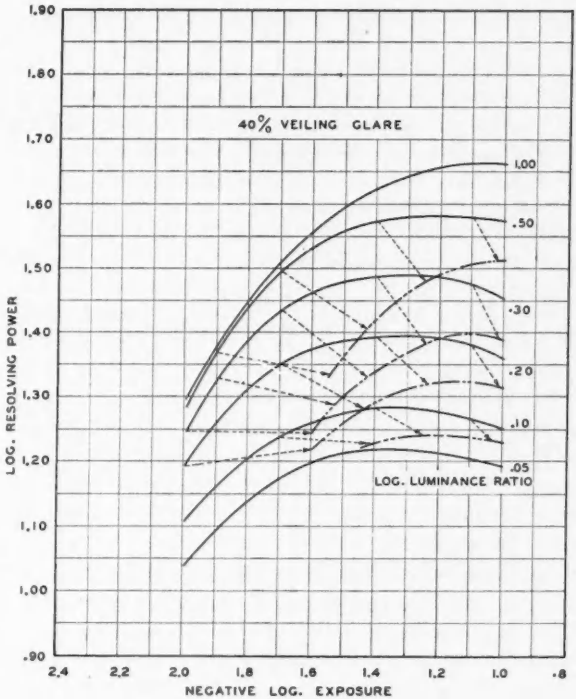

Fig. 7. Same as Fig. 5 for 40% veiling glare.

Discussion of Results

Considering a log luminance ratio of 0.20, Fig. 5 shows that 10% veiling glare changes the log resolving power by about −0.03, i.e., a reduction of about 7%, in the typical exposure range. This amount is of the same order as the variation in lens–film resolving power from lens to lens in good quality survey lenses (2) and is therefore not serious. On the other hand 20 and 40% cause losses of about 12 and 20% respectively. The latter amounts are great enough to be undesirable but frequently occur in practice, as will be seen in the next section.

Instead of considering the effect of veiling glare as a loss of resolving power it may be thought to constitute a loss of camera speed. Thus if film speed is determined using the resolving power criterion suggested by L. E. Howlett (1), then the minimum acceptable exposure (i.e., that giving 90% of the maximum resolving power when the log luminance ratio is 0.20) is −1.70

for the film being considered, in the absence of veiling glare (see Fig. 6). To realize the same log resolving power (viz., 1.35) in the presence of 20% veiling glare on the other hand, the log exposure must be −1.35. This is an increase in log exposure of 0.35 or an increase in the exposure of over 100%. As a result a camera equipped with an $f/5.5$ lens having 20% veiling glare would be effectively no faster in cases where resolving power is the prime consideration than one with an $f/8$ lens free from glare, assuming the same quality in other respects. While this admittedly may exaggerate the situation (for example if the minimum criterion had been 95% of the maximum, the loss in speed would have been infinite) it is felt nevertheless that the effect is more serious than is generally realized. To state the effect generally: for the useful range of exposures any resolving power obtainable in the presence of veiling glare can be achieved with less exposure if the glare is reduced. This effective increase of camera speed is more significant than gain of transmission if lens surfaces are coated to reduce reflection. An example is described in the section "Veiling Glare in Some Existing Cameras" that follows. Corresponding changes of photographic speed as determined by density criteria can be seen by considering Figs. 1 and 2.

It is interesting that for very low exposures 10 or 20% veiling glare increases the resolving power. It is this effect that is sometimes used in spectrographic work to detect very faint lines by deliberately fogging the photographic plate. However, over the range of exposures used in aerial photography the glare causes a loss of resolution.

Since the change of resolving power has been determined for the film alone, it might be argued that the results would not be valid for a lens–film combination. However it is felt that the conclusions would be the same in the latter case because the lens–film resolving power does not generally differ greatly from the resolving power of the film alone when fast relatively coarse grained film is used, as is the case in aerial photography.

Measurement of Veiling Glare

The amounts of veiling glare caused by inherent defects in camera–lens combinations have been determined for several widely used aerial cameras. The method of measurement was to photograph a field of view, which was of uniform luminance except for a black spot subtending an angle of about one degree, with the camera under test. A specially constructed tunnel shown diagrammatically in Fig. 8 was used to provide this field.

In the film plane of the camera a small calibrated optical step wedge was placed so that part of the bright field became exposed through it. An example of the pictures that resulted is reproduced in Fig. 9. After processing the film carefully, using brush development, suitable temperature control, etc., densities were read for the image of the steps of the printed wedge, the black spot, and the field. The characteristic curve of the film was plotted from the wedge densities and the log exposure difference between the images of the black spot

and the background obtained from the curve as indicated in Fig. 10. The antilog of the value obtained is the ratio: $\frac{\text{Glare}}{\text{Glare} + \text{Image light}}$. If this ratio is called R then the per cent veiling glare is given by: $\frac{R}{1 - R} \times 100$.

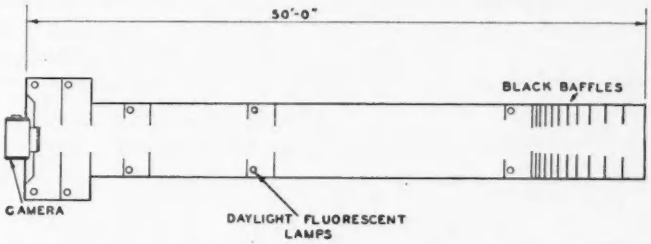

FIG. 8. *Diagrammatic view of the tunnel used to measure veiling glare in aerial cameras. The sections of the tunnel containing the lights are painted white; the rest is black.*

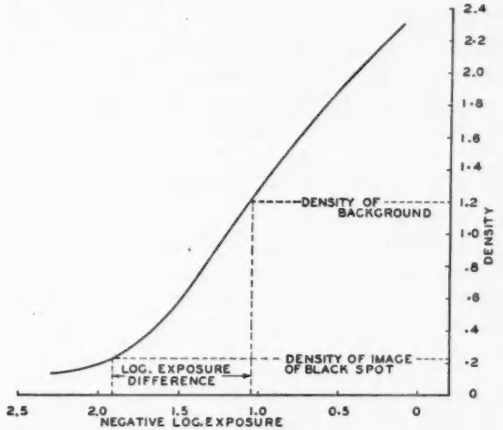

FIG. 10. *Characteristic curve of the film shown in Fig. 9 plotted from the wedge included in the picture. The dotted lines indicate how the log exposure difference between the image of the black hole and the background is determined.*

The value for "Glare + Image light" was measured in the immediate neighborhood of the point in the field where the veiling glare was being determined. This is in general different from a value averaged over the whole field of view because of vignetting, the cosine effect, variation over the field of the amount of flare, and so on. The choice of the former value is obviously the logical one in view of the method of determining effects on resolution discussed in the previous sections.

Recalling the discussion in the second paragraph of the introduction it is seen that, because the black spot used in the measurement described above

subtends about a degree, only light that is thrown at least a half degree from the edge of the geometrical image is included in the value obtained for the glare light. This is an arbitrary amount, and no attempt is made to justify it in this paper except to say that veiling glare has been used to describe only that light which is scattered over a "relatively large" area. In the case where secondary images are formed by reflection between lens surfaces it is clear that the scattered light may involve any area, as the secondary image may be very much out of focus or in focus and coincident with the primary image.

It is apparent that the method described above gives the per cent veiling glare that is effective when the camera is used in service because the color sensitivity, diffuseness of pickup of energy, etc., is identical in the test and in service use, provided the same kind of film is used. Conditions have necessarily been idealized in that a uniformly bright field of view has been used but this does not lead to serious error except in special circumstances, such as cases when the sun is in or nearly in the field of view, which cases must be considered separately.

The usual objections to photographic photometry such as reciprocity law failure, variation in processing, etc., are obviously not valid here because of the method used. Reproducibility of measurements has been found consistent with the practical considerations involved. For example, three separate tests on the axis of Camera *D* in Table I gave the values: 20, 25, 24% respectively.

Veiling Glare in Some Existing Cameras

The glare found in several widely used aerial cameras is shown in Table I. *A* and *B*, a short focal length reconnaissance camera and a survey camera respectively, are representative of cameras having fair correction. The cones are painted black inside and are large enough so that there is little tendency for light to be reflected specularly on to the film. Neither camera has coated

TABLE I

Camera	Veiling glare on axis, %	Veiling glare at edge of field, %
A	13	7½
B	22	8
C	35	11
C'	11	9
D	23	14
E	7	4

The identification of the cameras mentioned in the preceding table is as follows:

A is an F24 reconnaissance camera.

B is a Fairchild K 17b with a 6 in. Bausch & Lomb Metrogon lens.

C and C' represent a Williamson O.S.C. with a 6 in. Ross W.A. Survey lens.

D is a Fairchild F224 Cartographic camera with a Metrogon lens.

E is an F52 camera with a 36 in. F/6.3 N.R.C. Booth Telephoto lens.

lenses, but the curvatures of the lens surfaces of Camera *A* are not very steep. Camera *B* has steeply curved lenses, and coating the lenses would likely reduce the glare to a value close to that of Camera *A*. The results given in the preceding section indicate that these cameras have lost about 10% of their potential resolving power because of veiling glare. This amount is not serious although it would be worthwhile to reduce it, especially in Camera *B*.

Camera *C* is a recently designed aerial survey camera that is well baffled. The unusually high veiling glare was found to be caused by reflections from the lens surfaces, which are very steeply curved, with the result that reflections at large angles of incidence cause light to be thrown back into the camera. *C'* is the same camera after the lens was coated with antireflection films. The glare has been reduced to an unobjectionable amount.

Another recently designed survey camera with not much more than normal glare under normal conditions is Camera *D*. However, apparently in the interests of compactness, the cone was designed to fit the outside rays very closely, with a disregard for veiling glare, and no field limiting baffle was provided outside the lens. The result is slightly increased glare (especially at the edge of the field) under normal conditions, viz., when the field of view is of nearly uniform luminance. When very bright sources such as clouds or lakes with the sun reflected from them are imaged on the inside of the cone, serious glare results. From measurements on the camera and on aerial negatives showing lakes it was found that glare of over 35% could be expected frequently.

Camera *E* is a well designed long-focal-length reconnaissance type with relatively flat lens curves. Fig. 11 shows typical variation of glare with angle in the field.

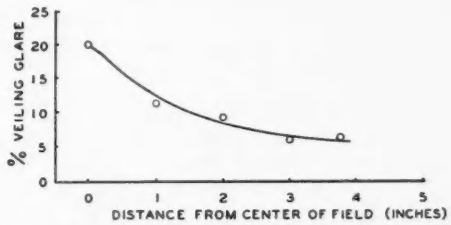

FIG. 11. *Curve showing typical variation of veiling glare across the field of view of an aerial camera.*

Conclusion

From the foregoing results it is seen that in an aerial camera in which reasonable care has been taken in design, veiling glare will be of the order of 10 to 15%, corresponding to a reduction in resolving power in the typical exposure range of about 10%. Whereas this amount is undesirable it is not serious and it is generally not practical to reduce it.

It is also evident however that lack of care in design might result in veiling glare of the order of 40%. This would cause a loss of resolving power of over 20% or an equivalent serious loss of speed.

To keep veiling glare at a minimum it is recommended that the lens surfaces be coated to reduce reflection if there are many elements or if the surfaces are steeply curved, as is usually the case with wide angle lenses. There should be a field limiting cone outside the lens. The lens tunnel should be large, well baffled, and blackened on the inside.

Whereas the experimental results given above are for aerial cameras and one photographic emulsion, the general conclusions apply to photography in general.

Acknowledgment

The author wishes to express his gratitude for the invaluable assistance of Dr. L. E. Howlett and P. A. Tate in this research.

References

1. HOWLETT, L. E. Can. J. Research, A, 24 : 1. 1946.
2. HOWLETT, L. E. Can. J. Research, A, 24 : 15. 1946.
3. JONES, L. A. and CONDIT, H. R. J. Optical Soc. Am. 31 : 638. 1941.
4. JONES, L. A. and WOLFE, R. N. J. Optical Soc. Am. 35 : 559. 1945.
5. ROYAL AIRCRAFT ESTABLISHMENT, Technical Note, No. 190 (Ph. 513/GCB/57). June, 1942.

RELATIVE YIELDS OF THE D-D REACTIONS AT LOW ENERGIES[1]

By T. P. Pepper

Abstract

By the simultaneous detection of the p, T, and He^3 particles in a thin window proportional counter the concurrent nuclear reactions $D(d,p)T$ and $D(d,n)He^3$ have been investigated throughout the deuteron energy range 26 to 63 kev. The ratio of the yield of the reaction $D(d,p)T$ to that of the reaction $D(d,n)He^3$ was found to be 1.15 ± 0.15 throughout this energy range. There is some slight evidence for an increase in this ratio towards lower bombarding energies.

Introduction

The bombardment of deuterium with deuterons produces the concurrent nuclear reactions

$$D(d,p)T \qquad Q = +4 \text{ Mev.}$$

and

$$D(d,n)He^3 \qquad Q = +3.3 \text{ Mev.}$$

which will be referred to collectively as the D–D reactions. Various aspects of these reactions have been reported in the literature. When the present work was done early in 1948, however, the literature contained no reference to the simultaneous measurement of the D–D reactions at *low* energies. In addition it appeared that no study of the yields had been made using *similar* methods of monitoring the two reactions, as, for example, the detection of the charged products from each reaction as herein described. The present work was undertaken to show that the yields from both reactions could readily be measured simultaneously and under identical conditions. This method could therefore provide a simple means of obtaining the ratio of the yields at low energies.

Reasons for the present experiment are suggested below. Measurement of the reactions $D(d,n)He^3$ by means of the He^3 particles would provide a useful standard of neutron emission. Obtaining the relative yields of the two D–D reactions would permit a neutron standard to be established from measurements of the yield of the more readily detectable protons and tritons. Knowledge of the ratio of the yields of the D–D reactions as a function of bombarding deuteron energy might prove useful in estimating the relative importance of the Coulomb and centrifugal barriers in the formation of the reaction products.

[1] *Manuscript received March 10, 1949.*

Contribution from the Nuclear Physics Branch, Chalk River Laboratory, Division of Atomic Energy Research of the National Research Council of Canada. Issued as N.R.C. No. 1956. This work was part of a thesis submitted to McGill University in partial fulfillment of the requirements for the degree of Doctor of Philosophy, October 1948.

Experimental Method

A small 50 kv. accelerator, designed and built by D. Roaf, employed a conventional 25 kv. voltage-doubler circuit. The ion source was a radio-frequency positive ion source designed and built by A. J. Bayly and A. G. Ward (1). The ion beam was employed without resolution. It consisted, as described by Ward and Bayly, of about 200 μa. mixture of masses 1 to 6, the odd integral masses being due to hydrogen impurities in the deuterium. Approximately 50% of the total beam was atomic heavy hydrogen: the relative intensities of D^+, DD^+, and DDD^+ were 6, 2, and 1: the relative energies were E, $E/2$, and $E/3$. The yields at energy E were one to two orders of magnitude greater than those at $E/2$ or $E/3$. To a good approximation, therefore, the observed yields were due to the higher energy, more intense atomic deuteron beam. It is the energy of this beam that is quoted throughout. For extracting and focusing the ions two separate 0 to 10 kv. power supplies were available. Thus an ion had a maximum energy of 70 kev. The voltage was measured directly by observing the current through a 50 megohm chain of carbon resistors. Since the present method of determining the relative yields of the D–D reactions did not require precise determination of this voltage, the resistor chain was not calibrated for voltage or thermal variations.

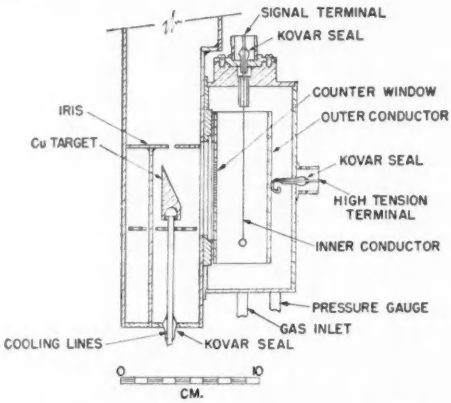

FIG. 1. *Cross sectional view of a water-cooled copper target for condensing the deuterons and proportional counter for detecting protons, tritons, and He^3 particles.*

Fig. 1 represents a cross-sectional view of target and cylindrical counter. The deuterium target was a condensation target, i.e., a water-cooled copper target onto which the impinging ions condensed, forming a deuterium layer that was then bombarded by succeeding deuterons in the beam. The resultant particles from the D–D reaction, i.e., 3 Mev. protons, 1 Mev. tritons, 2.4 Mev. neutrons, and 0.8 Mev. He^3 particles, penetrated a thin Formvar window and entered the sensitive volume of the proportional counter in a cone of semiangle 20°. This degree of collimation was effected by an array

of 0.040 in. holes drilled in a 0.1 in. steel plate, which supported the Formvar window. During the experiment, windows of 0.25 and 0.12 mgm. per cm.^{2} were used. A thin layer of gold was sputtered onto the Formvar windows to render them conducting and to reduce the light entering the counter from the deuteron beam and target. The minimum path length in the counter for the charged particles was 3 cm. For most of the runs, methane was used as counter filling. The final series of runs was made, however, using *n*-octane vapor at room temperature (7). The counter was operated with a gas amplification of approximately 100. The ionization pulses were further amplified, sorted according to size, and counted.

Experimental Results

The experimental procedure was arranged, first, to identify the three groups of pulses observed on the pulse analyzer (8), and, second, to obtain the relative yields of the D–D reactions. The results are most readily presented by referring to representative pulse distributions observed.

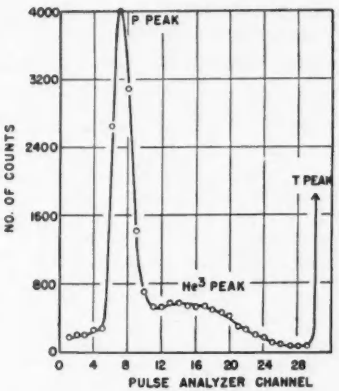

FIG. 2. *Proton, triton, and He^3 pulses from the D–D reactions. Methane-filled proportional counter at pressure of 30 cm. of mercury. Formvar window 0.25 mgm. per cm.^{2} Energy = 39 kev.*

Figs. 2, 3, and 4 show the three groups of pulses labelled as subsequently identified. In Fig. 2 (counter pressure, 30 cm. of mercury) the He^3 peak is broad and spreads across the sharper, less energetic proton peak, while the triton peak falls entirely in Channel No. 30, the last channel, of the pulse analyzer. This channel counted all pulses above a certain size. By reducing the pressure in the counter the triton peak emerges as shown in Fig. 3 (counter pressure, 18 cm. of mercury) to become a well resolved peak while the He^3 peak is somewhat sharpened and the proton peak has receded into the noise background of Channel No. 1. By still further reducing the pressure in the counter the relative positions of the triton and the He^3 peaks were interchanged, as

expected (Fig. 4). At counter pressures of 1.9 cm. of mercury the He^3 peak became sharp and similar to the proton or triton peak.

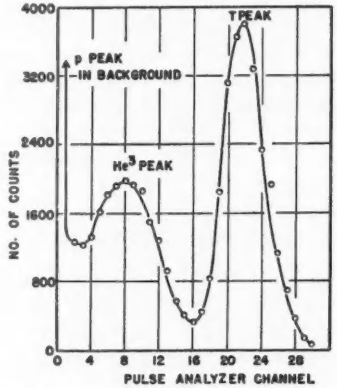

FIG. 3. *He^3 and triton pulses from the D–D reactions. Methane-filled proportional counter at pressure of 18 cm. of mercury. Formvar window 0.25 mgm. per cm.² Energy = 60 kev.*

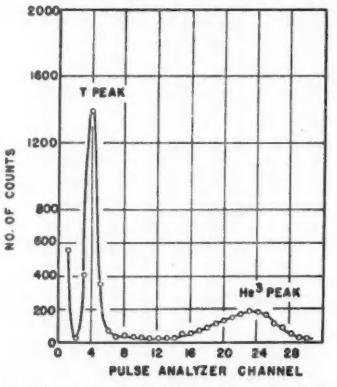

FIG. 4. *Triton and He^3 pulses from the D–D reactions. Methane-filled proportional counter at pressure of 3.5 cm. of mercury. Formvar window 0.12 mgm. per cm.² Energy = 43 kev.*

The ratio of the yields of the D–D reactions was obtained in three ways from the resolved proton, triton, and He^3 peaks. These are best illustrated with reference to Figs. 2 and 4.

Method A

For the counter filled with methane to a pressure of 30 cm. of mercury (Fig. 2) the triton pulses fell in Channel No. 30. By counting these pulses and the pulses associated with the combined proton and He^3 peaks, the ratio of the number of counts $\frac{T}{(p + He^3) - T}$ can be obtained. This is equivalent to the ratio T/He^3.

Method B

Again from Fig. 2 the ratio p/He^3 can be obtained by direct interpolation of the He^3 peak beneath the p peak.

Method C

For the counter filled with methane to a pressure of 3.5 cm. of mercury the T and He^3 peaks were resolved as illustrated in Fig. 4. Upon an arbitrary assignment of those counts lying between the main portions of the T and He^3 peaks a straightforward deduction of the ratio T/He^3 is obtained. Two extreme cases were considered: the one apportioned the ambiguous counts so as to maximize the ratio T/He^3, the other to minimize it. The largest spread encountered in all the cases considered was 14%. The consistent cleanness of the T peak and the characteristic straggling of the He^3 peak lead to an arbitrary weighting of 2 : 1 in favor of assigning the doubtful counts to the He^3 peak.

Ratios obtained by Methods *A*, *B*, and *C* are each treated as equivalent to the ratio of the yields of the reactions $D(d,p)T$ and $D(d,n)He^3$. Had the peaks been completely resolved from one another and any spurius background, all three methods would have given the same results. The three methods are presented and employed therefore to indicate the amount of uncertainty introduced by the imperfect resolution. Averaging of the results removes in large part the errors associated with any one of the methods outlined above.

Each method was applied at various deuteron energies from 26 to 63 kev. The ratios so obtained are presented in Table I.

TABLE I

MEASUREMENT OF YIELDS OF $D(d,p)T$ AND $D(d,n)He^3$

	d-energy kev.	Counter filling, in cm. Hg	Ratio of yields
		CH_4	
Method *A*			
Ratio calculated			
$\frac{T}{(p + He^3) - T}$	27	30	1.07
	39	30	1.06
	59	30	1.10
Method *B*	34	30	0.99
Ratio calculated	40	30	1.07
$\frac{p}{He^3}$	45	30	1.11
	51	30	1.12
	56	30	1.12
	62	30	1.12
Method *C*	27	3.4	1.35
Ratio calculated	31	3.5	1.19
$\frac{T}{He^3}$	44	3.5	1.20
	52	3.5	1.16
		C_8H_{18}	
	26	0.5 - 1.0	1.31
	61	0.5 - 1.0	1.28

Discussion of Results

Method *C* was applied to runs made using a window 0.12 mgm. per cm.^{2}, i.e., half the thickness of the one providing the data for Methods *A* and *B*. This was permitted by the lower pressure requirements of Method *C*. That the ratios obtained by Method *C* are some 8% higher than those obtained by Methods *A* and *B* may indicate selective absorption of the He^3 particles by the window. The ratios 1.31 and 1.28 deduced using Method *C* at bombarding energies 26 and 61 kev. were obtained using *n*-octane vapor at room temperature. These ratios are in satisfactory agreement with those obtained using methane at about six times the pressure.

The possibility of selective absorption of the charged products by small irregularities in the surface of the target was considered but thought to be unlikely, as indicated by the following argument. To the deuteron beam the target depth was just that for the *energy* of the deuteron beam. This depth l was never greater than 63 kev. The target made an angle of approximately 30° with the deuteron beam. The particles entering the counter therefore penetrated a maximum target of l tan $(30 \pm 20)°$. For a perfectly smooth target only the shortest range particles (He^3 of 4 mm. air equivalent) need be considered. The He^3 particles, would, on their way to the counter, lose less than 100 kev. in the target. With the windows used this would broaden but not decrease the He^3 peak. On the other hand, for a target with small metal spurs, the emitted particles might indeed be prevented from entering the counter. However, if such were the case for an appreciable fraction of the particles, those that did enter the counter would not form a defined peak. The fact that the He^3 particles did produce such a peak, which with adequate reduction of the counter stopping power could be sharpened to resemble the *p* or T peak, is good evidence against serious loss of the He^3 particles before entry into the counter. As a precautionary measure the copper target was always very highly polished with Hydro-Durexsil 700 paper and only in an up and down motion so that whatever grooves were formed would be in the plane containing the beam, the target, and the counter window.

The possibility that the measured ratio was altered by scattering of the emitted particles on their way to the counter was considered. Assuming the scattering to be of the same order of magnitude as that of deuterons on deuterium as reported by Blair *et al.* (2), the fraction of *p*, T, He^3 particles scattered before entry into the counter was found to be negligible.

The D–D reaction products are known to be anisotropically distributed in the center of mass system of co-ordinates. Bretscher, French, and Seidl (4) have measured the angular distribution of protons for deuteron energies 20 to 80 kev. They found that the angular distribution could be represented by the relation $N_\theta = N_{90}(1 + A \cos^2 \theta)$, where N_θ is the proton flux proceeding at an angle θ to the deuteron beam and N_{90} is the flux proceeding perpendicularly to the beam. The quantity A is a function of the deuteron energy

and increases linearly from 0.25 at 20 kev. to 0.45 at 80 kev. The angular distribution of the neutrons has not been determined at these low energies. At higher energies, however, the angular distributions are similar for protons and neutrons (3). It is therefore unlikely that they differ radically at low energies. In the case of identical angular distribution functions for protons and neutrons the ratio of the fluxes at $\theta = 90°$ can correctly be taken as the ratio of the total yields of the reactions D(d,p)T and D(d,n)He^3. In the extreme case, that the neutron flux is isotropic for the energies considered, the error so introduced is only 6%. That the angular distribution of the neutrons is markedly more asymmetric than that of the protons is very unlikely. It is improbable therefore that the error introduced by the angular distribution is more than 2%.

From Table I it is seen that the ratio of the yields of the reaction D(d,p)T and D(d,n)He^3 is 1.15 ± 0.15 throughout the energy range 26 to 63 kev. Assuming that the results obtained using the thinner window and Method *C* are the more reliable there is some slight evidence that the ratio increases toward lower deuteron energies.

Blair *et al.* (3) have found that throughout the energy range 1 to 3.5 Mev. the ratio of the cross sections of the reactions D(d,p)T and D(d,n)He^3 is almost constant and equal to 0.9. The reaction D(d,n)He^3 was detected by means of the He^3 in a proportional counter, but owing to the high energy of the scattered deuterons the He^3 particles and protons were not monitored simultaneously but at different times using windows of different thickness. At the low deuteron energies of the present experiment, the scattered deuterons could not enter the counter, and hence the charged products could readily be detected together.

Coon and co-workers (5, 6) have investigated the D–D reaction throughout the energy range 100 to 300 kev. and have found that the ratio of the cross sections of the reactions D(d,p)T and D(d,n)He^3 is 0.6 at 300 kev. and 1.0 at 130 kev. Their results indicate by extrapolation that at still lower energies the ratio exceeds unity. These results were obtained by detecting the protons in an ionization chamber at angles of 20°, 45°, and 90° to the deuteron beam and the neutrons in a surrounding manganese sulphate solution. The relative cross sections therefore required the use of a neutron standard, a complication not met when the reactions are detected entirely by the charged particles. The present results are consistent with those of Coon *et al.*, extrapolated to lower energies.

Acknowledgments

The author wishes to acknowledge with thanks the assistance of Mr. A. G. Ward for supervision of the work, Mr. G. C. Hanna for the designing of the electronic equipment, and Dr. B. W. Sargent for an encouraging interest in the work and aid in presenting the details of the experiment.

References

1. BAYLY, A. J. and WARD, A. G. Can. J. Research, A, 26 : 69. 1948.
2. BLAIR, J. M., FREIER, G., LAMPI, E., SLEATOR, W., JR., and WILLIAMS, J. H. Phys. Rev. 74 : 1594. 1948.
3. BLAIR, J. M., FREIER, G., LAMPI, E., SLEATOR, W., JR., and WILLIAMS, J. H. Phys. Rev. 74 : 1599. 1948.
4. BRETSCHER, E., FRENCH, A. P., and SEIDL, F. G. P. Phys. Rev. 73 : 815. 1948.
5. GRAVES, A. C., GRAVES, E. R., COON, J. H., and MANLEY, J. H. Phys. Rev. 70 : 101. 1946. *See also* M.D.D.C. 207.
6. MANLEY, H., COON, J. H., and GRAVES, E. R. Phys. Rev. 70 : 101. 1946. *See also* M.D.D.C. 206.
7. PEPPER, T. P. Rev. Sci. Instruments, 20 : 222. 1949.
8. WESTCOTT, C. H. and HANNA, G. C. Rev. Sci. Instruments 20 : 181. 1949.

THE SPECIFIC HEAT OF NAPALM*–GASOLINE GELS[1]

By G. O. Langstroth[2] and K. H. Hart

Abstract

The heat capacities of gasoline, Napalm, and various Napalm–gasoline gels have been measured in the range −50° C. to 50° C. by the method of mixtures, using an ordinary type of Richard's adiabatic calorimeter. The specific heat in calories per gram per Centigrade degree at a temperature T° C. within this range is given to within 2% by the relation

$$S_T = 0.479 - 0.00054C + 0.00092T,$$

where C denotes the Napalm concentration in per cent by weight. Concentrations of 0% and 100% are included. These data supplement earlier results on thermal conductivity.

The thermal conductivity of Napalm–gasoline gels has been determined previously (2) over the temperature range −50° to 50° C. with Napalm concentrations from 0 to 10% by weight. Specific heat data for the same temperature range with Napalm concentrations from 0 to 100% are presented in this article.

Apparatus and Procedure

The determinations were made by the method of mixtures with the ordinary type of Richard's adiabatic calorimeter. The cylindrical brass calorimeter vessel (diameter, 2 in.; height, 4 in.) was mounted on an insulating support inside a water-tight brass jacket (diameter, 3 in.; height, 5½ in.). The jacket was immersed in a motor-stirred water bath of 3 gal. capacity. Samples were introduced to the calorimeter vessel through a tube soldered to the top of the jacket and extending just above the bath level; normally the tube was closed with a cork. The calorimeter vessel was provided with a hinged top, which was opened or closed by a thread extending through the tube. The water in it was stirred manually by means of a small copper vane mounted on a plastic rod that passed through the top of the jacket.

A copper–constantan thermocouple, with one junction in contact with the calorimeter vessel and the other in the bath, was connected directly to the terminals of a galvanometer. A difference of 0.003° C. between the calorimeter and bath temperatures produced a deflection of 1 mm. Changes in bath temperature involved in maintaining adiabatic conditions while the sample and calorimeter contents attained equilibrium were read to 0.001° C. from a Philadelphia differential thermometer. Bath temperatures were read to 0.01° C. from a calibrated mercury thermometer.

Samples to be measured were placed in cylindrical containers of thin brass closed by screw caps with thin gaskets. The containers had a diameter of

[1] *Manuscript received March 3, 1949.*
Contribution from the Physics Department, University of Alberta, Edmonton, Alta.

[2] *Present address: Experimental Station of the Defence Research Board of Canada, Suffield, Alta.*

* *Napalm is a commercial product consisting of a basic aluminum soap of naphthenic, oleic, and palmitic acids in the approximate ratio 1 : 1 : 2.*

2 cm., a height of 7 cm., a volume of 20 cc., and a mass of 18 gm. The gasket weighed about 0.1 gm. No leakage was detected.

The bath used to bring the samples to the desired initial temperature before introduction to the calorimeter had a capacity of about 1 gal. It was similar to that used previously in conductivity measurements (2). The bath liquid was water for temperatures above, and methyl alcohol for those below, 0° C. Temperature constancy was maintained by the operation of a heating element with a toluene thermostat control working against a cooling tube containing acetone and carbon dioxide snow. Vertical brass tubes about 7 in. long and 1 in. in diameter with their tops just above the liquid level served as dry receptacles for the sample containers. The bath temperature was measured to 0.01° C. by potentiometric determination of the e.m.f. of a copper–constantan thermopile of three couples in series, calibrated at the steam, ice, and carbon dioxide snow points. It exhibited periodic fluctuations of 0.01° C. above 0° C., and of 0.05° C. below 0° C., but no drift occurred over periods of several hours.

Before insertion in the constant temperature bath, the sample containers were placed in shields designed to minimize heat losses or gains during the four second interval required for transfer from the bath to the calorimeter. A shield consisted of a brass tube just large enough to hold a container. It was closed permanently at the upper end and was corked at the lower. In transferring a sample from the bath to the calorimeter, the shield was held over the tube in the calorimeter jacket, the cork was removed, and the sample container was lowered into the calorimeter by means of a thread passing through the top of the shield.

A graded series of gels was prepared by mixing appropriate quantities of Napalm and gasoline with mechanical stirring for half an hour. The gasoline was supplied by the Research Council of Alberta. It had a tetraethyl lead content of 3.4 cc. per gal., and a specific gravity of 0.702. About 15 gm. of the gel to be examined was placed in a sample container and brought to the desired initial temperature by insertion for at least one hour in the constant temperature bath. The temperature attained by it was taken to be equal to the mean bath temperature over the latter part of this period. The temperature of the weighed mass of distilled water in the calorimeter vessel and also that of the calorimeter bath was so adjusted that the value attained after adding the sample was as nearly as possible 21.00° C. On transfer of the sample to the calorimeter, adiabatic conditions were achieved as nearly as possible by additions of warm or cold water to the calorimeter bath. On attainment of thermal equilibrium the temperature change of the bath, and so of the water in the calorimeter vessel, was determined from the initial and final readings of the differential thermometer. The final temperature was read to 0.01° C. from the bath thermometer. The heat capacity of the sample between its initial and final temperature was calculated in the usual way, the heat capacities of the calorimeter vessel, stirrer, and sample container being

taken into account. The heat capacity between the initial temperature and 21.00° C. was calculated from this value by application of a small correction.

From 100 to 140 gm. of water was used in the calorimeter vessel; its temperature never exceeded 24° C. nor fell below 18° C. Temperature changes caused by introduction of the sample were from 2° to 4° C. The specific heat of water was taken as 1.000 cal. per gm. per Centigrade degree. In view of the small departures from 21° C., use of this value introduced an error of less than 0.1%.

The heat capacity of the calorimeter vessel and stirrer was determined in tests in which 5 to 8 gm. of distilled water at 0° C. was added to 20 to 30 gm. of water in the vessel, with a resulting temperature drop of about 3° C. The mean value for the 21° C. region was 16.5 ± 0.2 cal. per °C. The heat capacity of each sample container was calculated from the masses and specific heats of brass and the gasket material. On the average these contributed respectively about 0.05 and 1.6 cal. per °C. to the heat capacity of the loaded container (9 to 10 cal. per ° C.). The specific heat of the gasket was determined from measurements on sample containers filled with disks of the material. It was found to be 0.52 cal. per gm. per Centigrade degree. Since the gasket accounted for only about 0.5% of the heat capacity of the loaded containers, variations with temperature were not measured. The specific heat of commercial brass was determined from heat capacity measurements on a 150 gm. cylinder by the method described above. The data are given in Table I. The heat capacities H_{21}^{θ} between the initial temperature θ and 21.00° C. are described to better than 1% by the relation

$$H_{21}^{\theta} = -1.859 + 0.0885\theta + 0.000019\theta^2 \qquad (1).$$

Consequently the specific heat S_T at T° C. is given in calories per gram per Centigrade degree by

$$S_T = 0.0885 + 0.000038T \qquad (2)$$

over the temperature range of Table I.

TABLE I

OBSERVED HEAT CAPACITIES IN CALORIES PER GRAM BETWEEN θ AND 21.00° C. FOR A SAMPLE OF COMMERCIAL BRASS ROD, AND THE DEVIATIONS FROM THEM OF THE VALUES GIVEN BY EQUATION (1)

θ (°C.)	Cal./gm.	% Dev.	θ (°C.)	Cal./gm.	% Dev.
50.15	2.63	0.0	−21.27	−3.74	0.3
49.64	2.59	−0.4	−29.85	−4.49	0.2
40.18	1.72	0.6	−39.76	−5.33	−0.4
33.40	1.11	0.9	−49.53	−6.19	−0.2
0.00	−1.85	−0.5	−50.77	−6.32	0.3

In preliminary tests the bath temperature was maintained equal to that of the water in the calorimeter over periods of more than half an hour without detectable change in the reading of the differential thermometer. It follows

that heat exchange with the exterior and heat loss by evaporation were negligible over the period required for making a determination. Other tests showed that 100 rather vigorous strokes of the stirrer caused a temperature rise of only 0.005° C. in the water in the calorimeter. Since in making a determination only three or four gentle strokes were used on about three occasions during the course of heat exchange, the stirring was not sufficient to cause a detectable rise in temperature. As a check on over-all reliability, the average specific heat of copper was determined for the ranges 21° to 50° C. and 21° to 58° C. The mean of six determinations was 0.0932 cal. per gm. per Centigrade degree, in agreement with a value of 0.0930 cal. per gm. per Centigrade degree calculated from the results of Bronson *et al.* (1).

Results of Heat Capacity Measurements

Measured heat capacities between various initial temperatures θ and 21.00° C. are given in Table II for gasoline, Napalm, and gasoline–Napalm gels of four different concentrations.

TABLE II

OBSERVED HEAT CAPACITIES IN CALORIES PER GRAM BETWEEN θ AND 21.00° C. FOR GASOLINE, NAPALM, AND VARIOUS GASOLINE–NAPALM GELS, AND THE DEVIATIONS FROM THEM OF THE VALUES GIVEN BY EQUATION (4). PERCENTAGE NAPALM CONCENTRATIONS BY WEIGHT ARE GIVEN AT THE HEAD OF EACH PAIR OF COLUMNS.

θ, °C.	0.0		5.0		7.5		10.0		12.5		100	
	Obs.	% Dev.	Obs.	% Dev.	Obs.	% Dev.	Obs.	% Dev.	Obs.	% Dev.	Obs.	% Dev.
50.15	15.09	−1.2	14.89	−0.5	14.87	−0.6	14.92	−0.7	14.77	−0.4	13.24	1.4
49.64	14.79	−0.8	—	—	—	—	—	—	—	—	—	—
44.61	12.05	−0.4	11.89	0.3	11.96	−0.2	11.91	0.3	11.74	0.9	10.72	0.7
40.18	9.84	−1.3	—	—	—	—	—	—	—	—	—	—
39.81	—	—	—	—	—	—	9.43	0.3	—	—	8.47	1.2
39.73	9.56	−0.9	9.38	0.4	9.20	2.3	—	—	9.40	−0.4	—	—
33.42	6.24	0.3	—	—	—	—	—	—	—	—	—	—
30.52	4.72	1.1	4.62	2.8	4.63	1.9	4.63	2.4	4.79	−1.7	4.38	−1.1
0.00	−10.47	−1.9	−10.07	1.4	−10.18	0.1	−10.10	0.5	− 9.95	1.7	− 9.03	0.4
−11.17	−15.66	−0.6	−15.41	0.4	−15.35	0.5	−15.47	−0.6	−15.30	0.2	−13.88	−0.9
−21.27	−20.22	0.2	−20.01	0.6	−20.19	−0.4	−20.03	0.0	−19.99	−0.2	−18.00	−0.5
−29.85	—	—	—	—	—	—	−23.89	−0.1	—	—	−21.54	−0.8
−31.26	−24.85	−0.2	−24.49	0.7	−24.65	−0.2	—	—	−24.40	0.2	—	—
−39.76	−28.59	−0.1	−28.32	0.2	−28.48	0.5	−28.28	−0.1	−28.23	−0.2	−25.25	0.0
−49.53	−32.85	0.1	−32.38	0.9	−32.53	0.2	−32.45	0.1	−32.36	0.1	−29.08	−0.3
−50.77	−33.62	−0.7	−33.06	0.5	−33.23	−0.3	−33.12	−0.3	−33.11	−0.5	−29.50	−0.1
Average	—	0.7	—	0.8	—	0.7	—	0.5	—	0.6	—	0.7

Discussion

An examination was made of two types of empirical relation to describe the heat capacity data of Table II. The one finally adopted was the power series

$$H_{21}^{\theta} = -P + Q\theta + R\theta^2, \qquad (3)$$

where H_{21}^{θ} denotes the heat capacity in calories per gram between the initial temperature θ and 21.00° C., and P, Q, and R are constants. The values of the constants were first determined by fitting the equation by the method of least squares to the data independently for each Napalm concentration, including 0% and 100%. Plots of P, Q, and R against the Napalm concentration C then showed a linear relation between the first two and C, but no detectable dependence on C of the small constant R. The equations of the lines in the P and Q plots were substituted for P and Q in Equation (3) to express explicitly the dependence of H_{21}^{θ} on Napalm concentration. The value of R was taken to be the mean value for the entire data. On this basis Equation (3) became

$$H_{21}^{\theta} = -10.27 + 0.012C + (0.479 - 0.00054C)\,\theta + 0.00046\,\theta^2. \quad (4)$$

The values of H_{21}^{θ} calculated from Equation (4) showed an average deviation of 0.7% from the 69 observed values, as may be seen from Table II. The maximum deviation was 2.8%. There were three deviations greater than 2%, and 11 between 1% and 2%. Two of the former, and four of the latter were associated with data for the initial temperature closest to 21.00° C., and for these the experimental error is expected to be greatest; the average deviation for the $\theta = 30.52°$ data was 1.8%. Equation (4) satisfies the requirement that H_{21}^{θ} should effectively vanish when $\theta = 21.00°$ C. Calculated values of H_{21}^{21} for the concentrations in the order given in Table II are 0.03, −0.01, −0.02, 0.00, 0.00, and 0.06 cal. per gm.

It follows from Equation (4) that the specific heat S_T in calories per gram per Centigrade degree at any temperature T° C. between 50° and −50° C. and any Napalm concentration C in per cent by weight, is given by

$$S_T = 0.479 - 0.00054C + 0.00092T. \quad (5)$$

This relation is considered to be good to about 2%. Although no data were obtained between $C = 12.5\%$ and $C = 100\%$, there is no reason to expect serious errors from interpolation for this region.

References

1. Bronson, H. L., Chisholm, H. M., and Dockerty, S. M. Can. J. Research, A, 8 : 282. 1933.
2. Langstroth, G. O. and Zeiler, F. Can. J. Research, A, 26 : 50. 1948.

THE NUCLEAR MOMENTS OF P^{31} [1]

By M. F. Crawford and J. Levinson[2]

Abstract

Hyperfine structures have been observed in the $3s4s\ ^3S_1 - 3s4p\ ^3P^0_{0,1,2}$ transitions of P IV with a 21 ft. concave grating and in the $4s\ ^2S_{1/2} - 4p\ ^2P^0_{3/2}$ transition of P III with a transmission echelon. The half-widths of the lines, excited in an electrodeless discharge, were reduced by mixing neon with the phosphorus vapor and by using a condenser of small capacity. Their intensities were increased by discharging the condenser through the exciting coil nine times per half-cycle by means of a rotating spark gap. The structures of the P IV lines confirm $I = 1/2$ and show that μ, the nuclear magnetic moment, is positive. $\mu = 1.15 \pm 0.05$ n.m. and $\mu = 1.11 \pm 0.1$ n.m. are obtained from the P IV and P III structures, respectively.

Introduction

The nuclear magnetic moments of nearly all the nuclei lighter than Yt with odd atomic number and odd mass number are known. P^{31} is one exception. Its spin, $I = \frac{1}{2}$, has been determined from alternating intensities in the band spectrum of diatomic phosphorus vapor (1, 10). Its magnetic moment has been investigated by Tolansky (14): he found no resolvable hyperfine structure in any of the 13 lines of the second spectrum of phosphorus studied by him, and concluded that the nuclear gyromagnetic ratio, g, is anomalously small. However, these lines of P II would have very narrow structures even for a g-value corresponding to a magnetic moment of the order of one nuclear magneton (3).

The fourth spectrum of phosphorus is more favorable for a determination of the magnetic moment. The transitions $3s4s\ ^3S_1 - 3s4p\ ^3P^0_{0,1,2}$ in P IV (2, 13) should have hyperfine structures of the order of seven times larger than the widest structure in the lines studied by Tolansky. Accordingly these transitions were investigated. An electrodeless discharge was used to excite the fourth spectrum, and the effects of source conditions on the half-widths of the lines were studied. The reduction effected in the half-widths made it possible to resolve hyperfine structures and determine the magnetic moment.

Experimental

The light source was an electrodeless discharge in a mixture of phosphorus vapor and neon in a quartz tube 75 cm. long and 2.5 cm. in diameter. The discharge was observed through a plane window at one end. An exciting coil 50 cm. long was wound tightly on mica wrapped around the central portion of the tube. Neon was circulated through the discharge tube. The construction and operation of the circulating and purifying system are described

[1] *Manuscript received February 5, 1949.*
Contribution from the Department of Physics, University of Toronto, Toronto, Ontario.

[2] *Holder of a Fellowship under the National Research Council of Canada, 1946–1947. Now at the Research Laboratory of Electronics, Massachusetts Institute of Technology, Cambridge, Massachusetts.*

in the book by Tolansky (15). Freedom from hydrogen and mercury in the discharge tube is essential since both appreciably quench the higher spectra of phosphorus.

A schematic diagram of the exciting circuit is shown in Fig. 1. The oil condensers, *C*, combined in series as shown, had a capacity of 0.002 μf. The exciting coil, *D*, consisted of 118 turns of 1.5 mm. copper wire, and had an

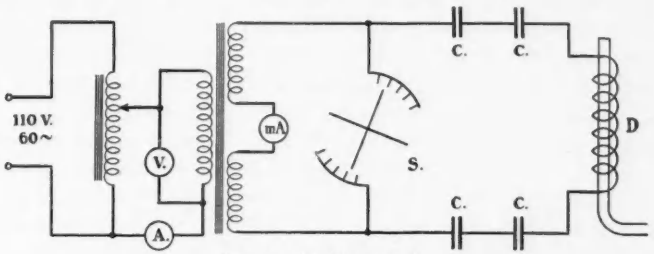

FIG. 1. *Exciting circuit.*

inductance of 27.5 μh. It was found empirically that smaller values of the capacity resulted in sharper lines, but reduced the intensity appreciably. In order to use small capacity without loss of intensity, the method of multiple discharge per half-cycle was adopted. The condensers were discharged through the coil by the rotating spark-gap, *S*, which was synchronous with the applied voltage. The number of discharges per half-cycle was determined by the number of fixed terminals per quadrant, and as many as nine were used. With the above value of the capacity the condensers charged up to approximately the same potential before each discharge. The charging current was supplied by a 1.5 kva., 220 : 75,000-v. transformer. Its input was controlled by a 1.5 kva. autotransformer and was adjusted to give a sparking voltage of approximately 20,000 v.

The best compromise between intensity and half-width for P IV lines was obtained with the electrical conditions described above and a pressure of 1 mm. of neon. Since the discharge tube was operated at room temperature, the partial pressure of the phosphorus vapor was that of yellow phosphorus at room temperature. The effects of source conditions were not investigated in sufficient detail to warrant much speculation on the mechanism of the excitation process. However, the empirical results indicate that the line widths of the higher spectra depend more upon the velocities acquired by ions in the exciting field than upon other factors, and thus show that data relevant to the theory of discharges in gases at low pressure can be obtained from the study of line contours.

The spectrograph was a 21 ft. concave grating in a modified Eagle mounting with a plate holder 12 ft. long. It was in a constant temperature room separated from the source room except for a small opening through which the light entered. The 3350 Å region was recorded in the fourth and fifth orders

simultaneously. In the fifth order, which is the more intense, the theoretical resolving power is 400,000.

Ilford Zenith plates were used and developed in Ilford metolhydroquinone developer. A Corning red–purple Corex filter was placed before the slit to reduce the background and the overlapping of orders. Although the plates were grainy, traces obtained with a Leeds and Northrup microphotometer were relatively smooth because a sufficiently long portion of the line was scanned to average out fluctuations. The separations, as well as the intensities of the hyperfine structure components, were determined from the traces.

An accurate calibration of the emulsion was obtained from the nonuniform intensity distribution along a spectral line due to the astigmatism of the concave grating, as first suggested by Dieke (5). Dieke's method is applicable only if the slit is uniformly illuminated and the grating is uniformly reflecting along the length of a ruling. Since these conditions were not fulfilled, his method was modified to incorporate the principle of the "Two-Line Method" described by Churchill (4). On a concave grating spectrogram the relative intensity distribution along the length of a spectral line is the same for all lines in a narrow spectral region. Thus the densities of two selected lines measured at equal distances from the centers of the lines represent a constant intensity ratio independent of the distance from the centers. By measuring corresponding densities at a number of distances from the centers of the lines the characteristic curve can be determined if the intensity ratio of the two lines is known. If the intensity ratio is not known, the characteristic curve can be plotted only on an arbitrary log I scale.

In this investigation the intensity ratio of the transitions $^3S_1 - {}^3P_1^0$ (3364 Å) and $^3S_1 - {}^3P_0^0$ (3371 Å) was used to determine the log I scale uniquely. This ratio was first measured using a characteristic curve obtained from a stepped-slit exposure on another plate of the same emulsion number, and was within 10% of the ratio 3:1 given by multiplet theory for LS coupling. This is the order of agreement expected when the standard is not on the same plate as the spectrum. Thus it was deemed justifiable to use the theoretical ratio 3:1 to determine the log I scale of the characteristic curve obtained by the Two Line Method. The intensity ratios for hyperfine structure components and for the lines of the fine-structure multiplet as determined with this calibration are consistent with theory to within 5% as shown in Fig. 2.

This consistency is appreciably better than that obtained with a stepped-slit calibration, particularly at low densities. This is not unexpected since the Two Line Method uses the lines themselves, and hence is independent of source fluctuations and variation of emulsion sensitivity over the plate. Further, the background corrections can be made with greater precision.

Results

The intensity contours of the three P IV lines studied are given by the heavy lines in Fig. 2, (*a*), (*b*), (*c*). They were obtained from the microphotometer

traces of the best plate. Traces of seven other plates showed no appreciable departure in form from those of the best plate. Relative intensities obtained from several of these plates agreed with those obtained from the best plate to within 10%, and half-widths agreed to within 2%. In our judgment the contours obtained from the best plate are reliable to better than 5%, and are probably more accurate than a simple average of the contours obtained from all the plates.

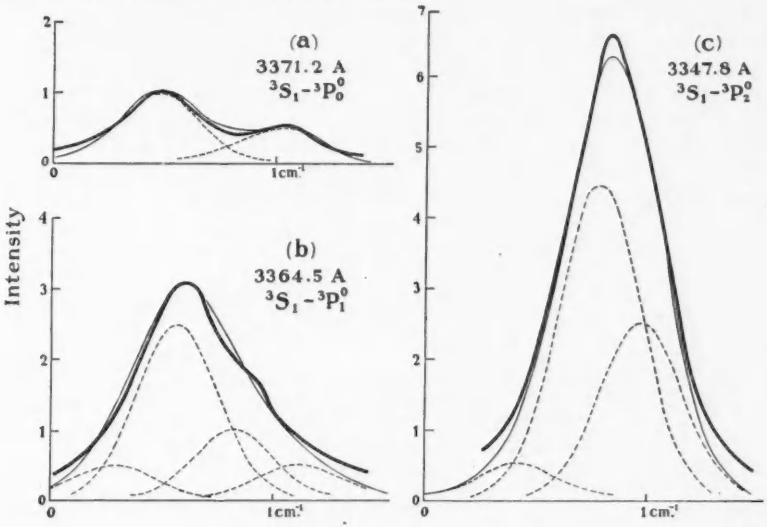

FIG. 2. *Intensity contours*

The dashed contours in Fig. 2 represent the theoretical hyperfine structure components, assumed to have a Gaussian distribution. They are based on the theoretical patterns shown in Fig. 3, (*a*), (*b*), (*c*). These patterns are drawn for $I = \frac{1}{2}$ and a positive nuclear magnetic moment. The relative intensities are shown in Fig. 3 by the heights of the lines representing the components and were obtained from the formulae of Hill (9). The hyperfine structure separations given in terms of g in Fig. 3 are calculated as described below. The theoretical line contours shown in Fig. 2 as light continuous lines are the sums of the dashed contours of the components. Only two experimentally derived data were used in plotting the theoretical contours: 0.44 cm.$^{-1}$ as the half-width of a component, deduced from 3348 Å; and 0.54 (5) cm.$^{-1}$ as the separation of the hyperfine structure states of $^3S_1$, obtained from the measured separation of the peaks (0.49 ± 0.02 cm.$^{-1}$) in 3371 Å by correcting for the small overlapping of the components. The intensity unit for both the theoretical and the experimental contours is the intensity of the stronger peak of 3371 Å.

The presence of just two hyperfine structure components in the pattern of 3371 Å with a measured intensity ratio of 1.98 proves uniquely that $I = \frac{1}{2}$, the value obtained by Ashley (1) and Jenkins (10) from the molecular spectrum.

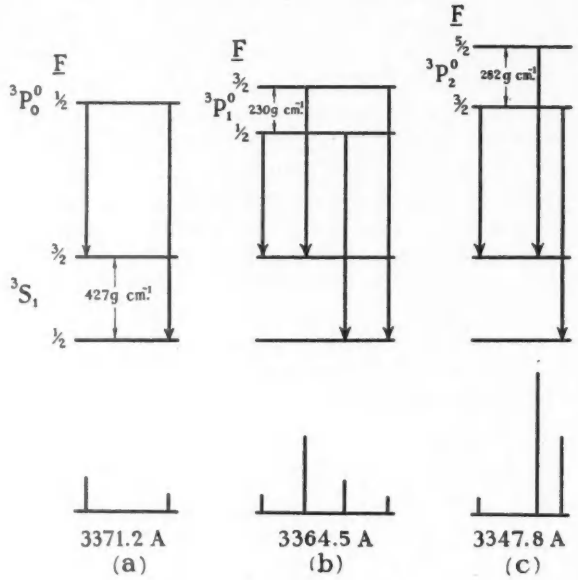

FIG. 3. *Theoretical patterns.*

The hyperfine structure splitting of the $^3S_1$ level for $I = \frac{1}{2}$ is given by (7, 8)

$$\Delta(^3S_1) = \frac{3}{2} \cdot \frac{1}{2} \cdot (a_{3s} + a_{4s}) \, . \, K \text{ cm.}^{-1}; \tag{1}$$

where

K is a relativistic correction and has the value 1.02 for an s electron of phosphorus,

$$a_{ns} = \frac{8}{3} R\alpha^2 \frac{Z_i \, Z_0^2}{n_e^3} \cdot g \text{ cm.}^{-1}, \tag{2}$$

R is the Rydberg constant,

α is the Sommerfeld fine-structure constant,

Z_i is the inner effective nuclear charge and equals 15 for an s electron of phosphorus.

Z_0 is the outer effective nuclear charge,

n_e is the effective principal quantum number,

g is the ratio of the nuclear magnetic moment in Bohr magnetons to the nuclear angular momentum in Bohr units.

Thus,

$$a_{ns} = 232.8 \, Z_0^2 g / n_e^3 \text{ cm.}^{-1} \, . \tag{3}$$

The values of Z_0^2/n_e^3 are different for the two electrons of $3s4s\ ^3S_1$, and are not obtainable directly. Since the Rydberg formula for the term value gives only Z_0^2/n_e^2, Z_0 or n_e must be determined explicitly for each electron. For the $3s$ electron Z_0^2/n_e^2 is evaluated by equating it to the term value, in Rydberg units, of the $3s4s$ configuration of P IV relative to the $4s$ configuration of P V. A value of n_e to be used with Z_0^2/n_e^2 is obtained as follows: n_e of the $3s$ electron of P V evaluated from Robinson's data (13), $T = 524{,}463$ cm.$^{-1}$ and $Z_0 = 5$, is 2.287. This is an approximate value of n_e for the $3s$ electron in the $3s4s$ configuration of P IV. It is true that $Z_0 = 5$ is too large for the $3s$ electron, by perhaps 10%, when the shielding by the $4s$ electron is taken into account; but the term value, $T = 524{,}463$ cm.$^{-1}$, taken from the P V analysis is also too large by 12% compared to the energy required to remove the $3s$ electron from the $3s4s$ configuration of P IV, namely $T = 460{,}384$ cm.$^{-1}$. These two errors tend to compensate. Since Z_0 probably is between 5 and 4.5, the value of n_e obtained in this manner should not be in error by more than $\pm$ 5%. Using $n_e = 2.287$ and $T = 460{,}384$ cm.$^{-1}$ for the $3s$ electron,

$$Z_0^2/n_e^3 = T/R \,.\, n_e = 1.83_5 \,. \tag{4}$$

Substituting this value in (3),

$$a_{3s} = 427 \text{ g cm.}^{-1} \,. \tag{5}$$

For the $4s$ electron of the $3s4s$ configuration, Z_0 is taken as 4, then n_e is 3.061, as calculated from the term value, 187,423 cm.$^{-1}$, of $^3S_1$ relative to $3s\ ^2S$ of P V. Thus from (3)

$$a_{4s} = 130 \text{ g cm.}^{-1} \,. \tag{6}$$

Substitution of (5) and (6) in (1) gives

$$\Delta\ (^3S_1) = 425 \text{ g cm.}^{-1} \,. \tag{7}$$

The experimentally determined value of $\Delta\ (^3S_1)$ is 0.54 (5) cm.$^{-1}$, and the hyperfine structure is normal. Thus by Equation (7), $g = +\ 0.00128$. However, Fermi and Segrè (6) have shown that if the quantum defects for an s-electron term sequence are not constant the right hand side of Equation (3) must be multiplied by a correction factor. From Robinson's data for the ns terms of P III and P V and for the $3sns$ terms of P IV the correction factor for the $3s$ electron is 1.016 and for the $4s$ electron 1.025. These corrections increase the coefficient of g in Equation (7) by 2%, and give $g = +\ 0.00125 \pm 0.00005$. The nuclear magnetic moment, μ, in nuclear magnetons then is $+\ 1.15 \pm 0.05$ n.m.

The separations of the levels of the $3s4p$ configuration are consistent with Houston's equations and show that the coupling departs somewhat from LS. The wave function for the triplet level with $J = 1$, designated as $\{^3P_1^0\}$, can be expressed as a linear combination of the triplet and singlet wave functions in pure LS coupling, designated as $[^3P_1^0]$ and $[^1P_1^0]$ respectively. Using Robinson's term values (13),

$$\{^3P_1^0\} = 0.994\,[^3P_1^0] - 0.106\,[^1P_1^0]. \tag{8}$$

Equation (8) shows that the departure from LS coupling is small, and that the 3:1 intensity ratio assumed for the two lines used to calibrate the emulsion is valid to within 1%. However, the departure is significant in the calculation of the hyperfine structure splitting of the $^3P_1^0$ level.

For this calculation (3) it is necessary to express the wave function as a linear combination of the jj wave functions of the two levels with $J = 1$. Designating these as [1/2, 1/2] and [1/2, 3/2], to indicate their origin in the jj subgroups,

$$\{^3P_1^0\} = 0.873\,[1/2, 1/2] + 0.488\,[1/2, 3/2]\,. \tag{9}$$

The coefficients in Equation (9) when substituted in the formulae of Breit and Wills (3) for intermediate coupling give the following relation for the splitting of the $^3P_1^0$ level:

$$\Delta(^3P_1^0) = \frac{3}{2}(0.327\,a_{3s} + 1.09\,a_{4p}), \tag{10}$$

where

$a_{3s} = 427\ g\ \text{cm.}^{-1}$ from Equation (5),

$a_{4p} = \dfrac{\Delta\nu g}{(l + \frac{1}{2})Z_i} = 10.6\ g\ \text{cm.}^{-1}$.

$\Delta\nu = 207\ \text{cm.}^{-1}$, the separation between the $J = 0$ and $J = 2$ levels,

$Z_i = 13$, obtained from $\Delta\nu$ by the spin doublet formula,

$l = 1$.

Relativistic corrections are included in the numerical coefficients of Equation (10). Thus, $\Delta(^3P_1^0) = 228\ g\ \text{cm.}^{-1} = 228 \times 0.00128\ \text{cm.}^{-1}, = 0.29\ \text{cm.}^{-1}$, using the uncorrected value of g obtained from the $^3S_1$ splitting.

An experimental value of $\Delta(^3P_1^0)$ was obtained by comparing the observed contour of 3364 Å with the contours predicted using $\Delta(^3S_1) = 0.54(5)\ \text{cm.}^{-1}$ and a series of values of $\Delta(^3P_1^0)$. The comparison gave a fairly unique value, $\Delta(^3P_1^0) = 0.27 \pm 0.04\ \text{cm.}^{-1}$. The contour plotted using this value, which is $0.02\ \text{cm.}^{-1}$ smaller than the calculated splitting, matched the observed contour very well, including the hump on the high-wave-number side. This is evident from Figs. 3, (*b*), 2, (*b*); a small decrease in the splitting of $^3P_1^0$ increases the separation of the two central components and produces a hump on the side of the contour. However, the difference between the calculated and the experimental value of $\Delta(^3P_1^0)$ is within the assigned error which takes into consideration both the precision of the matching and the 4% error in the value of $\Delta(^3S_1)$ used in the analysis of the contour. Although this error is relatively large because of the incomplete resolution, the contour is compatible only with $I = \frac{1}{2}$. A similar analysis of the contour of 3348 Å gave $\Delta(^3P_2^0) = 0.39 \pm 0.11\ \text{cm.}^{-1}$. By calculation (3), $\Delta(^3P_2^0) = 282\ g\ \text{cm.}^{-1} = 0.36\ \text{cm.}^{-1}$. Thus, the hyperfine structures of these two lines, as well as that of 3371 Å, are consistent with $I = 1/2$ and $\mu = +1.15 \pm 0.05$ n.m.

The third spectrum of phosphorus was also investigated with a transmission echelon. The transition $4s^2S_{1/2} - 4p\ ^2P_{1/2}^0$ (4246 Å) (11, 13) was resolved into

two components with a separation of 0.11 ± 0.01 cm.$^{-1}$ However, only one good spectrogram was obtained before two plates of the echelon became "uncontacted." The resolved structure on this spectrogram gave $\Delta(4s^2S_{1/2}) = 0.12 \pm 0.01$ cm.$^{-1} = K \cdot a_{4s}$. Thus by Equation (3) with a Fermi–Segrè correction factor of 1.026, $\mu = +1.11 \pm 0.1$ n.m.

During the writing of this report a letter was published by Pound (12) in which he gave $\pm 1.1314 \pm 0.0013$ n.m. as the nuclear magnetic moment of P^{31} obtained by the magnetic resonance method. Our values agree with his within the error set by us on the basis of experimental accuracy alone. In addition our results show that the nuclear magnetic moment is positive and confirm $I = 1/2$.

References

1. Ashley, Muriel F. Phys. Rev. 44 : 919. 1933.
2. Bowen, I. S. Phys. Rev. 39 : 8. 1932.
3. Breit, G. and Wills, L. A. Phys. Rev. 44 : 470. 1933.
4. Churchill, J. R. Ind. Eng. Chem., Anal. Ed. 16 : 653. 1944.
5. Dieke, G. H. J. Optical Soc. Am. 23 : 274. 1933.
6. Fermi, E. and Segrè, E. Z. Physik, 82 : 729. 1933.
7. Goudsmit, S. Phys. Rev. 43 : 636. 1933.
8. Goudsmit, S. and Bacher, R. F. 34 : 1501. 1929.
9. Hill, E. L. Proc. Natl. Acad. Sci. U.S. 15 : 779. 1929.
10. Jenkins, F. A. Phys. Rev. 47 : 783. 1935.
11. Millikan, R. A. and Bowen, I. S. Phys. Rev. 25 : 600. 1925.
12. Pound, R. V. Phys. Rev. 73 : 1112. 1948.
13. Robinson, H. A. Phys. Rev. 51 : 726. 1937.
14. Tolansky, S. Z. Physik, 74 : 336. 1932.
15. Tolansky, S. High resolution spectroscopy. Methuen & Co. Ltd., London. 1947.

THE GAMMA RAYS OF RADIUM (B + C)[1]

By K. C. Mann and M. J. Ozeroff

Abstract

An experiment has been performed to verify the gamma-ray energy spectrum of Radium (B + C) as reported by Latyshev and associates. The spectrum was obtained by measuring the energies of photoelectrons ejected from a thin lead radiator by means of a thin-lens magnetic beta-ray spectrometer. The spectrum obtained failed to reveal the presence of transitions other than those reported by C. D. Ellis. Comparative results are presented.

Introduction

The gamma rays of RaB and RaC have been reported in detail by Ellis and coworkers (5) from measurements of the energies of internal conversion electrons and of photoelectrons ejected from high atomic number materials. Later, Latyshev and his associates (1, 2, 8, 9, 10) measured the energy distribution of positrons formed in the process of internal pair production as well as internal conversion electron energies. They were able to report the detection and measurement of all the gamma rays found by Ellis above 2 m_0c^2 (1.02 Mev.) plus 10 new gamma rays, the comparative intensities of the latter being high enough for reasonably easy detection. It is strange that these gamma rays were not found by Ellis, in spite of the extreme care which characterized his work, and for this reason it seemed advisable to investigate again the gamma-ray spectrum of radium in an effort to eliminate these uncertainties.

Apparatus and Method

The source used in this investigation was a silver "needle" containing 10 mc. of radium in equilibrium with its disintegration products. Gamma rays from this source were studied in a thin-lens magnetic beta-ray spectrometer of the type described by Deutsch, Elliott, and Evans (3). For this purpose the gamma rays were allowed to eject into the spectrometer photoelectrons from a thin lead foil 50 mgm. per cm.^{2} in thickness. The momentum distribution of the photoelectrons was measured by varying the focusing current through the spectrometer's lens coil. For detection of electrons, a bell-type Geiger–Müller counter was used with a mica window 4 mgm. per cm.^{2} thick.

The spectrometer was calibrated using the well known F-line of Thorium B. The momentum corresponding to this conversion line has been accurately determined (4, 11) and is

$$H\rho = 1385.6 \text{ gauss-cm.}$$

The thorium source was prepared by precipitation as a sulphide from a thorium nitrate solution on a thin backing of mica. When used in the spectrometer

[1] *Manuscript received March 15, 1949.*

Contribution from the Department of Physics, University of British Columbia, Vancouver, B.C.

the conversion line was quite sharp and gave a calibration constant for the spectrometer of 486.0 gauss-cm. per ampere.

Observations of photoelectron peaks indicate that the resolution of the spectrometer, $\frac{\Delta(H\rho)}{H\rho}$, is 4% at half-peak intensity.

Results

Fig. 1 shows the curve obtained with the spectrometer, using the radium source. The solid curve is the composite curve of photoelectron peaks and Compton electron background, the latter arising from a brass absorber used to eliminate all primary beta rays. The dotted curve represents the Compton electrons alone, taken with lead radiator foil removed.

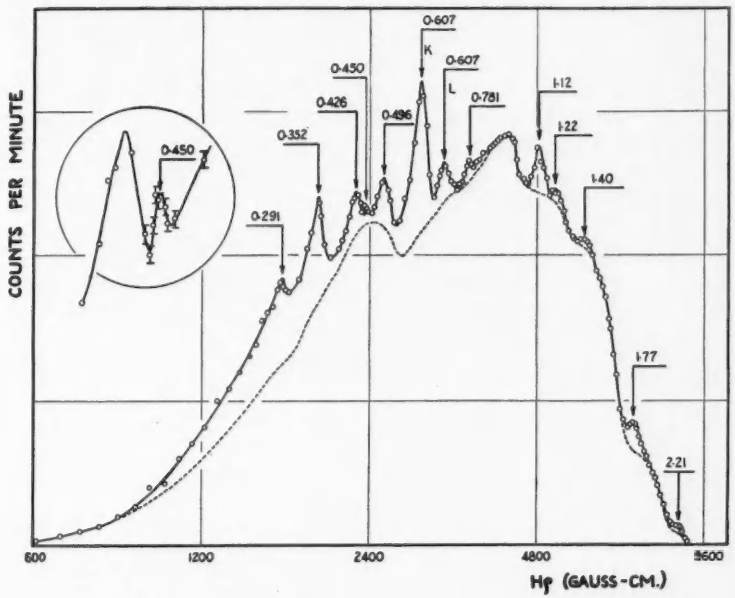

FIG. 1. *The gamma ray spectrum of Radium (B + C).*

The values of the energies in Mev. assigned to each photoelectron peak are the gamma-ray energies, calculated as the sum of the photoelectron energy plus the shell binding energy of lead. All peaks, with one exception, were assumed to be due to photoelectrons ejected from the *K*-shell, since this is most probable. For these, the *K*-shell binding energy used was 0.088 Mev. (taken from X-ray absorption limits (7)). In the one exception, a smaller peak following the 0.607 Mev. gamma ray was found to be 72 kv. more energetic and so was identified as an *L*-shell peak of the same gamma ray.

Table I compares the energies and relative intensities of the gamma rays found in this investigation with those reported by Ellis and coworkers, and by Latyshev. The relative intensities have been calculated on a basis of peak height above background corrected for variation of photoelectric cross section, using published curves (6).

TABLE I

Lines marked "i.c." denote internal conversion measurements.
Lines marked "p.e." denote photoelectric measurements.
Lines marked "i.p." denote internal pair measurements.

Ellis and coworkers	Latyshev and coworkers		Present investigation	
Gamma-ray energy, Mev.	Gamma-ray energy, Mev.	Relative intensity	Gamma-ray energy, Mev.	Relative intensity
0.0529 i.c.				
0.2406 i.c.				
0.2571 i.c.				
0.2937 i.c.			0.291	*
0.3499 i.c.			0.352	*
0.4260 p.e.			0.426	9
			0.450	4
0.4980 p.e.			0.496	14
0.6067 i.c.	0.606 i.c.		0.607	74
0.766 i.c.	0.766 i.c.		0.781	13
0.933 i.c.	0.933 i.c.			
	1.11 i.p.			
1.120 i.c.	1.120 i.c.		1.12	9
	1.21 i.p.	23		24
1.238 i.c.	1.234 i.c.			
1.379 i.c.	1.370 i.c.			
	1.39 i.p.	49	1.40	23
1.414 i.c.	1.414 i.c.			
	1.52 i.p.	29		
	1.62 i.p.	22		
	1.69 i.p.	17		
	1.75 i.p.	100	1.77	100
1.761 i.c.	1.761 i.c.			
	1.82 i.p.	17		
	2.09 i.p.	15		
2.193 i.c.	2.20 i.p. + i.c.	41	2.21	25
	2.40 i.p.	21	2.40	*

* *Not estimated.*

The 2.40 Mev. gamma ray reported in this paper does not appear as a photoelectron peak. It was assumed that a weak gamma ray must be responsible for the Compton recoil electron distribution of the upper energy end of the curve. Choosing the end point of this distribution by inspection to be 2.14 Mev., the gamma-ray energy responsible can easily be shown to be 2.40 Mev., with an uncertainty of the order of $\pm 3\%$.

As used in this investigation, the spectrometer is somewhat insensitive to gamma rays of energy less than 0.250 Mev. because of the long electron path with its attendant scattering and the relatively thick counter window and lead

radiator foil. Hence the low energy rays reported by Ellis did not appear here. In addition, conversion coefficients strongly affect the comparison of results. For example, the 1.414 Mev. transition is known to be almost completely converted and, as a result, it does not appear at all in our measurements.

One faint peak from a 0.450 Mev. gamma ray was found which has not been reported previously. Its intensity is so low that it is certainly near the limit of detection of the spectrometer.

An inspection of the comparative results indicates a radium gamma-ray spectrum along the Ellis pattern. Little evidence of the extra gamma rays reported by Latyshev and coworkers was found. However, all photoelectron peaks above 1 Mev. are relatively weak compared to the admittedly high Compton background and it is possible that the latter may have masked the missing lines.

Techniques are now being developed in this laboratory in an attempt to reduce the Compton background, which if successful should increase the sensitivity of the spectrometer to low intensity gamma rays. The authors hope to be able to make a further report of this research in the near future.

Acknowledgments

This investigation was made possible by a Grant-in-aid of Research from the National Research Council of Canada to one of us (K.C.M.). The junior author (M.J.O.) is indebted to the National Research Council for the award of a Studentship. In addition, grateful acknowledgment is made to the British Columbia Cancer Research Institute for the use of the radium source used here, and to the Consolidated Mining and Smelting Co. of Trail, B.C., for a gift of lead used for protective baffles.

References

1. Alechanov, A. and Latyshev, G. D. Compt. rend. acad. sci. U.R.S.S. 20 : 429. 1948.
2. Constantinov, A. A. and Latyshev, G. D. J. Phys. U.S.S.R., 5 : 249. 1941.
3. Deutsch, M., Elliott, L. G., and Evans, R. Rev. Sci. Instruments, 15 : 7. 1944.
4. Ellis, C. D. Proc. Roy. Soc. (London), A, 138 : 318. 1932.
5. Ellis, C. D. Proc. Roy. Soc. (London), A, 143 : 350. 1934.
6. Goodman, C. The science and engineering of nuclear power. Addison-Wesley Press Inc., Cambridge, Mass. 1947.
7. Handbook of Chemistry and Physics, 30th ed., p. 2013. Chemical Rubber Publishing Co., Cleveland, Ohio. 1948.
8. Kulchitsky, L. A. and Latyshev, C. D. J. Phys. U.S.S.R. 4 : 515. 1941.
9. Latyshev, G. D. Revs. Modern Phys. 19 : 132. 1947.
10. Latyshev, G. D., Kompaneetz, A. F., Borisov, N. P., and Gucak, J. H. J. Phys. U.S.S.R. 3 : 251. 1940.
11. Wang, K. C. Z. Physik, 87 : 633. 1934.

CANADIAN JOURNAL OF RESEARCH

Notes on the Preparation of Copy

GENERAL:—Manuscripts should be typewritten, double spaced, and the **original and one extra copy** submitted. Style, arrangement, spelling, and abbreviations should conform to the usage of this Journal. Names of all simple compounds, rather than their formulae, should be used in the text. Greek letters or unusual signs should be written plainly or explained by marginal notes. Superscripts and subscripts must be legible and carefully placed. Manuscripts should be carefully checked before being submitted, to reduce the need for changes after the type has been set. If authors require changes to be made after the type is set, they will be charged for changes that are considered to be excessive. **All pages, whether text, figures, or tables, should be numbered.**

ABSTRACT:—**An abstract of not more than about 200 words, indicating the scope of the work and the principal findings, is required.**

ILLUSTRATIONS:

(i) *Line Drawings:*—All lines should be of sufficient thickness to reproduce well. Drawings should be carefully made with India ink on white drawing paper, blue tracing linen, or co-ordinate paper **ruled in blue only**; any co-ordinate lines that are to appear in the reproduction should be ruled in black ink. Paper ruled in **green, yellow, or red should not be used** unless it is desired to have all the co-ordinate lines show. Lettering and numerals should be neatly done in India ink preferably with a stencil (**do not use typewriting**) and be of such size that they will be legible and not less than one millimeter in height when reproduced in a cut three inches wide. All experimental points should be carefully drawn with instruments. Illustrations need not be more than two or three times the size of the desired reproduction, but the ratio of height to width should conform with that of the type page. **The original drawings and one set of small but clear photographic copies are to be submitted.**

(ii) *Photographs:*—Prints should be made on glossy paper, with strong contrasts; they should be trimmed to remove all extraneous material so that essential features only are shown. Photographs should be submitted **in duplicate**; if they are to be reproduced in groups, one set should be so arranged and mounted on cardboard with rubber cement; the duplicate set should be unmounted.

(iii) *General:*—**The author's name, title of paper, and figure number should be written in the lower left-hand corner (outside the illustration proper) of the sheets on which the illustrations appear.** Captions should not be written on the illustrations, but typed on a separate page of the manuscript. All figures (including each figure of the plates) should be numbered consecutively from 1 up (arabic numerals). **Each figure should be referred to in the text.** If authors desire to alter a cut, they will be charged for the new cut.

TABLES:—Titles should be given for all tables, which should be numbered in Roman numerals. Column heads should be brief and textual matter in tables confined to a minimum. **Each table should be referred to in the text.**

REFERENCES:—**These should be listed alphabetically by authors' names, numbered in that order, and placed at the end of the paper.** The form of literature citation should be that used in the respective sections of this Journal. **Titles of papers should not be given in references listed in Sections A, B, E, and F, but must be given in references listed in Sections C and D.** The first page only of the references cited in papers appearing in Sections A, B, and E should be given. **All citations should be checked with the original articles.** Each citation should be referred to in the text by means of the key number; in Sections C and D the author's name and the date of publication may be included with the key number if desired.

The *Canadian Journal of Research* conforms in general with the practice outlined in the *Canadian Government Editorial Style Manual*, published by the Department of Public Printing and Stationery, Ottawa.

Reprints

Fifty reprints of each paper without covers are supplied free. Additional reprints, if required, will be supplied according to a prescribed schedule of charges. On request, covers can be furnished at cost.